INFORMATION TO USERS

This manuscript has been reproduced from the microfilm master. UMI films the text directly from the original or copy submitted. Thus, some thesis and dissertation copies are in typewriter face, while others may be from any type of computer printer.

The quality of this reproduction is dependent upon the quality of the copy submitted. Broken or indistinct print, colored or poor quality illustrations and photographs, print bleedthrough, substandard margins, and improper alignment can adversely affect reproduction.

In the unlikely event that the author did not send UMI a complete manuscript and there are missing pages, these will be noted. Also, if unauthorized copyright material had to be removed, a note will indicate the deletion.

Oversize materials (e.g., maps, drawings, charts) are reproduced by sectioning the original, beginning at the upper left-hand corner and continuing from left to right in equal sections with small overlaps.

Photographs included in the original manuscript have been reproduced xerographically in this copy. Higher quality 6" x 9" black and white photographic prints are available for any photographs or illustrations appearing in this copy for an additional charge. Contact UMI directly to order.

Bell & Howell Information and Learning
300 North Zeeb Road, Ann Arbor, MI 48106-1346 USA
800-521-0600

AEROBIC GLYCOLYSIS IN RESPONSE TO VISUAL STIMULATION STUDIED BY POSITRON EMISSION TOMOGRAPHY (PET): PRELIMINARY APPLICATION TO MITOCHONDRIAL DISORDERS

Manouchehr S. Vafaee

Dept. Neurology and Neurosurgery

McGill University, Montreal

May 1999

A Thesis submitted to the

Faculty of Graduate Studies and Research

in partial fulfillment

of the requirements for the degree of

Doctor of Philosophy

in Neurological Science

National Library of Canada
Acquisitions and Bibliographic Services
395 Wellington Street
Ottawa ON K1A 0N4
Canada

Bibliothèque nationale du Canada
Acquisitions et services bibliographiques
395, rue Wellington
Ottawa ON K1A 0N4
Canada

Your file Votre référence

Our file Notre référence

0-612-55389-2

Canada

ABSTRACT

Adenosine triphosphate (ATP) is the main source of energy supply for tissue. It is provided either by conversion of glycogen to lactate (anaerobic glycolysis) or by oxidation of glucose (aerobic glycolysis) which is a more efficient way of energy production. The process of aerobic glycolysis, also called oxidative phosphorylation, utilises molecular oxygen (O_2) as the oxidant and occurs in mitochondria. Therefore, normal function of mitochondria and normal supply of O_2 is vital for cellular work.

We have used positron emission tomography (PET) and investigated the issue of oxygen consumption in the visual cortex following stimulation with a colorful visual paradigm. The stimulus was capable of activating visual neurons involved in color processing. We have further investigated the behavior of the oxygen consumption and blood flow in the visual cortex with respect to the rate of stimulation using the same visual stimulus designed in the previous study. We also studied a few available patients who suffered from mitochondrial diseases and compared the results with those obtained from the normals with the aim of shedding some light on the pathophysiology of these disorders.

RÉSUMÉ

L'adénosine triphosphate (ATP) représente la principale source d'énergie pour les tissus. La synthèse d'ATP s'effectue par le biais de deux mécanismes distincts: 1) la conversion du glycogène en lactate (glycolyse anaérobie); 2) l'oxydation du glucose (glycolyse aérobie). Cette dernière représente probablement la voie de production d'énergie la plus efficace. La glycolyse aérobie, également appelée phosphorylation oxydative, utilise l'oxygène moléculaire comme oxydant et siège au sein des mitochondries. Ainsi, le fonctionnement et l'apport d'O_2 normaux sont vitaux pour assurer une fonction cellulaire adéquate.

Nous avons étudié la consommation d'oxygène dans le cortex visuel suivant l'activation des neurones impliqués dans le traitement de la couleur a l'aide de la tomographie par émission de positons chez le sujet normal. Nous avons, de plus, étudié les variations de la consommation d'oxygène et du flux sanguin dans le cortex visuel selon la fréquence de stimulation. Enfin, nous avons répété ces études chez quelques patients souffrants de maladies mitochondriales. Les résultats obtenus chez ces derniers ont été comparés à ceux obtenus chez le sujet normal afin de mieux comprendre la pathophysiologie sous-tendant ces maladies.

ACKNOWLEDGEMENTS

I sincerely thank Dr. Albert Gjedde my co-supervisor for his boundless contribution throughout the course of this work. This study would not have been completed without his constructive criticisms and scientific expertise. I truly appreciate his vast wealth of understanding. Having the opportunity to work with him not only gave me the chance to learn science from him but also the human aspect of science, without which, science is not meaningful.

I also wish to thank Dr. Ernst Meyer my other co-supervisor for his support and believing in me from the beginning which gave me the momentum to start my project.

I am grateful to Dr. Alan Evans for his overall support as well as his efforts in creating such a congenial and effective multidisciplinary environment at the PET unit.

I extend my special gratitude to my advisory committee members, Drs. Tomáš Paus and Eric Shoubridge for devoting their time to me and making themselves available whenever I needed. I sincerely appreciate their contribution to this work.

I would also like to thank Drs. Hidehiko Okazawa and Pedro Rosa for their extremely constructive and helpful criticisms and comments which helped me to improve the quality of my research and data.

Special thanks are due to Dr. Paul Cumming who read the thesis and provided me with valuable comments.

I also extend my appreciation to Mr. Peter Neelin for providing expert image analysis, our cyclotron staff for providing the radioisotopes, our technicians and Ms. Paule Joanne Toussaint for their assistance with PET experiments as well as Ms. Catherine Bleicher for helping me to prepare the French version of the abstract.

Finally I would like to acknowledge the support of my inspiring and valuable friends throughout the course of this work especially Mrs. Lori Billinghurst which helped me to boost my confidence whenever I needed.

This work was supported by Medical Research Council (Canada) grant SP-30, the Isaac Walton Killam Fellowship Fund of the Montreal Neurological Institute, the McDonnell-Pew Program in Cognitive Neuroscience, and Medical Research Council (Denmark) grants 12-1633 and 12-1634.

This thesis is dedicated to my family for their unconditional support, encouragement, and love.

TABLE OF CONTENTS

CONTRIBUTIONS OF AUTHORS

Chapter 2 is a published manuscript, **Increased oxygen consumption in human visual cortex: Response to visual stimulation**, by M.S. Vafaee, S. Marrett, E. Meyer, A.C. Evans, A. Gjedde, *Acta Neurol Scand, 98:85-89, 1998.* The original source code for the creation of visual stimulus was provided by S. Marrett. and E. Meyer contributed to the design of the study. I performed all of the experiments and data analysis. E. Meyer, A.C. Evans, and A. Gjedde assisted me in writing the manuscript.

Chapter 3 is based on the manuscript, **Frequency-dependent changes in cerebral metabolic rate of oxygen during activation of human visual cortex**, by M.S. Vafaee, E. Meyer, S. Marrett, T. Paus, A.C. Evans, A. Gjedde, *J Cereb Blood Flow Metab 19:3:272-277. 1999.* E. Meyer assisted me with the design of the study. S. Marrett provided the source code for creation of the stimulus. I performed all of the experiments and data analysis and T. Paus helped me with the latter. E. Meyer, T. Paus, A.C. Evans, and A. Gjedde contributed to the writing of the manuscript.

Chapter 4 is based on the manuscript, (submitted to the J Cereb Blood Flow Metab) **Increased oxygen consumption in visual cortex consistent with model of oxygen delivery**, by M.S. Vafaee, A. Gjedde. I designed the study based on the model of oxygen delivery proposed by A. Gjedde. I performed the experiments, and analyzed the data. A. Gjedde helped me to interpret the data

and assisted me in writing the manuscript.

Chapter 5 is based on the manuscript (to be submitted to the Annals of Neurology), **Cerebral metabolic rate of oxygen ($CMRO_2$) and cerebral blood flow (CBF) in mitochondrial encephalomyopathy: A PET study**, by M.S. Vafaee, E. Meyer, A.C. Evans, A. Gjedde. I performed the experiments, analyzed the data and wrote the manuscript. E. Meyer, A.C. Evans, and A. Gjedde contributed to the writing of the manuscript.

OUTLINE AND SCOPE OF THESIS

This thesis is the compilation of a general introductory chapter plus four manuscripts that have been either published (chapters 2 and 3) or have been submitted (chapter 4) or are in the process of submission (chapter 5).

The work carried out for the preparation of this thesis, including literature review, experimentation, presentation and application of the results, is summarized here following the structure outlined below.

Chapter 1 (introduction) is devoted to a comprehensive overview of biochemical and physiological mechanisms underlying energy production in the body and diseases associated with defects of energy production. I shall also briefly touch upon the physiology of the visual system (and specifically color vision) since this project focused mainly on energetics of the visual cortex. In addition, the physics of PET is reviewed. A treatment of the theory and methods of kinetic modeling which are often used in physiology and biochemistry for PET measurements of dynamic process such as cerebral blood flow completes chapter 1.

In chapter 2, I tested the hypothesis that oxygen metabolism in human visual cortex could be enhanced by a carefully designed and sufficiently complex visual stimulus. The details of the experiment presented in this chapter have been published in *Acta Neurol Scand. 98:85-89. 1998* .

In chapter 3, I present the first evaluation with PET of the response of oxygen consumption in the visual cortex as a function of the frequency of a visual

stimulus capable of enhancing oxygen metabolism, as described in chapter 2. The results of the experiment presented in chapter 3 have been published as a full-length manuscript in the *J Cereb Blood Flow Metab, 19:3:272-277, 1999.*

In chapter 4. I examined further the behavior of blood flow and oxygen metabolism in response to the frequency of visual stimulus described in chapter 2. I verified the hypothesis that an oxidative index (oxygen consumption / blood flow) shall vary in a predicted manner by theory. The results have been submitted as a full-length manuscript to the *J Cereb Blood Flow Metab.*

Chapter 5 is devoted to the comparison of the results of our previous experiments (in normal subjects) with results obtained in patients suffering from a disease of oxidative metabolism. The contents of this chapter are as a manuscript to be submitted to the *Annals of Neurology.*

Finally, in chapter 6. I critically discuss the results of four series of experiments performed during the course of this dissertation project, both with patients and normals. Based on the results obtained from the normal subjects using the same methodology, I also propose a general conclusion regarding the issue of the coupling or uncoupling between blood flow and oxygen metabolism. Moreover, I suggest more investigations to be performed to shed more light on this important issue.

CHAPTER 1

GENERAL INTRODUCTION

A. The process of energy production

1.1 Energy metabolism

Metabolism, in its broadest sense, refers to the sum of chemical reactions carried out in an organism. Within this great scheme, the chemical structure of a compound formed within or entering the organism may undergo a series of rearrangements, additions, and deletions in successive reactions catalyzed by enzymes of the metabolic pathway. The energy requirements of the humans vary markedly with age, sex, and physical activity level. A healthy adult maintaining constant body weight takes in and expends about 2500 kcal per day (Clarke and Sokoloff, 1994). This energy is used in muscular contraction, for transport of substrates and ions across cell membranes, for synthesis of expendible substances such as hormones and digestive enzymes, for repair and replacement of damaged tissues. If the net energy intake exceeds the body's energy expenditure, the excess can be stored in the form of fat and glycogen. Carbohydrates, lipids, and proteins are metabolized for energy in varying proportions, depending on diet and physical activity level. Much of the energy used by the body is derived from oxidation of glucose to carbon dioxide and water. If a mol of glucose (180 g) were burned, its complete oxidation would yield 686 kcal of thermal energy.

In living cells, glucose is not oxidized into carbon dioxide and water instantly,

but in a series of biochemical reactions involving numerous intermediate compounds. This process releases the energy of oxidation in manageable portions, and much of the theoretical yield of 686 kcal/mol is captured in "high-energy" phosphorylated nucleotides. The four common high-energy nucleotide tri-phosphates are guanosine triphosphate (GTP), cytosine triphosphate (CTP), uraciltriphosphate (UTP), and adenosine triphosphate (ATP). Of these the most important is ATP while the others are specifically required in some reactions but are interconvertible with ATP (Clarke and Sokoloff, 1994). Hydrolysis of the bond holding terminal phosphate group of ATP yields adenosine diphosphate (ADP) and inorganic phosphate ($H_2PO_4^-$) with a free energy change of about 7.3 kcal/mole. This free energy is used for endothermic reactions catalyzed by specific ATP-dependent enzymes.

1.2 Aerobic and anaerobic metabolisms

There are two basic mechanisms for the generation of ATP. The first is referred to as substrate-level phosphorylation in which a phosphorate group is transferred to ADP from a phosphorylated metabolic intermediate. Substrate-level phosphorylation takes place in the cytoplasm and is the only mechanism by which ATP can be generated in the absence of oxygen.

The second means of ATP production, oxidative phosphorylation, occurs in the inner mitochondrial membranes, requires oxygen, and produces most of the

ATP used by aerobic organisms (some bacteria do not need O_2). Oxidative phosphorylation and the reaction sequence that serves it are referred to collectively as oxidative or "aerobic metabolism". However, one step in the pathway of oxidative metabolism also involves substrate-level phosphorylation . The latter is less economical than aerobic metabolism because the end product, lactate, still has a high energy content (aerobic metabolism yields 15 times more energy than anaerobic metabolism).

1.3 Electron carriers: NADH and $FADH_2$

The process of exchanging electrons between two molecules is an oxidation-reduction reaction in which the donor molecule is oxidized while the recipient molecule is reduced. Most of the potential energy in glucose is first captured by oxidation-reduction reactions. A key element in such reactions is the participation of co-enzymes. The most important electron-carrying co-enzymes are nicotinamide adenine dinucleotide and flavine adenine dinucleotide. The oxidized forms of these co-enzymes are abbreviated NAD^+ and FAD, respectively, the reduced forms are NADH and $FADH_2$ (Ahmed and claiborne, 1989).

The electron-carrying co-enzymes are present in living cells in only very small concentrations. At some steps in the pathway of energy metabolism, the oxidized coenzymes are converted to NADH and $FADH_2$. If there were no means to regenerate NAD^+ and FAD, all of the oxidized co-enzymes would quickly be converted

to the reduced forms, and the reaction steps requiring the oxidized forms would stop. Under aerobic conditions an effective solution to the problem of regenerating oxidized coenzymes is to couple their regeneration to reduction of oxygen to O_2^-, a multistep process called "terminal oxidative metabolism". The overall reactions are:

$$NADH + H^+ + 1/2\ O_2 \rightarrow NAD^+ + H_2O$$

$$FADH_2 + 1/2\ O_2 \rightarrow FAD + H_2O$$

In each of those reactions, two electrons are transferred to atomic oxygen (1/2 O_2), resulting in O_2^- . Each O_2^- immediately reacts with two H^+ to form H_2O. The advantage of this reaction is that some of the free energy of reduced co-enzyme can be used to phosphorylate ADP (oxidative phosphorylation). Also, the end product of the process is metabolic water, which is more easily disposed of by cells than lactate.

1.4 Glycolysis

The first step in the energy metabolism of glucose is glycolysis (Fig. 1.1). All of the reactions of the glycolytic pathway, except for the last, are indifferent to the presence or absence of oxygen. Anaerobic glycolysis occurs in the absence of oxygen or in simple organisms that lack mitochondria, and yields lactate as its end product. In aerobic glycolysis, the glycolytic pathway is the first step in complete oxidation of glucose, and the pyruvate produced (in the next-to-last step)

is not converted to lactate but enters a second pathway of intermediary oxidative metabolism, that ultimately completes its oxidation to CO_2 and H_2O (Fig. 1.2A).

In the first step of glycolysis, catalyzed by hexokinase, glucose is converted to glucose-6-phosphate, a reaction fueled by ATP. This step is rate controlling because hexokinase is saturated and the reaction is endothermic. The second reaction of glycolysis is the isomerase-driven conversion of glucose-6-phosphate to fructose-6-phosphate. In the next several steps in glycolysis, the 6-carbon ring of glucose is broken into two 3-carbon fragments, yielding two molecules of glyceraldehyde-3-phosphate, and ultimately two molecules of pyruvate. Conversion of two glyceraldehyde-3-phosphate molecules to two pyruvate molecules generates four ATP molecules by substrate level phosphorylation, two molecules of NADH, and 56 kcal/mol of heat. Since two ATP molecules were used in the initial steps of glycolysis, the net yield is two ATPs per glucose molecule. Conversion of one molecule of glucose to two molecules of pyruvate results in production of two molecules of NADH which must be reoxidized if glycolysis is to continue. In the aerobic organisms, the pyruvate enters the pathway of intermediate oxidative metabolism, and the NADH is reoxidized by the terminal oxidative metabolism, resulting in a substantial additional phosphorylation of ADP. If a cell does not have the enzymes of the oxidative pathway, or if oxygen is not available, NAD^+ is generated by converting pyruvate to lactate, with no energy gained from production of NADH (Fig. 1.2B).

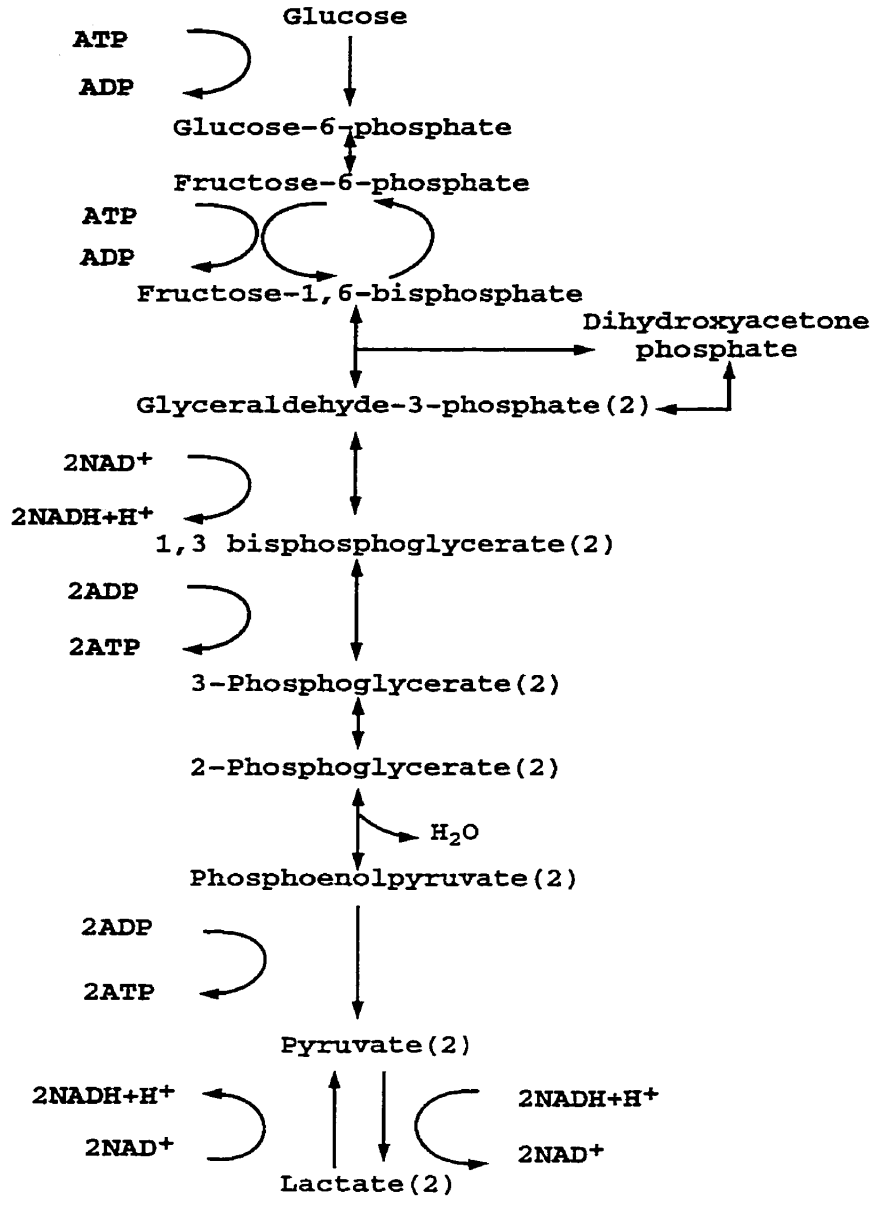

Figure 1.1 The reactions of glycolysis. The initial reactions involve the phosphorylation of glucose and consumption of ATP. Later reactions produce ATP with a net gain of two ATP molecules per molecule of glucose consumed. The end product of glycolysis is pyruvate.

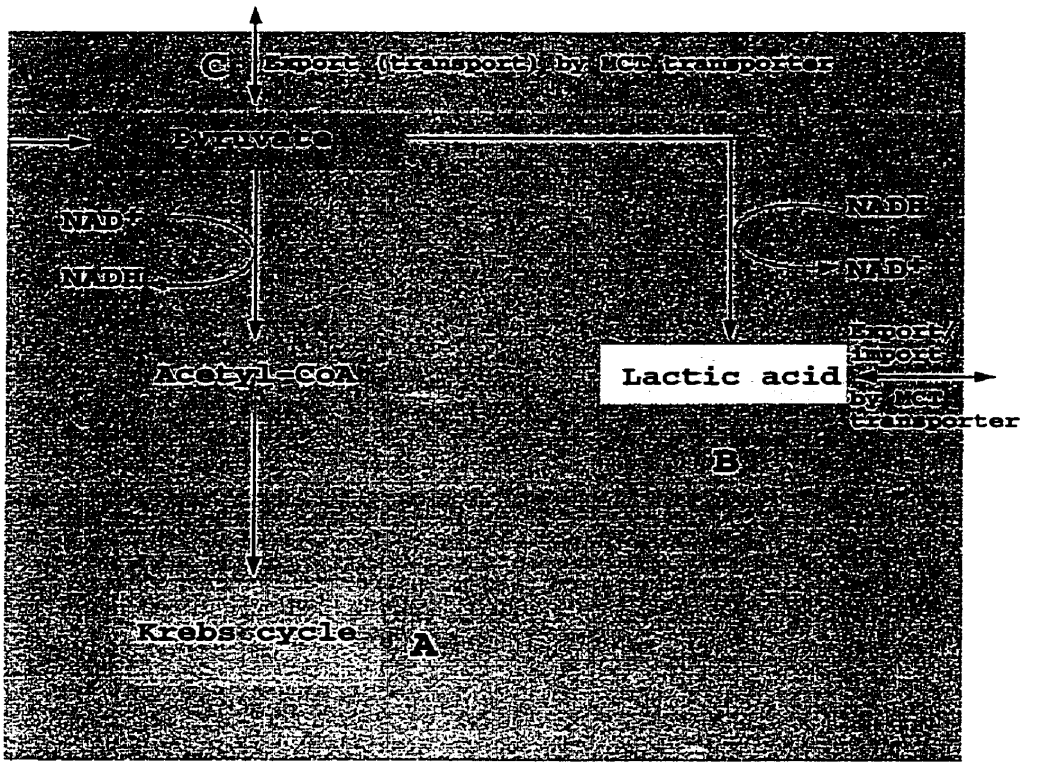

Figure 1.2 Alternative fates of pyruvate. Pyruvate can enter the Krebs cycle via acetyl-CoA (A) or be converted to lactic acid to regenerate NAD^+ (B), or leave the cell by export (C).

1.5 Intermediary oxidative metabolism: The Krebs cycle

After transport into the mitochondria, pyruvate produced into the pathway in aerobic glycolysis is prepared for entry into the pathway of intermediary oxidative metabolism by decarboxylation. This complex reaction that releases CO_2, is coupled to reduction of NAD^+ to NADH, and requires the participation of coenzyme A (CoA). The active site of coenzyme A is a sulfhydryl (-SH) group, so the free form of CoA is CoASH. When CO_2 is removed from pyruvate, the two remaining carbon molecules are substituted for the H of the sulfhydryl group of CoASH, forming acetyl-CoA which is the carrier of acetyl groups in several important steps of energy metabolism.

The Krebs cycle (Fig. 1.3) named after its discoverer Krebs, is a closed sequence of eight reactions that occurs in the interior (matrix) of mitochondria. In the first step of the cycle, an acetyl-CoA combines with a molecule of oxaloacetate (a 4-carbon carboxylic acid) to form citrate (a 6-carbon acid). In subsquent steps, the 6-carbon backbone is decarboxylated twice, releasing two molecules of carbon dioxide; four pairs of electrons are transferred to electron-carrier coenzyme (3 to NAD^+ and 1 to FAD); and one ATP molecule is formed by substrate phosphorylation. Since each glucose entering the glycolytic pathway forms two molecules of pyruvate, the cycle makes two turns for each glucose metabolized.

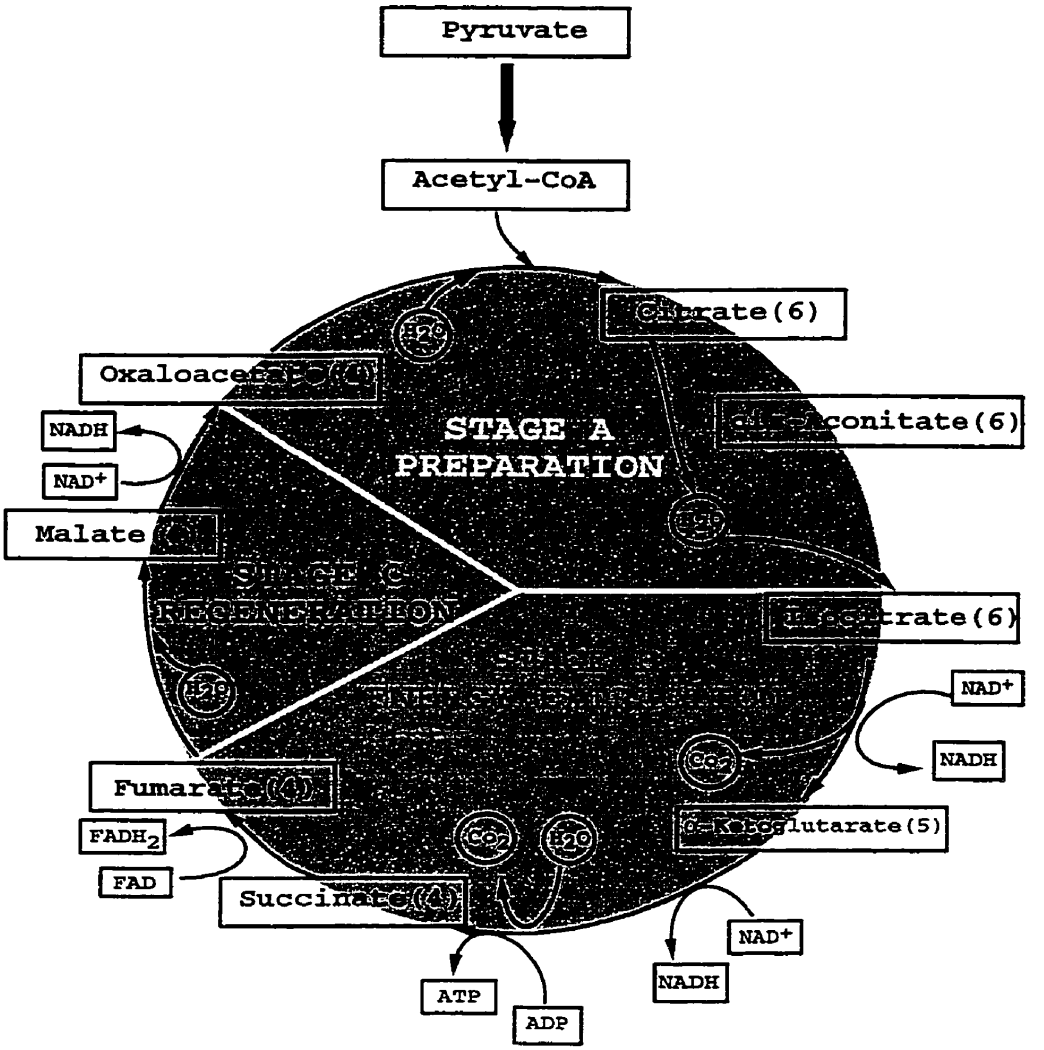

Figure 1.3 In the Krebs cycle, pyruvate, amino acids, and fatty acids transfer 2-carbon segments to coenzyme A to form acetyl-CoA. At the end of the cycle, energy is captured in the form of NADH and $FADH_2$.

1.6 Mitochondrial respiratory chain and oxidative phosphorylation (OXPHOS)

At the point of pyruvate decarboxylation and at four points along the Krebs cycle, electrons are transferred to NAD^+ or FAD. These electrons are subsequently passed to oxygen in the reactions of terminal oxidative metabolism. These reactions are carried out by the electron transport chain (respiratory chain), a series of enzyme complexes in the inner mitochondrial membrane which is relatively impermeable to ions (Fig. 1.4). The inner compartment of the mitochondrion, enclosed by the inner membrane, is the matrix in which Krebs cycle takes place. NADH and $FADH_2$ generated from the Krebs cycle act as electron donors to the series of transport enzymes of the inner mitochondrial membrane. Concomitantly, ejection of protons across the inner mitochondrial membrane results in an electrochemical proton gradient, which stores potential energy. Thus, oxidative phosphorylation is the process by which the transfer of reducing equivalents (electrons) to oxygen is coupled to the synthesis of ATP (Beal et al., 1993).

The electron transport chain consists of a complex of enzymes (Wallace, 1992). Complex I (NADH dehydrogenase), the main point of entry to the electron transport chain, is composed of 26 subunits, seven of which are encoded by mitochondrial DNA. Complex II (succinate dehydrogenase), another entrance to the electron transport chain, consists of five subunits that are encoded by nuclear DNA. Complex III (ubiquinol-cytochrome-c-reductose) has 11 subunits, with one sub-

unit (cytochrome-b) encoded by mitochondrial DNA. Complex IV (cytochrome-c-oxidase) is composed of 13 units, with three encoded by mitochondrial DNA, and complex V (ATP synthase) is composed of 12 subunits, with two subunits encoded in the mitochondrial genome. The mitochondrial DNA and certain peculiarities of the synthesis of mitochondrial proteins has led to the proposition that mitochondria are evolutionarilly derived from an ancient infection of an anaerobic organism by a smaller aerobic organism.

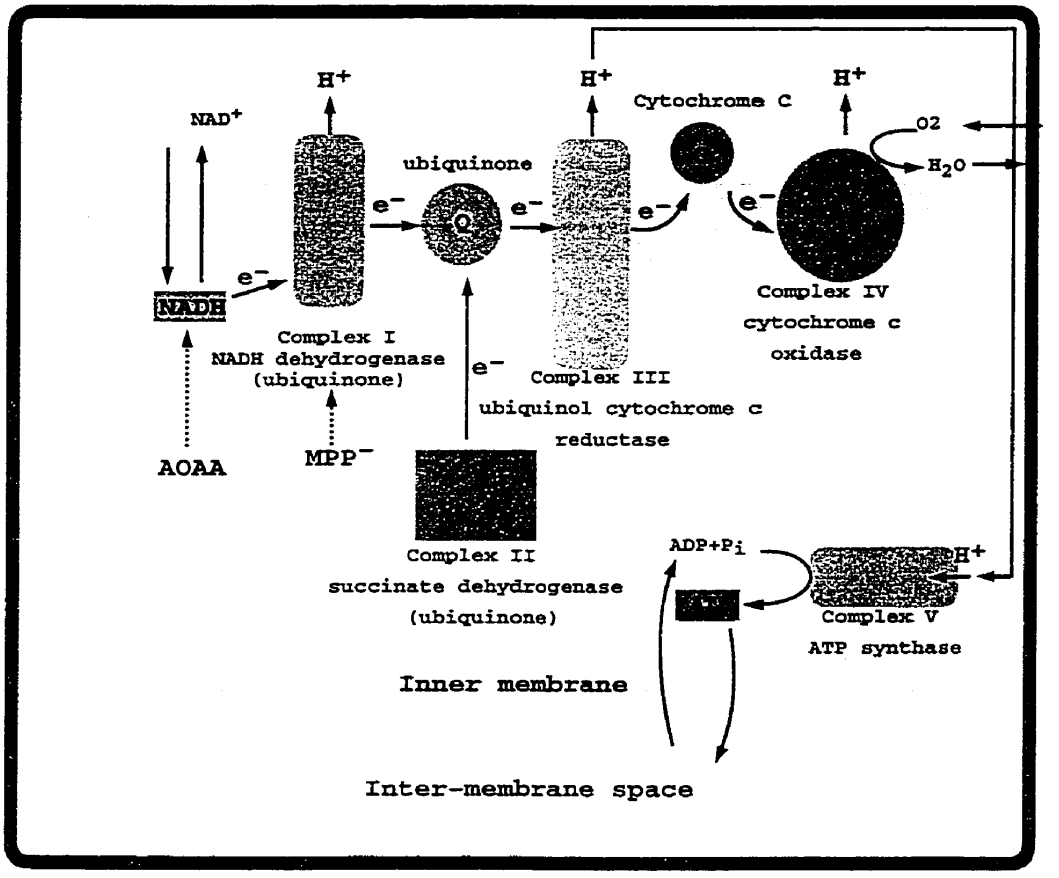

Figure 1.4 The complexes of the electron transport chain are located in the inner mitochondrial membrane. Electrons from NADH enter the chain through the complex I; those from $FADH_2$ are accepted by coenzyme Q. At three of the complexes, the energy released in transfer of electrons through the complex drives pumping of H^+ across the inner mitochondrial membrane. The last carrier in the chain, cytochrome c oxidase, transfers electrons up to molecular oxygen, reducing it to water. The hydrogen ions drive the phosphorylation of ADP tp ATP by the f-type ATPase.

1.7 Oxidation-phosphorylation coupling

Although some of the energy can be quickly obtained from glucose or glycogen, through anaerobic glycolysis, most of the energy derives from the oxidation of carbohydrates and fatty acids in the mitochondria. The common metabolic precursor of sugars and fats is acetyl CoA, which enters Krebs cycle. Oxidation of one molecule of acetyl CoA results in the reduction of three molecules of NAD and one of FAD. These so-called reducing equivalents pass through a chain of carriers in a series of coupled oxidation-reduction events. At three steps along this chain, the free energy released is used by proton pumps to create an electrochemichal gradient for protons across the inner mitochondrial membrane. The released energy charges the inner mitochondrial membrane, converting the mitochondrion into a veritable biological battery. The final hydrogen acceptor is molecular oxygen, and the product is water. This oxidation process is coupled to ATP synthesis from ADP and inorganic phosphate (P_i) and catalyzed by the mitochondrial f-type ATPase.

The vast majority of mitochondrial proteins are encoded in nuclear DNA. Disruption of the electron transport chain could therefore occur by mutation in either mitochondrial of nuclear DNA.

1.8 Structure of the mitochondrial genome

Mitochondria have their own genetic material in the form of small, double-

stranded, circular DNA molecules (mtDNA). The human mitochondrial genome has been sequenced completely (Anderson et al., 1981) and contains 16569 bases. Mammalian mtDNA codes for two ribosomal RNAs (rRNA), 22 transfer RNAs (tRNA), and 13 proteins. The absence of introns (noncoding DNA sequences) contrast sharply with nuclear-encoded genes. As mitochondrial genes are derived entirely from the oocyte, their inheritance is maternal (Giles et al., 1980). Thus, diseases caused by primary mtDNA mutation are transmitted in the maternal lineage. There are several thousand copies of mtDNA in most cells.

1.9 Diseases of mitochondrial metabolism

Two major classification of mitochondrial diseases have been proposed (DiMauro, 1992). One is based on genetics and the other on biochemistry.

1.9.1 Genetic classification of mitochondrial diseases

The genetic classification scheme divides mitochondrial diseases into three groups as follows:

1) Defects of mtDNA which include point mutation and deletion or duplications

2) Defects of nuclear DNA (nDNA)

3) Defects of communication between nDNA and mtDNA

1.9.1.1 Defects of mtDNA which include point mutation and deletion or duplications

Point mutation:

a. Mitochondrial encephalomyopathy with ragged red fibers (MERRF)

The clinical features of MERRF include myoclonic jerks of limb, generalized convulsive seizures, cerebellar ataxia of upper and lower extremities, hearing impairment, optic atrophy, retinopathy, and myopathy (Fukuhara et al., 1980; Wallace et al., 1988). Although most symptoms are progressive, the relative frequency and severity of those manifestations are quite variable, even within the same family. Although it is generally believed that the onset of symptoms occurs during the second part of the first decade of life, onset has also been reported as late as the fourth decade (Karpati and Shoubridge, 1993). Laboratory tests can confirm the diagnosis. The most characteristic abnormality is the presence of an A-to-G point muation in mtDNA at nucleotide position 8344 of the lysine tRNA gene ($tRNA^{lys}$) (Shoffner et al., 1990). Skeletal muscle biopsies and leukocytes are both suitable for showing the mutation which seems to be present in the great majority of cases in which there is clinical evidence of maternal transmission.

The progressive clinical course of MERRF is not explained fully. Since there is no evidence for an age-related relative increase of mutant mtDNA copies at the expense of wild-types, this mechanism is unlikely to explain the progressive course. On the other hand, there is an age-related overall decline of OXPHOS

even in normal people, and this, coupled with reduced OXPHOS due to the mutation, could reduce OXPHOS below tissue-specific thresholds with advancing age (Wallace, 1992).

b. Mitochondrial encephalomyopathy, lactic acidosis, and stroke-like episodes (MELAS)

The most characteristic feature of the clinical phenotype of MELAS consists of attacks of severe headache and vomiting with or without convulsions (Montagna et al, 1988). Brain imaging by computerized tomography or magnetic resonance reveals cerebral lesions, low-density white matter lesions, focal cortical atrophy, and calcifications in the basal ganglian. The brain pathology is consistent with ischemic necrosis without blood vessel occlusions (Pavlakis et al., 1984).

In 85% to 90% of all case the predominant mtDNA mutation observed is a point mutation (A for G substitution at nucleotide 3243 of mtDNA) in the gene coding for the leucine tRNA ($tRNA^{leu}$) (Goto et al., 1990). There is a wide range of heteroplasmy in both muscle and leukocytes, with a convincingly direct connection between a higher mutant/wild-type ratio and the severity of the phenotype (Montagna et al., 1988). Biochemical studies revealed that this mutation results in a severe reduction of the activities of complexes I and IV of the electron transport chain (Montagna et al., 1988).

c. Leber's hereditary optic neuropathy (LHON)

In its typical form, symptoms and signs of LHON are restricted to the optic

nerve and consist of sudden and severe severe visual failure with central scotomata and, often, swelling of the optic nerve heads (Karpati and Shoubridge, 1993). In patients with a family history of the disease, it is transmitted maternally. Another clinical feature of LHON is the relatively late onset of visual failure (average 27.6 years). This late onset might be explained by the age-related natural decline of OXPHOS activity (Karpati and Shoubridge, 1993).

The first mtDNA abnormality demonstrated in about 50% of LHON cases was a base substitution (G for A at nucleotide position 11778), substituting an arginine for histidine at amino acid 340 in the ND4 subunit of complex I (Wallace et al., 1988). When hemoplasmic (uniformly mutant type), the mutation produces blindness; in heteroplasmic (mixture of mutant and wild types) cases (14%), there are no visual symptoms (Wallace, 1992). Three additional missense point mutations have been reported in LHON at nucleotide positions 3460 and 4160, affecting the ND1 subunit of complex I, and at nucleotide position 15257, affecting cytochrome b (Huoponen et al., 1991; Brown et al., 1992; Howell et al., 1991).

Deletions:

a. Kearns-Sayer syndrome (KSS)

The evidence for a primary role of mitochondria in Kearns-Sayer syndrome was obtained recently by demonstration of major deletions in the mtDNA (Holt et al., 1988; Moraes et al., 1989).

The core of the clinical syndrome is a progressive, asymmetrical, nonfluctuating paresis of multiple extraocular muscles bilaterally. In addition, eyelid ptosis, a peculiar form of pigmentary degeneration of the retina, and heart block (Karpati and Shoubridge, 1993). Other common features are myopathy, stunted growth, cerebellar defecits, and endocrine abnormalities. Onset is during the first or second decade of life. Cerebrospinal fluid protein level almost always is elevated. Muscle biopsy shows numerous ragged red fibers. The disease is progressive and fatal outcome usually is due to cardiac arrest.

The most common mtNDA deletion involves 4977 base pairs and is found about 40% of patients (Schon et al., 1989). About 20% of the patients do not have detectable deletions (Moraes et al., 1991), and two patients with KSS were shown to have an mtDNA duplication (Poulton et al., 1989).

b. Progressive external ophthalmoplegia (PEO)

PEO is a sporadic syndrome with abnormal ocular motility very similar to that described in KSS. The mtDNA defect is indistinguishable from that of KSS however, the relative proportion of mtDNA deletions in nonmuscle tissue usually is extremly low. About 50% of patients with PEO have detectable mtDNA deletions (Moraes et al., 1989). A significant proportion of patients without deletions have been shown to carry the 3243 point mutation that is commonly associated with MELAS (Ciacci et al., 1992).

Pearson's marrow/pancreas syndrome (a relatively rare disease of young chil-

dren) and familial diabetes mellitus are two other examples of mitochondrial disorder caused by deletions.

1.9.1.2 Defects of nuclear DNA

The vast majority of mitochondrial proteins are encoded by nDNA, synthesized in the cytoplasm, and then imported into the mitochondria. Defects of genes encoding the proteins or controlling the importation mechanism will cause mitochondrial disease, which will be transmitted by mendelian inheritance. From a biochemical point of view, all components of mitochondrial metabolism can be affected.

1.9.1.3 Defects of communication between nDNA and mtDNA

The nDNA controls many functions of the mtDNA, including its replication. It is conceivable that mutations of nuclear genes cause alterations in the mtDNA expression. Two human diseases have been attributed to this mechanism (DiMauro, 1992). The first is associated with multiple mtDNA deletions and is characterized clinically by ophthalmoplegia, weakness of limb and repiratory muscles, and early death. It is assumed that a primary mutation in nDNA makes mtDNA prone to develop subsequent deletions. The second disease is associated with mtDNA depletion in one or more tissues, most commonly in muscle. Depending on the tissue affected and the severity of the mtDNA decrease, the clinical picture can be a rapidly fatal congenital myopathy, a slightly more benign myopathy of childhood. It is postulated that an nDNA mutation may impair mtDNA replication.

1.9.2 Biochemical classification of mitochondrial diseases

The biochemical classification is based on the five major steps of mitochondrial metabolism and accordingly divides mitochondrial diseases into five groups as follows:

1. Defects of mitochondrial transport
2. Defects of substrate utilization
3. Defects of the Krebs cycle
4. Defects of oxidation/phosphorylation coupling
5. Defects of the respiratory chain

1.10 Oxidative stress, mitochondrial dysfunction, and neurological disorders

Mutations of mtDNA are associated with a wide spectrum of disorders encompassing the myopathies, encephalopathies, cardiopathies, in addition to organ specific presentations such as diabetes mellitus and deafness. The pathogenesis of mtDNA mutations is not fully understood although it is assumed that their final common pathway involves impaired oxidative phosphorylation mainly caused by a respiratory chain defect. It is puzzling how mitochondrial mutations, which all affect the respiratory chain, produce different phenotypes. Defective oxidative phosphorylation caused by mitochondrial dysfunction, has also been reported to be involved in the pathogenesis of neurodegenerative diseases. There is per-

suasive evidence that oxidative stress is involved in brain damage of patients with Alzheimer's, Parkinson's or Huntington's diseases. Therefore, the study of oxidation-phosphorylation behavior in normals and comparison of such behavior in neurological patients can shed a great deal of light on the pathophysiology of these disorders. It was our intention throughout this project to study this vital physiological factor. To so do. we needed to measure blood flow and oxygen consumption.

Most *in vivo* measurements of cerebral energy metabolism in humans, have been made in the brain as a whole, representing the mass-weighted average of the metabolic activities in all the component structures of the brain. As this average, must obscure transient and local events in individual brain regions, it is not surprising that many studies of altered cerebral function failed to demonstrate corresponding changes in energy metabolism. The [^{14}C]deoxyglucose method of Sokoloff and Kety (1977) made it posssible to measure glucose utilization simultaneously in many structures within the central nervous system. This method was used to identify the regions with altered functional and metabolic activites in a variety of physiological. pharmacological and pathological states in rat brain (Sokoloff, 1977). Originally the method used autoradiography of brain sections for localization. Later developments of positron emission tomography (PET) made it possible to adapt this tracer methodology to human use as well (Hoffman and Phelps, 1986).

B. Visual system

1.11 Information processing and pathways

The visual system is believed to be the most complex of sensory systems and yet the most well-studied. The auditory nerve has about 30,000 fibers, the optic nerve one million, more than all dorsal root fibers entering the entire spinal cord combined (Mason and Kandel, 1991).

Visual perception occurs in two stages. Light entering the cornea is first projected to the back of the eye where it is converted into an electrochemical signal by specialized receptors in the retina. The human retina contains two types of photoreceptors, known as rods and cones. Cones are responsible for day and color vision while rods, which function in dim light, mediate night vision, when most stimuli are too weak to excite the cone system. However, cones perform better than rods in all visual tasks other than the detection of dim stimuli. Cone-mediated vision is of higher acuity than rod-mediated vision, and provides better resolution of rapid changes in the visual image, i.e., better temporal resolution. Cones also mediate color vision. The rod system is more sensitive than the cone system but is achromatic. These differences in performance are due partly to properties of the rods and cones themselves and partly due to the connections these cells make with other neurons in the retina. The retina modifies and processes the signals evoked by light in the photoreceptors and transmits them to higher brain centers via retinal ganglion cells. The axons of ganglion cells, form the optic

nerve, which projects to three subcortical targets; the lateral geniculate nucleus of the thalamus, the pretectal area of midbrain and the superior colliculus (Kandel, 1991). Of the three subcortical regions receiving direct input from retina, only one, the lateral geniculate nucleus, processes visual information eventually resulting in visual conscious perception. The pretectal area of midbrain uses inputs from the retina to produce pupillary reflexes, whereas the superior colliculus, uses its input to generate eye movements.

The majority of retinal axons terminate in the lateral geniculate nucleus, the principal subcortical region that processes visual information for perception. The lateral geniculate nucleus of primates contains six layers of cell bodies separated by intervening layers of axons and dendrites. The layers are numbered from 1 to 6 (ventral to dorsal). The two most ventral layers of nucleus, which contain relatively large cells, are known as the magnocellular layers; their main retinal input is from P_α ganglion cells in the retina also called M cells (after the layers in which they terminate). The four dorsal layers are known as the parvocellular layers and receive input from P_β ganglion cells in the retina, also called P cells. The M cells seem to mediate the initial analysis of movement of the visual image across the retina, whereas the P cells are concerned with the analysis of image structure and color vision.

The first relay point in visual processing where receptive field properties change significantly is the primary visual cortex (Brodmann's area 17) also know as vi-

sual area 1 (abbreviated as V1). It is also called striate cortex because it contains prominent stripes of white matter. The human visual cortex is about 2 mm thick and consists of six layers of cells between the pial surface and underlying white matter (Fig. 1.5). One of these, layer 4, the principal layer of inputs from the lateral geniculate nucleus, is further subdivided into four layers (sublaminae): 4A, 4B, 4Cα, and 4Cβ. M and P cells of lateral geniculate nucleus terminate in different layers and even in different sublaminae (Fig. 1.5). The axons of M cells terminate principally in sublamina 4Cα: the axons of one group of P cells terminate principally in sublamina 4Cβ. Axons from a third group of cells, located in the interlaminar region of the lateral geniculate nucleus, terminate in layer 2 and 3, where they innervate patches of cells called "blobs". The primary visual cortex also contains several types of resident interneurons. Spiny stellate and pyramidal neurons, both of which have spiny dendrites, are excitatory and use glutamate or aspartate as their neurotransmitter. Smooth stellate cells are inhibitory and use GABA as their neurotransmitter. Pyramidal cells project out of the primary visual cortex, whereas both types of stellate cells are local neurons.

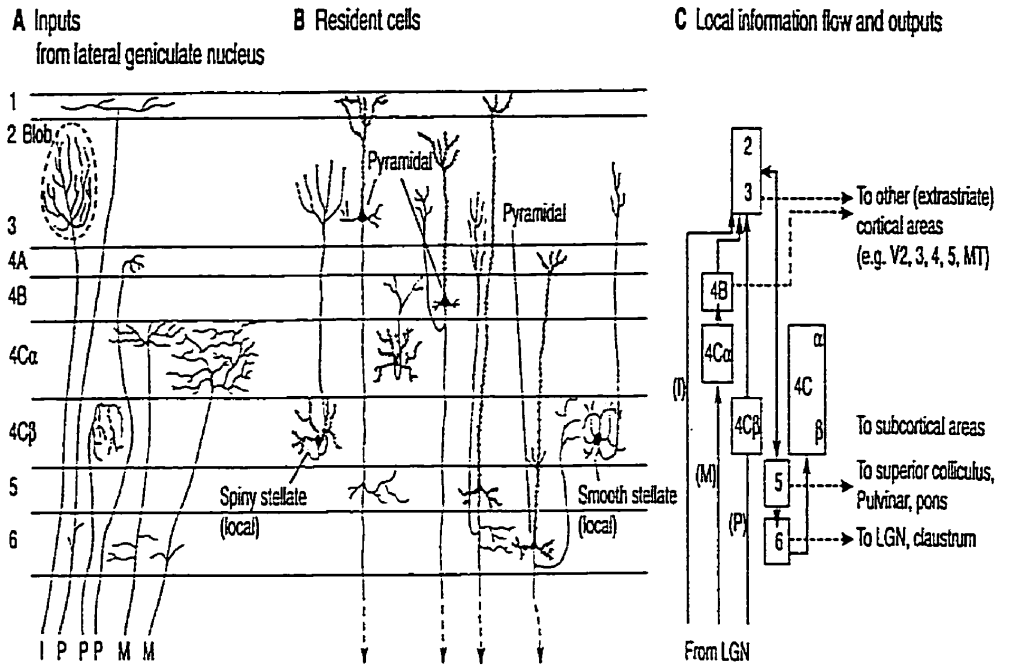

Figure 1.5 The primary visual cortex has six distinct anatomical layers, each with characteristic synaptic connections. **A** Most afferent fibers from the lateral geniculate nucleus terminate in layer 4. Axons of type P cells terminate primarily in layer 4Cβ, with monr inputs to 4A and 1, while axons from type M cells terminate primarily in layer 4Cα. Collaterals of both types of cells also terminate in layer 6. Cells of the intralaminar regions of the lateral geniculate nucleus terminate in layers 2 and 3. **B** Pyramidal and spiny stellate and smooth stellate cells (resident neurons) make up the primary visual cortex. Pyramidal cells project out of the cortex, whereas both types of stellate cells are local neurons. **C** Information flow and output from primary visual cortex. (Adapted from Lund, 1988).

Like the somatosensory cortex, the primary visual cortex is organized into narrow columns, each measuring about 30-100 μm wide and 2 mm deep. The anatomical layout of the orientation columns has been demonstrated in electrophysiological experiments using several methods, including those employing spectral changes in voltage-sensitive dye. The systematic shifts in axis of orientation relative to the visual field from one column to another is occasionally interrupted by "blobs", which are peg-shaped regions of cells in layers 2 and 3 of V1 and rich in oxidative enzyme, cytochrome-oxidase (Wong-Riley, 1984; Horton, 1984; Livingstone and Hubel, 1984a and 1984b) (Fig 1.6). These blobs are separated by intervening regions that stain lighter for cytochrome oxidase, called "interblob" regions (Fig. 1.7). These cells within blobs receive direct connections from the lateral geniculate nucleus and are sensitive to color and not to orientation. In addition to columns devoted to axis of orientation and blobs related to color, a third alternating system of columns is devoted to the left or right eye. Theses ocular dominance columns are important for binocular interaction (Hubel and Wiesel, 1972).

Beyond the striate cortex (V1) lies V2 and the other visual representations in the extrastriate cortex. Tootell (1985) discovered cytochrome-rich patches in V2, instead of blobs, the darkly stained cytochrome-rich patches in V2 take the form of alternating thick and thin stripes separated by pale interstripes.

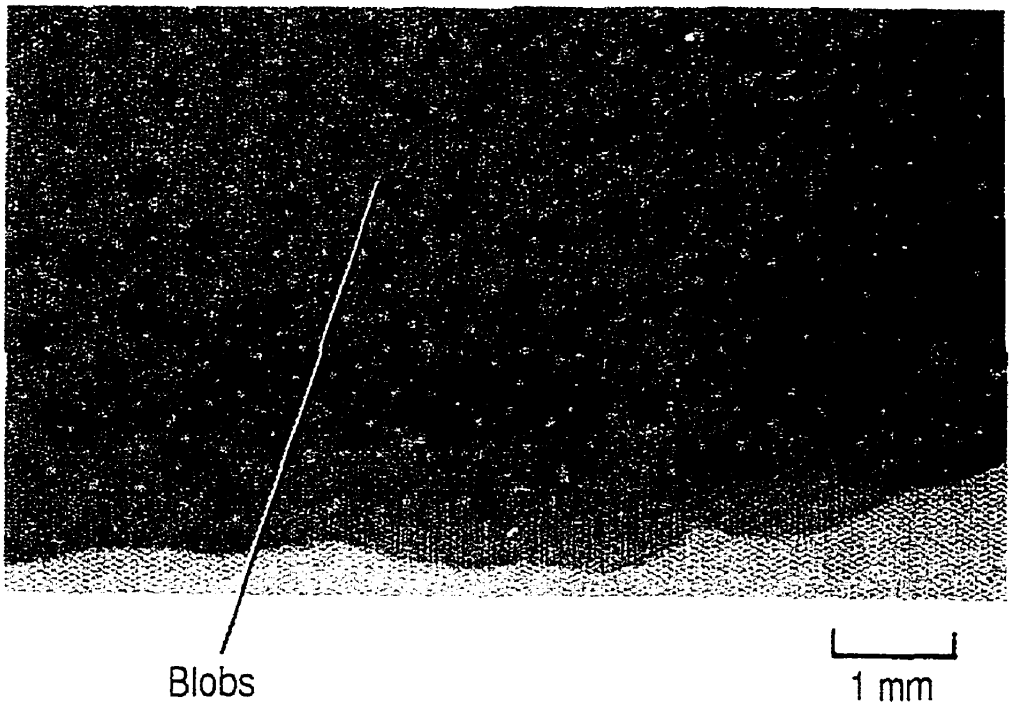

Figure 1.6 The distribution of the mitochondrial enzyme cytochrome oxidase in the superficial layers of the visual cortex, as seen in tangential sections of area 17 of the macaque monkey. The rows of dark patches or *blobs* represent areas of heightened enzymatic activity. This is thought to represent heightened neuronal activty in the *blobs* because of lower response selectivity of these cells. (Courtesy of DY. Ts'o, CD. Gilbert, and TN. Wiesel)

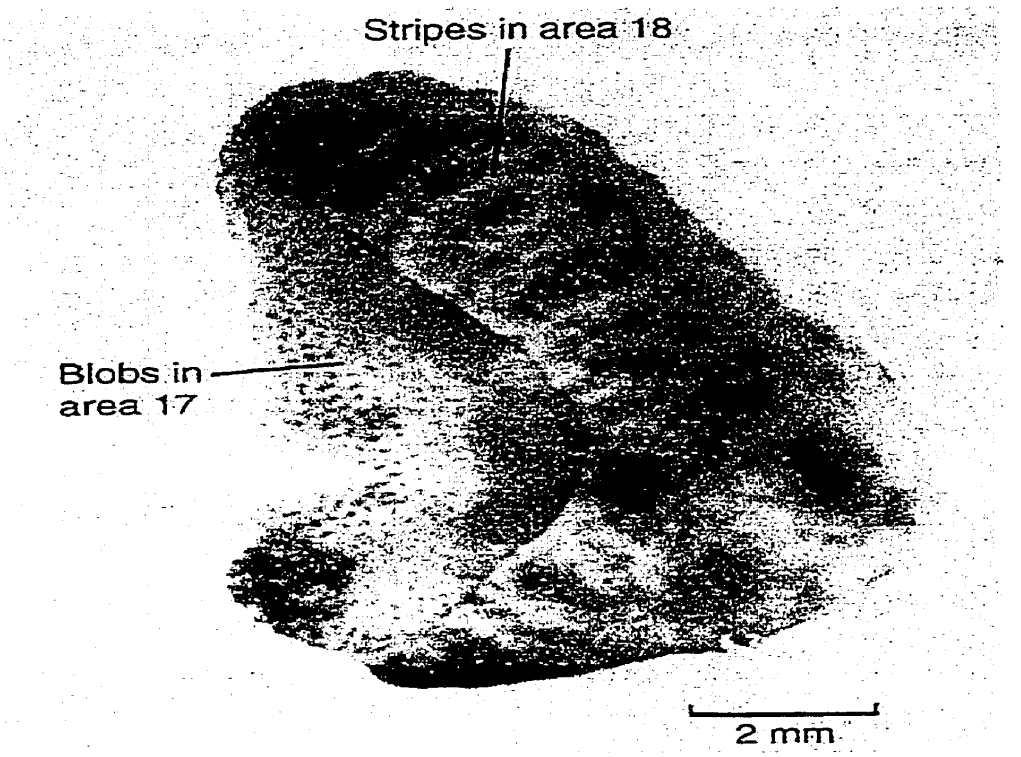

Figure 1.7 Section from the occipital lobe of a squirrel monkey at the border of areas 17 and 18 reacted with cytochrome oxidase. The cytochrome oxidase stains the *blobs* in area 17 and it stains the *stripes* (both thick and thin) in area 18. (Courtesy of M. Livingstone)

Hubel and Wiesel found that most neurons above and below layer 4 respond only to stimuli that are substantially more complex than those that excite cells in the retina and lateral geniculate nucleus (Hubel and Wiesel, 1959, 1962). They also found that small spots of light which are effective stimuli in the retina, lateral geniculate nucleus, and in the input layers of cortex 4C, are completely ineffective in layers of the visual cortex other than the blob regions. Neurons in all regions, except the blobs, do not have circular receptive fields. They respond only to stimuli having linear properties, such as a line or bar. Hubel and Wiesel categorized the cells (in what we know now to be the regions outside the blobs) into two major groups, known as simple and complex cells based on their specific responses to linear stimuli.

The organization of the output connections from the primary visual cortex is similar to that of somatosensory cortex. There is output from all layers except 4C, and in each layer the principal output neurons are the pyramidal cells. The neurons in layer 2 and 3 make associational connections; they project to other higher visual cortical regions, such as Brodmann's area 18 (V2, V3) and 19 (V4). Neurons in layer 4B project to the medial temporal lobe (V5 or MT). Neurons in layer 5 project to superior colliculus, the pons, and the pulvinar nucleus of the thalamus. Neurons in layer 6 project back to the lateral geniculate nucleus and claustrum (a grey band inserted between the putamen and insular cortex). Both pulvinar and claustrum are thought to be important for visual attention.

1.12 Color vision

The human eye is sensitive to wavelengths of light from 400 to 700 nanometers. Throughout this range, the sensitivity to the color of monochromatic light changes gradually from blue, through green, to red. People with normal color vision can readily match the color of any spectral composition of light by combining in an appropriate way three primary colors: red, green, and blue. This property of color vision, called trivariancy, results from three types of light-absorbing cone photoreceptors, each with a different visual pigment (Gouras, 1991). The theory of trivariant vision attributes color perception to the activity of three primary cone classes in the retina. This theory explains a large variety of data on color perception. For example, the combination of green and red is seen as yellow, and combination of all three is perceived as white. However, trivariancy alone fails to explain some important aspects of color perception.

The first is that certain colors cancel one another in such a way that they are never perceived in combination. For example, we cannot perceive reddish green or bluish yellow colors, even though we can readily see reddish blue (magenta), reddish yellow (orange), greenish yellow, or bluish green (cyan). Red and green lights can be mixed so that all traces of the original redness or greenness are lost.

This perceptual cancellation of colors led Ewald Hering to propose the "opponent process" theory (1964). According to this theory, the three primary colors have mutually antagonistic (or opponent) pairs: red-green, yellow-blue, and white-

black. Hering postulated that these three color pairs are organized in the retina in three "color-opponent" neuronal channels. Accordingly, one channel responds in one direction (excitation or inhibition) to red and in the opposite direction to green. When properly balanced with the precise mixture of red and green, this channel produces no net output. The second channel opposes the sensations of yellow and blue, a third opposes white and black. The outputs from these cone mechanisms are combined in opponent fashion, starting in the retina and lateral geniculate nucleus, and then in the cortex, in a way that can explain color opponency (Gouras, 1991).

The color opponent theory explains why certain colors originating from the same point in visual space cancel one another. It does not, however, explain the phenomenon of "simultaneous color contrast", which occurs across, rather than within the bounderies of a perceived object. For example, a grey object seen in a background of red has a green tinge: in a background of green it has a red tinge. In these situations, cone mechanisms appear to "facilitate" one another, rather than to cancel. The so-called "double-opponent" cells in the visual cortex have properties that can explain, at least in part, simultaneous color contrast.

Retinal ganglion cells and cells in the lateral geniculate nucleus of primates fall into several classes based on the way in which inputs from the three types of cones are combined. Most cells fall into two important classes: the concentric broad-band cells and the color-opponent cells. The broad-band cells respond to

the "brightness" of the center of object (as opposed to the brightness of the surround) and do not contribute to the perception of color.

Information about color is transmitted by color-opponent cells. In most of these cells the antagonism is between the R and G cones, which occurs within an antagonistic center-surround receptive field structure. Thus, the center receives inputs from R or G cones, and the larger antagonistic surround receives input from the other cones. These cells are called single-opponent, to distiguish them from "double-opponent" cells in the visual cortex. The response of single-opponent cells to different stimuli demonstrates that they transmit information about both color and achromatic brightness contrast. The responses of these cells to white or yellow light show the same center-surround antagonism as in broad-band cells because G or R cones absorb white or yellow light to similar degrees. When illuminated with white light they respond preferentially to small spots on either the center of their receptive field, or in the surround. At the same time these cells respond strongly to large spots of monochromatic light of the appropriate wavelength. The R-center/G-surround cells respond best to red, while the G-center/R-surround celss respond best to green light. Thus, these cells do not respond only to chromatic stimuli. It is impossible to know, for example, whether a strong excitatory response from an R-center/G-surround cell is due to a large red spot or a small bright spot of any color applied to the center of its receptive field. The visual cortex has the red-green double-opponent cells that do respond

selectively to chromatic stimuli.

Color information is processed by double-opponent cells in the blob zones

Many retinal ganglion cells fall into two general classes: the large M cells with fast conduction velocities, which project to the magnocellular layers of the lateral geniculate nucleus, and the smaller P cells, which project to the parvocellular layers. The broad-band cells can be either M-type or P-type, while single-opponent cells are exclusively P-type ganglion cells. Thus, the parvocellular layers relay all color information to the cortex in addition to information about achromatic contrast. The parvocellular cells form synapses in the layer 4Cβ; neurons in this layer project to layers 2 and 3 (Fig. 1.8). The color-sensitive cells in these layers are heavily concentrated in "blob" zones. The cells in the blobs are not selective for orientation, while most cells in the large interblob areas are selective for orientation, but are not chromatic. It is thought that the same single-opponent parvocellular cells provide color contrast information to the cells in the blobs, and also provide achromatic brightness contrast information to cells in the interblob regions. Cells in the magnocellular layers projects to layer 4Cα, which in turn projects to layer 4B. All cells in these two layers are sensitive to achromatic contrast and show orientation selectivity. Thus, in the visual cortex, chromatic and achromatic information is segregated into separate channels.

As mentioned before, the parvocellular interblob system appears to process information for the perception of form, the parvocellular-blob system codes for

the perception of color, and the magnocellular system for the perception of movement. These three pathways project to separate interdigitating strips in V2. The magnocellular-interblob pathway then projects to V5, which contains cells sensitive to movement. The parvocellular-blob system projects to V4, the area described by Zeki (1988), in which color sensitive cells are predominant.

In the cortex, inputs from the single-opponent cells are combined to create so-called double-opponent cells, concentrated in the blob zones as stated above. These cells also have an antagonistic center-surround receptive field organization, but the cone organization of receptive field is quite different from that of the single opponent cells. Instead of one type of cone operating in the center and another in the surround, each type operates in all parts of the receptive field, but has different actions in either the center or surround. For example, in some double-opponent cells, R cones excite in the center and inhibit in the surround while G cones do the opposite. They inhibit in the center and excite in the surround. These cells respond best to a red spot in the center against a green background, and they are more selective for chromatic stimuli than the single-opponent cells.

In summary, color information is processed in a specialized pathway in the brain. The segregation of color information from information about form and movement starts in the retina. Information about color is processed by parvocellular-blob system, which projects from the lateral geniculate nucleus by segregate channels to cortical areas V1, V2, and V4.

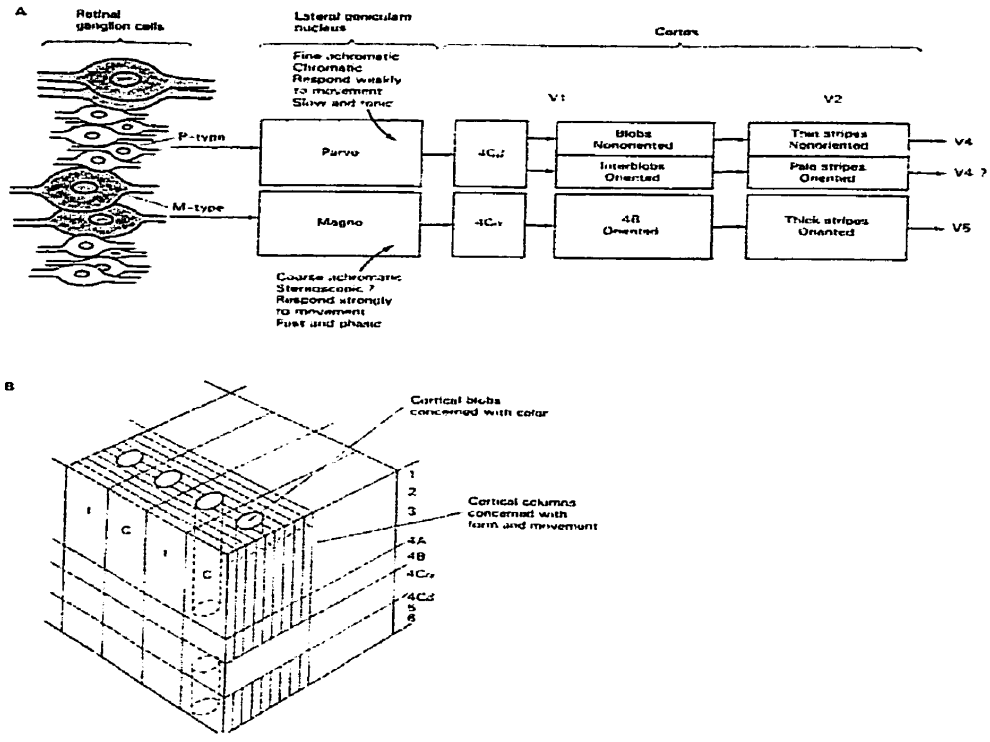

Figure 1.8 Color information is processed in the parvocellular-blob system. (Livingstone and Hubel, 1984a).

A. Different aspects of the visual image are processed by separate pathways in the retina, lateral geniculate nucleus, and cortex.

B. *Blobs* in the primary visual cortex contain double-opponent cells responsive to simultaneous color contrast (color across boundries). The *blobs* are located in both the ipsilateral (I) and contralateral (C) ocular diminance columns and make up a system that is parallel to ocular dominance and orientation columns, whose cells are concerned with edges and contours.

C. Positron emission tomography (PET)

1.13 The Physical Basis of PET

Unstable proton-rich nuclei decay by two processes: (a) by electron capture (EC), where the nucleus captures an orbital electron, or (b) by β^+ decay, where a proton is transformed into a neutron with emission of a positron and a neutrino. The positron is the antiparticle of the electron having the same mass but opposite charge. After travelling a short distance in a dense medium, the positron will combine with an electron and undergo annihilation. Upon annihilation, the masses of the electron-positron pair (equivalent to 2×511 keV) are converted to electromagnetic radiation. In order to conserve both energy and linear momentum, the electromagnetic radiation appears in the form of two 511 keV gamma rays which are emitted under an angle of approximately 180° to each other (since the electron and the positron in general are never entirely at rest at the time of annihilation, there is always a net momentum with the result that the two annihilation photons are emitted at about 179.5° to each other). It is the annihilation radiation that can be detected externally. It is used to measure both the location and the quantity of a positron emitter in a medium.

A PET scanner consists of pairs of photon detectors arranged in a ring and connected to an electronic coincidence circuit which detects nearly coincident (within the coincidence resolving time of 20 nanoseconds) pairs of photon arriving at opposite sides of the ring. When a coincident event is detected, the information

is placed into a sinogram, a two dimensional matrix which retains information on the position and angulation of the coincidence line joining the center of two detectors involved. The external detection and localization of a positron emitter inside an object take advantage not only of the fact that the two annihilation photons are emitted at nearly 180° to each other, but also of the fact that they are created simultaneously. If the annihilation originates outside the volume between the two detectors, only one of the photons can be detected, and since the detection of a single photon does not satisfy the coincidence condition, the event is rejected (Hoffman and Phelps, 1986). Corrections are required for random coincidences, in which a coincident circuit is activated by two unrelated photons that happen to arrive nearly simultaneously; attenuation, the absorption of photons before the detectors are reached; and scatter, the deflection of photons from their initial collinear paths. The sinogram (two-dimensional array of coincidence projections which stores the information about the angles and positions of the coincidence events) is then used for tomographic image reconstruction. A variety of reconstruction algorithms have been used of which the convolution (filtered back-projection) method is the most widely used. Figure 1.9 illustrates the annihilation coincidence detection process.

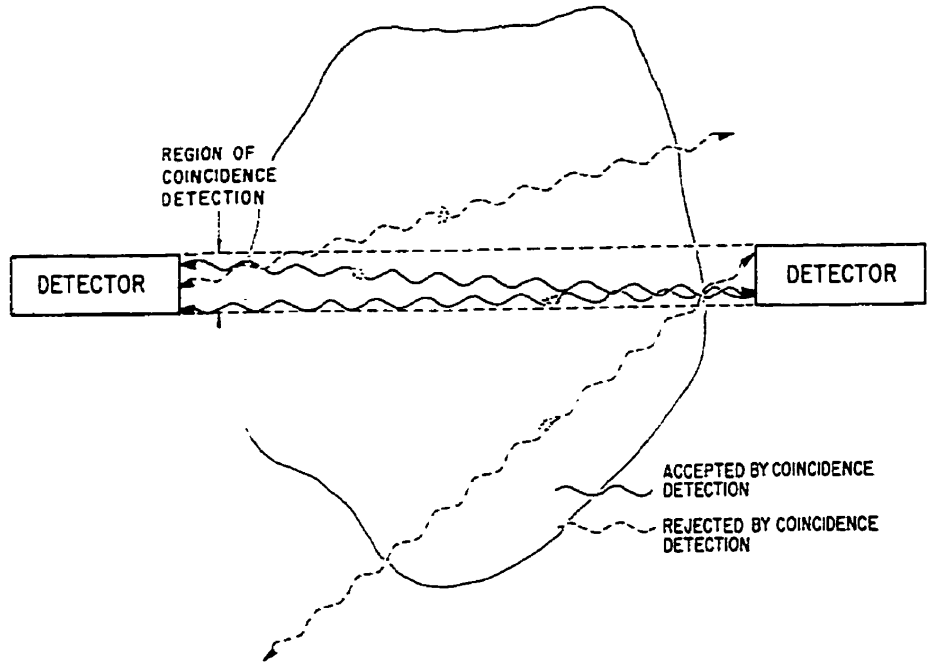

Figure 1.9 Principle of annihilation coincidence detection. Two gamma-rays are produced by annihilation of emitted positron and an electron in the medium. If two gamma-ray detectors are placed on opposite sides of positron emitting object, the detection of two annihilation photons simultaneously, or in coincidence, places the oroginal position of the annihilation in the space between the two detectors. Gamma rays from annihilations occuring outside this sensitive volume can interact with only one of the detectors per annihilation. By electronically selecting only those events seen in coincidence. all other events are rejected and the coincidence events are localized in the region between two detectors. (Courtesy of Hoffman and Phelps, 1986)

1.14 Early PET Studies

The use of positron emitting radioisotopes was first proposed in 1951 for the localization of brain tumors by Wrenn et al. (1951). Shortly afterward, Sweet and Brownell described the first practical non-tomographic positron imaging device in 1955. In 1966, Yamamoto and Robertson (1966) published the first physiological application of positron emission tomography. They used positron emitting ^{79}Kr for the measurement of cerebral blood flow. It became rapidly apparent that PET could be used for the noninvasive in-vivo determination of human biological function due to its ability to provide quantitative information not only of the tissue radioactivity concentration of a given radiotracer ($\mu Ci \cdot ml^{-1}$) but also, through the use of appropriate physiological models, of quantities such as cerebral blood volume (CBV), cerebral blood flow (CBF) as well as cerebral oxygen and glucose metabolic rates ($CMRO_2$; CMR_{glc}) (Phelps et al., 1979; Reivich et al., 1979; Raichle et al., 1983; Meyer, 1990; Ohta et al., 1992).

In practice, PET images visualizing these quantities may be reconstructed from contiguous slices to show transverse, coronal or sagittal views.

1.15 Major Applications of PET

The study of the hemodynamic and metabolic processes of CBF, CBV, $CMRO_2$ and CMR_{glc} represents a major area of cerebral PET research. Models have also been developed for the measurement of regional pH (Brooks et al., 1984; Alpert

et al., 1990) as well as for the study of blood brain barrier function (Gjedde et al., 1985; Gjedde and Kuwabara, 1990) and protein synthesis using labelled amino-acid (Bustany et al., 1985). Recently PET researchers have investigated the concentrations of neuroreceptors and transmitters using labelled radiopharmaceuticals (Mintun et al., 1984; Wagner, 1986). One research application of PET which has become particular fashionable over the past few years is the investigation of cognitive function by means of CBF activation studies (Fox et al., 1985). In such studies, correlation of function and anatomy is achieved by the 3-dimensional correlation of PET (function) and MRI (anatomy) information (Evans et al., 1992).

Although the research potential of PET has always been recognized, an increasing number of clinically useful applications have been identified recently. These include 1) identification of viable but compromised myocardium in patients with advanced ischemic heart disease (Schwaiger and Hicks, 1991) considered for bypass surgery, 2) distinction between recurring tumor tissue and radiation necrosis (Coleman et al., 1990), and 3) identification of seizure foci in epileptic patients (Engel et al., 1990). Other clinical applications might arise from the study of patients with transient ischemic attacks (Frackowiak, 1985) and acute stroke (Frackowiak and Wise, 1983; Powers and Raichle, 1985) using measurements of local cerebral blood flow, blood volume as well as oxygen and glucose metabolic rates. The study of neurotransmitter function in movement disorders (Brooks

and Frackwiak, 1989) (e.g. Huntington's and Parkinson's disease) as well as in mental disorders (Wong et al., 1986; Weiss et al., 1990, Minoshima et al., 1995) (e.g. schizophrenia, Alzheimer's disease) also promise some definite clinical applications. Finally, the presurgical evaluation of patients suffering from a number of cerebral lesions (arteriovenous malformations, tumors, epilepsy) located in so-called eloquent cortical areas (sensory-motor cortex, speech areas etc.) by means of functional CBF activation studies has been explored successfully (Leblanc et al., 1992; Leblanc and Meyer, 1990). It should be noted that a number of PET centers primarily dedicated to clinical applications have already been established.

1.16 Dynamic PET Studies

Functional information such as rCBF may be derived from a single PET image together with the appropriate blood data for calculation of the "input" of radioactivity to the brain (Jones et al., 1976; Frackowiak et al., 1980; Herscovitch et al., 1983; Raichle et al., 1983). A more flexible approach is to acquire a sequence of images (dynamic scan) and to calculate the kinetic parameter(s) defined as a mathematical model by means of a least squares regression, or curve fitting, procedure which produces the best match of the measured tissue time-activity curve with that predicted by the model (Gjedde et al., 1985). However, count rate restrictions together with the limited timing resolution of PET, and the computationally intensive task of serial image reconstruction and pixel-by-pixel curve

fitting all make the generation of functional images by this approach a difficult task. Computational modelling nevertheless has been used to estimate CBF for extended brain regions of interest (Koeppe et al., 1985; Iida et al., 1987; Lammertsma et al., 1989).

A computationally more efficient scheme of parameter estimation from dynamic scans, the so-called integrated projection technique, was proposed by Tsui and Budinger (1978) and implemented by Carson (1986) and Huang (1982, 1983) for the pixel-by-pixel determination of rCBF and partition coefficient p (the equilibrium tissue-blood partition coefficient of the tracer). This method takes advantage of the linearity of the tracer compartment model with regard to blood flow and the image reconstruction algorithm. The plasma and tissue concentration integrals appearing in their operational equations for CBF and p, are calculated on the projection of data rather than on individually reconstructed dynamic images. These modified projection sums are then used to reconstruct the two "integral" images required for the calculation of CBF and p.

With the weighted integration method described by Alpert (1984) and refined by Carson (1986), weighted images are generated by means of weighting functions that may be selected such that the variance of the desired parameter estimate, e.g. rCBF, is minimized. This method has been successfully used for the simultaneous determination of pixel-by-pixel images of regional CBF and distribution volume of water (Carson et al., 1986; Huang et al., 1983).

The generation of quantitative functional images such as CBF, CBV and $CMRO_2$ maps requires the knowledge of the arterial tracer concentration as a function of time. In the past, this information has been obtained from manual sampling of arterial blood at intervals as short as 5 s (Raichle et al., 1983). However, manual determination of the arterial input function requires accurate timing of sample withdrawal and counting times which makes it error prone and imposes a practical limit on the blood sampling rate. This method further demands numerous personnel and imposes an additional radiation risk to workers. Therefore, automated blood sampling systems have been recently developed to overcome these problems (Hutchins et al., 1986; Kanno et al., 1987; Nelson et al., 1990).

1.17 The Arterial Input Function

The determination of CBF and $CMRO_2$ by PET requires the measurement of the arterial ^{15}O tracer concentration, called the arterial input function, in addition to the quantification of the radioactivity distribution in the brain. The former information may be obtained by means of an automatic blood sampling system which requires appropriate corrections for tracer delay and dispersion. Automated blood sampling is superior to manual sampling in several ways. First, it demands minimum manual intervention and thus reduces the radiation hazard to personnel. Second, the sampling interval can be reduced to a fraction of a second. However,

corrections for external tracer delay (i.e. the time difference between the arterial site where blood is withdrawn and the detector where the count rate is measured) and external dispersion (i.e. the difference in the degree of distortion in the blood curve resulting from the dispersion of the tracer bolus in the additional length of catheter from the peripheral sampling site to the detector) must be carefully applied to the blood data acquired with such blood sampling systems (Iida et al., 1987; Eriksson et al., 1988).

1.18 Principles of kinetic modeling

1.18.1 Tracer kinetic techniques

Tracer kinetic techniques are generally used in physiology and biochemistry to trace dynamic processes, such as blood flow, substrate transport, and biochemical reactions (Kety and Schmidt, 1948; Lassen and Perl, 1979). In fact, tracer methods constitute one of the major techniques for increasing our knowledge of the biochemical, transport, and hemodynamic base of body functions. A tracer is a measurably labeled substance introduced into the system in a quantity so low that physiological steady-state is unperturbed. Measurements are then taken as a function of time, and the characteristics of the dynamic process of interest are inferred from the radioactivity recordings. The complexity of the inference process varies a great deal, depending on the pharmacokinetics of the tracer, the dynamic process defining its uptake, and the kinetics of its binding in brain. In

some cases, the time of tracer appearance at the measurement location or the rate of increase or decrease of the measured tracer concentration directly provides the information required without any modeling (Lassen and Perl, 1976).

Modeling is commonly used to investigate, understand, or predict phenomena in science or engineering. Models appear in different forms, e.g., physical, biological, and mathematical models. Here we refer particularly to the mathematical model. which describes the dynamic behavior of the tracer in terms of a mathematical representation. The information for the behavior of the tracer of the system is incorporated in the model by restricting the representation to a limited set of functions that are consistent with the known physiological information. With the mathematical representation, the number of variables required to characterize the tracer kinetic is reduced to a minimum.

1.18.2 Principle of tracer kinetics

We will describe the principle of tracer kinetic with the following classic example of an enzymatic process.

Fig. 1.10 illustrates a sequence of reversible chemical reactions for compound S (substrate) in a biochemical system. If the reactions are occuring at equilibrium, it is not easy to determine the rates of various reactions. Measuring the steady-state concentrations of reactants and products is not enough, although the concentration ratios are determined by the relative reactions rates. However, if a small amount of labeled compound S is added to the system (too small to perturb

the mass reaction), the amount of labeled compound appearing in other chemical forms will rise with some time delay and will later drop gradually, as shown in Fig. 1.10. From measurements of the time delay, and the rates of rise and fall in the concentration levels, the reaction rates can be estimated. The sensitivity of the tracer concentration to the reaction rates is illustrated by the large shape changes of the curves in Fig. 1.10 as a result of changing only the reaction rate constant of one reaction. This also illustrates how kinetic responses and reaction rates can change through changes in rate contants which have units of $time^{-1}$. The term "constant" indicates the fixed value of a rate constant in a particular steady-state condition and not that they are universal constants. They are in fact variables through which rates of reactions change.

The example illustrates the basic principle of tracer kinetic techniques, which utilize the concentration of tracer and the rate of its change with time to estimate the transport rates in a dynamic system. However, for most applications, the technique is usually more complicated than illustrated below with respect to selection of tracers, estimation of parameter values, and design of study procedure.

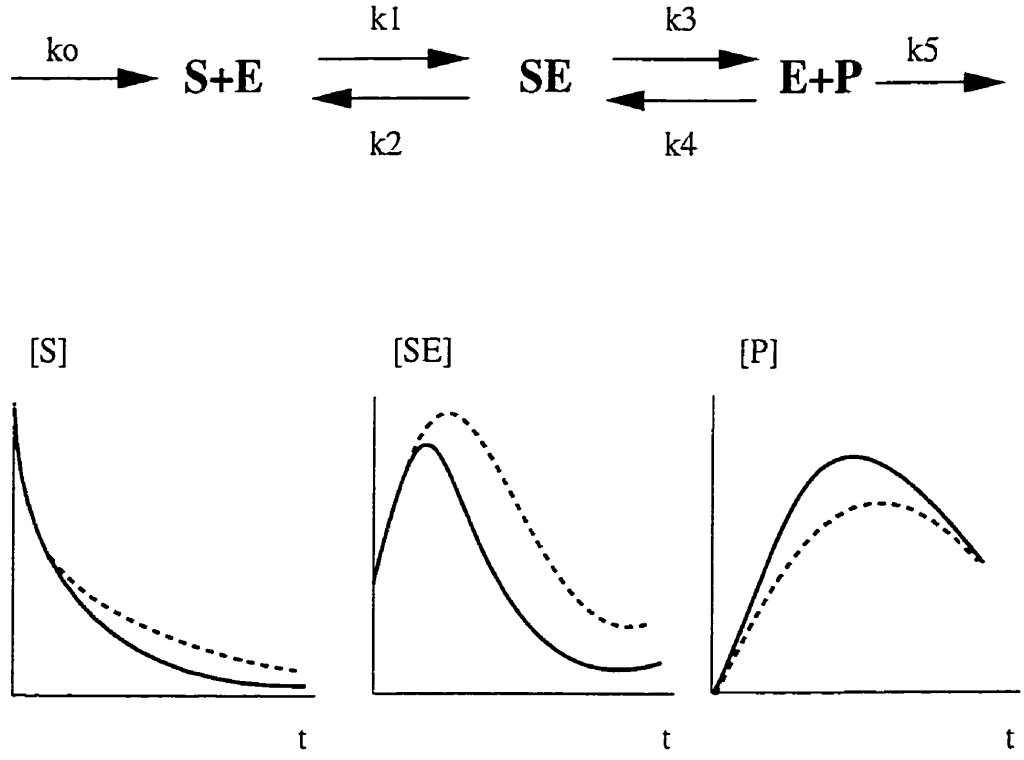

Figure 1.10 Illustration of the principle of tracer kinetics for measurement of chemical reaction rates. The chemical equation at the top shows that a substrate S binds with an enzyme E to form a complex SE which is further converted to a product P with release of E. If a small amount of a labeled substrate as a tracer is introduced at time zero, the tracer will go through all of the subsquent reactions. The time functions of the concentrations of the tracer at various steps can be used to estimate the reaction rates of various steps in the chemical pathway. If for example, the rate constant k3 is reduced by 50%, with all the other reactions kept constant, the tracer kinetic curves will be significantly changed (dotted curves), indicating the tracer kinetic curves are sensitive to speed of the reactions.

1.18.3 Basic assumptions of tracer kinetic techniques

In tracer kinetic technique, an appropriate tracer follows the dynamic process of interest. Usually, a tracer either is structurally related to the natural substance involved in the dynamic process (i.e., metabolic process) or has similar transport properties (i.e., for flow systems). Furthermore, the tracer is measurably tagged hence distinguishable from the natural substance that it traces. The degree of resemblance required between a tracer and its natural substances depends on the specific application and on the accuracy required. For example, most radiolabeled natural substances are chemically indistinguishable from the unlabeled compounds, and the small difference in mass are considered negligible for most physiological and biochemical applications (e.g. substituting radioactive ^{14}C, ^{13}C or ^{11}C for natural ^{12}C, or ^{3}H or ^{2}H for ^{1}H, or ^{13}N for ^{14}N).

The tracer is assumed by definition to be in a trace amount, so that the process being measured is not perturbed noticeably by the introduction of the mass. Otherwise, the measured results would reflect the effect of the tracer introduction and would not represent the process in its original state. In general, if the amount of tracer introduced is several orders of magnitude smaller than the natural substance i.e., its concentration is low relative to the relevant half-saturation constant, the perturbation caused by the tracer can be considered insignificant.

The dynamic process being evaluated with a tracer kinetic technique is usually assumed to be in a steady state. In other words, the rate of transport or

reaction of the system is not changing with time, and the amount of substance in any part of the system is constant during the evaluation period. Strictly speaking, there is no absolute steady state for biological system that may constantly change. However, the steady state condition is considered to be satisfied if the amount of change within the time of evaluation is small compared to the magnitude of the process itself.

1.18.4 Compartmental models

As stated earlier, mathematical models are generally used to incorporate known information about a process in order to provide a framework of representation allowing the interpretation of measurements. For tracer kinetic, there exist various kinds of mathematical models of widely different mathematical characteristics such as distributed versus nondistributed, compartmental versus noncompartmental, and linear versus nonlinear models (Carson et al., 1981 and 1983; Gjedde, 1995).

A compartmental model is usually represented by a number of compartments linked together by arrows indicating transport between compartments (Fig. 1.10). A compartment is defined as a space in which the tracer is distributed uniformly. The amount of tracer leaving a compartment is assumed to be proportional to the total amount in the compartment. The arrows indicate the possible pathways the tracer can follow. The symbol K (or k) next to the arrow is called rate constant, which has the dimension of inverse time and denotes the fraction of the total

tracer that would leave the compartment per unit time.

A compartmental model is consistent with the way we commonly describe or think of the transfer of tracer in the tissue or in the body. In addition, compartmental models offer many attractive mathematical properties that allow straightforward solutions or analyses of the characteristics of the models.

1.19 Oxygen-15 Studies With PET

Among the positron emitting radioisotopes frequently used in PET, oxygen-15 (^{15}O) has the shortest physical half-life ($T_{1/2}$=2.035 min) and the most energetic positron ($E_{max_{\beta+}}$=1.72 MeV). Both these facts have their consequences for the use of ^{15}O in PET imaging. The short physical half-life makes mandatory the on-site production of ^{15}O by a medical cyclotron. On the other hand, it allows multiple ^{15}O studies to be performed with the same subject within a short time with limited radiation exposure and negligible interference from residual radioactivity. This possibility has given rise to some exciting applications of ^{15}O such as metabolic mapping of functional activity of the brain by means of blood flow activation studies (Evans et al., 1992). The large positron energy of ^{15}O results in a resolution broadening effect of $\geq$ 1 mm (FWHM); therefore, greater uncertainty in the exact source of the positron emission event (Hoffman and Phelps, 1986). The major applications of ^{15}O in PET imaging, at present, are focused on the study of brain function (Mazziotta and Phelps, 1986). The compounds used include $C^{15}O$

for the measurement of cerebral blood volume (CBV), $C^{15}O$ and $H_2{}^{15}O$ for the measurement of cerebral blood flow (CBF), and $O^{15}O$ which, together with the former studies, allows the estimation of cerebral oxygen extraction fraction (E_{O_2}) and oxygen utilization rate ($CMRO_2$). Furthermore, the oxygen consumption of the brain has been measured directly from a single inhalation of $O^{15}O$ using the time-weighted integration method (Ohta et al., 1992).

1.20 Cerebral Blood Flow (CBF)

The measurement of regional CBF is one of the most frequently performed PET procedures. Often, PET/CBF investigations are carried out as independent studies e.g. in physiological blood flow activation studies (Evans et al., 1992) in which blood flow is the subjects of interest.

1.20.1 Theory

Most contemporary PET CBF methods using $H_2{}^{15}O$ are based on the Kety-Schmidt one-compartment model for diffusible inert tracers (Kety, 1951, 1960). However, because water is not a freely diffusible tracer (Eichling et al. 1974; Raichle et al., 1983), because its capillary first-pass extraction fraction, E_{H_2O}, is slightly lower than one. Therefore, an additional compartment is necessary to account for the non-extracted residual intravascular radioactivity. In the following paragraphs, the one- and two-compartment models are briefly described.

1.20.1.1 One-compartment Model

The one-compartment model assumes that water is perfectly diffusible, i.e. the transfer of tracer from blood to brain tissue is only limited by blood flow (Fig. 1.11A). In this model, a volume of tissue, V_t, is perfused with tracer which enters the compartment through the arterial blood stream at a flow F [ml·min^{-1}] and concentration C_a [Bq·ml^{-1}]. The compartment loses the tracer on the one hand through venous outflow with concentration C_v and, on the other hand, via radioactive decay (λ is the decay constant which, in the case of ^{15}O, is 0.34 min^{-1}). The rate of change in the amount of $H_2{}^{15}O$ in tissue, M, can then be expressed as:

$$\frac{dM}{dt} = F(C_a - C_v) - \lambda M \qquad (1.1)$$

Equation (1.1) is based on the Fick principle which expresses the law of conservation of mass, adapted here to include the physical decay of tracer (Kety, 1951). We define the tissue tracer concentration C=M/W_t [Bq·g^{-1}] and the venous, or compartmental, tracer concentration C_v=M/V_d [Bq·ml^{-1}], where W_t is the mass of the tissue element [g] and V_d the tracer distribution volume [ml]. We further define the equilibrium tissue-blood partition coefficient of the tracer, p=C/C_v = V_d/W_t [ml·g^{-1}], the tissue blood flow f=F/W_t [ml·min^{-1}·g^{-1}] and assume that C_a and C have been corrected for radioactive decay. Then, equation (1.1) becomes:

$$\frac{dC}{dt} = fC_a - (\frac{f}{p})C \tag{1.2}$$

With C and C_a being variable with time, integration of equation (1.2) with the initial condition $C(0) = 0$ yields:

$$C(t) = f \cdot \int_0^t C_a(\tau) e^{-\frac{f}{p}(t-\tau)} d\tau \tag{1.3}$$

Since PET, in general, does not measure the instantaneous tissue concentration, C(t), but rather its integral over a given time (frame length T_1 to T_2), the following operational equation is used to determine the blood flow, f:

$$C'(t) = \int_{T_1}^{T_2} C(t)dt = f \cdot \int_{T_1}^{T_2} e^{-k_2 t} \int_0^t C_a(\tau) e^{k_2 \tau} d\tau dt \tag{1.4}$$

where $C(t)$ is the total number of radioactive events per unit weight of brain tissue detected by the tomograph during the scan, C_a the arterial concentration and $k_2 = f/p$ describing the washout of tracer from the extravascular space.

1.20.1.2 Two-compartment Model

Since there is a diffusion barrier for $H_2{}^{15}O$ between the vascular compartment and the brain tissue, two compartments are necessary for the description of its dynamics (Ohta et al., 1990, 1996) (Fig. 1.11B). We define the unidirectional

clearance of a substance (e.g. $H_2{}^{15}O$) from blood by brain tissue, K_1, and its first-pass extraction fraction, E_{H_2O}, with F being the blood flow. These three quantities are related as follows: $K_1 = E_{H_2O}F$. If we further define k_2 as the fractional clearance (or rate constant), describing the washout of exchangeable tracer from the extravascular space and M_e as the quantity of exchangeable labeled material in the extravascular portion of the tissue, then Fick's equation can be written as:

$$\frac{dM_e}{dt} = K_1 C_a - k_2 M_e \tag{1.5}$$

Introducing the initial vascular volume of distribution for water in brain, V_0, so that

$$M = M_e + V_0 C_a \tag{1.6}$$

we arrive at the following solution for the total observable brain radioactivity, M:

$$M(T) = (K_1 + k_2 V_0) \int_0^T C_a(t)dt + V_0 C_a(T) - k_2 \int_0^T M(t)dt \tag{1.7}$$

From equation (1.7), K_1, k_2 and V_0 can be estimated by non-linear least-squares regression or by the weighted integration method (Alpert et al., 1984). CBF may then be calculated from the relation: $K_1^{H_2O} = E_{H_2O} \cdot \text{CBF}$ assuming that E_{H_2O} is known.

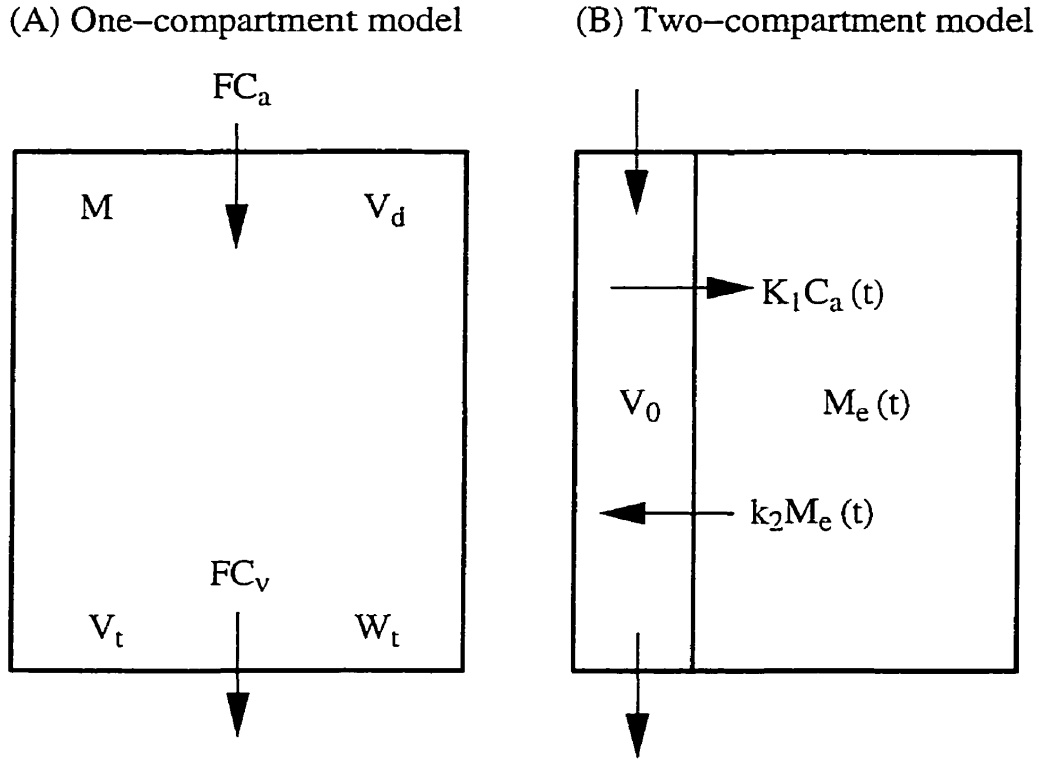

Figure 1.11 (A) One-compartment model for a freely diffusible inert tracer. A tissue element has volume V_t, mass W_t, tracer content M, and tracer distribution volume V_d. The tissue element is homogeneously perfused with blood flow F at arterial and venous tracer concentrations C_a and C_v. (B) Two-compartment model representing intravascular (blood) and extravascular (tissue) spaces separated by the blood-brain barrier for a diffusion-limited tracer with a first pass capillary extraction fraction of $E<1$. K_1 is the undirectional clearance of tracer from blood into tissue and k_2 is the rate constant which describes the washout of exchangeable tracer from tissue.

1.21 Cerebral Metabolic Rate of Oxygen ($CMRO_2$)

The *in vivo* determination of $CMRO_2$ was pioneered by Ter-Pogossian and associates (Ter-Pogossian et al., 1970; Raichle et al., 1976), who used the bolus injection of ^{15}O-labeled water and ^{15}O-oxyhemoglobin together with conventional external monitoring techniques to measure CBF and the first pass extraction fraction of oxygen (E_{O_2}). $CMRO_2$ was is then calculated as the product of CBF, E_{O_2}, and the arterial oxygen concentration, $C_a^{O_2}$. These results were validated by comparison with hemispheric $CMRO_2$ values obtained from direct measurements of differences in arteriovenous oxygen concentration and assuming E_{O_2}, to be equal to the net extraction fraction were at steady-state, $(C_a^{O_2}\text{-}C_v^{O_2})/C_a^{O_2}$ where $C_a^{O_2}$ and $C_v^{O_2}$ are the arterial and venous oxygen concentrations at steady-state.

Current PET techniques for the measurement of $CMRO_2$, which include the continuous inhalation or steady-state method of Frackowiak and associates (1980) and the sequential bolus approach of Mintun and colleagues (1984), are based on the same basic principle. With these techniques, $CMRO_2$ is calculated from a series of three PET studies which includes the measurements of CBF, CBV and oxygen extraction fraction, E_{O_2}. Such a multitracer study may last from 30 min (bolus method) to over an hour (steady-state method). Faster methods to measure $CMRO_2$ have been proposed (Huang et al., 1986; Meyer et al., 1987). Recently, Ohta et al. (1992) showed that $CMRO_2$ can be measured after a single inhalation of ^{15}O-labeled molecular oxygen. In this case, the bolus of labeled

hemoglobin is created by inhalation of $[^{15}O]O_2$. For that reason, the arterial time-activity curves from $CMRO_2$ studies and those obtained in CBF studies, where the tracer is injected intravenously, do not have the same shape. As in the case of CBF measurements, the arterial time-activity curves in $CMRO_2$ studies also require the corrections for tracer delay and dispersion.

1.21.1 Steady state and bolus inhalation methods

With both the steady state (Frackowiak et al., 1980) and the bolus inhaltion method (Mintun et al., 1984) in which a mixture of air and $[^{15}O]O_2$ is administered as a bolus in one or several deep inhalations, the calculation of $CMRO_2$ is based on a sequence of three distinct PET studies for the measurement of CBF, CBV and E_{O_2}. The CBV study is required to account for blood-born radioactivity in the calculation of E_{O_2}. Once these quantities are known, $CMRO_2$ is calculated as the simple product of $CBF \cdot E_{O_2} \cdot C_a^{O_2}$ where $C_a^{O_2}$ is the total oxygen content of arterial blood obtained from arterial samples.

1.21.2 One-step method (three-weighted integration technique)

Methods described above for calculation of $CMRO_2$ require three separate PET studies taking approximately 60 min for completion. Therefore, the results are prone to propagation of error, and violation of steady-state. Efforts have been made to estimate $CMRO_2$ from a single short PET study (Meyer et al., 1987; Huang et al., 1986). More recently, Ohta et al. (1992) introduced a two-compartment, three-weight integration method which allows the generation

of $CMRO_2$ maps on a pixel-by-pixel basis from a single short dynamic $[^{15}O]O_2$ bolus inhalation study.

The authors adopted the weighted integration method pioneered by Alpert et al. (1984) and refined by Carson et al. (1986). This method was originally used to estimate simultaneously the regional blood flow and partition coefficient for water in brain from 8-10 min radioactivity records obtained by PET. The observed and theoretically expected time-activity records were weighted with separate weights, $w_1(t)$, $w_2(t)$, and integrated, using an equation for which k_2, and eventually K_1 by back substitution, were estimated rapidly by means of look-up tables. As pointed out by Koeppe et al. (1987), this two-weight method may cause a significant parameter overestimation because it does not include a correction term for radioactivity remaining in the circulation. Therefore Ohta et al. modified the two-weight method to include a correction term for the vascular volume (Fig. 1.11B). This new approach which includes three weighting functions, was called the three-weight integration method. Using the analytical (autoradiographic) solution of equation 1.5 with the initial condition $M_e = 0$, equation 1.6 becomes

$$M(t) = K_1^{O_2} \int_0^t C_a(u) e^{k_2^{O_2}(u-t)} du + V_0 C_a(t) \qquad (1.8)$$

Successive multiplication of the left- and right-hand sides with the same weighting functions $w_1(t)$ to $w_3(t)$, and integration over time leads to three equations from which V_0 could be eliminated. Furthermore, the computational form for the

estimation of k_2 by the three-weighted method, equivalent to the two-weighted method leads to the equation in which the only unknown is k_2, which in turn could be estimated using a look-up table. With k_2 known, K_1 and V_0 could be calculated by solving the relevant equations.

In the following chapters, I focus on the behavior of oxidative metabolism in human cortex under different physiological circumstances. Specifically, I concentrate on the measurement of blood flow and oxygen consumption in visual cortex, a complex region of the human brain which has been extensively studied because of its fundamental role in defining human experience of the external world. I use PET to measure the absolute rates of blood flow and oxygen consumption. In all of the PET measurements, two-compartment, three-weight integration method will be used to estimate the physiological quantities of interest.

Rationale for the design of the experiment I

There are widely cited reports of a significant discrepancy between blood flow and oxygen consumption in sensory areas of the brain (Fox and Raichle, 1986; Seitz and Roland, 1992; Kuwabara et al., 1992; Ribeiro et al., 1993). This mismatch is of special interest in primate visual cortex. Although investigators unanimously report a significant increase of cerebral blood flow following the stimulation of the visual cortex by visual stimuli, the reports of the behavior of cerebral oxygen metabolism have been less clear, and mostly failing to demonstrate significant changes of oxygen consumption in the human visual cortex (Fujita et al. 1992; Ribeiro et al., 1993).

Staining for the oxidative enzyme cytochrome oxidase in primary visual cortex (V1) reveals an underlying organization of neurons in the superficial layers III and II into the so-called "blob" and "inter-blobs". As described before, cells in blob regions are involved in color processing. This suggests that color processing is subserved by a physiological process with relatively high demand for oxidative phosphorylation. Visual stimuli with different spatial frequency and chromatic content are reported to evoke different metabolic reponses in blob and non-blob regions of V1. Therefore, we investigated the possibility that stimulus parameters might influence the measured changes of $CMRO_2$ due to selective activation of neurons with different capacities for increasing oxidative metabolism. Combined histochemical and visual stimulation experiments in non-human primates

have demonstrated a differential increase of glucose uptake in the blobs using chromatic or medium-to-low spatial frequency stimuli (Tootell et al., 1988). The correspondence of this uptake pattern to the underlying oxidative enzyme distribution led us to hypothesize that increases energy demand produced by specific visual stimuli is met with elevated oxidative phosphorylation in the blobs. If this were the case, the blobs would correspond to an oxidative pathway. We therefore wanted to test the hypothesis that a medium spatial-frequency, chromatic stimulus (yellow and blue) would selectively activate neurons rich in cytochrome oxidase and produce an elevation in $CMRO_2$. If so, this stimulus could be used to evaluate $CMRO_2$ inconjunction with CBF assays in normal subjects and in patients suffering from diseases of oxidative metabolism.

CHAPTER 2

Increased oxygen consumption in human visual cortex: Response to visual stimulation

M.S. Vafaee, S. Marrett, E. Meyer, A.C. Evans, A. Gjedde

(Acta Neurol Scand, 98:85-89, 1998)

Abstract

To test the hypothesis that a sufficiently complex visual stimulus causes the consumption of oxygen to rise in the human visual cortex, we used positron emission tomography (PET) to measure the cerebral metabolic rate of oxygen ($CMRO_2$) during visual stimulation in six healthy normal volunteers. A yellow-blue checkerboard, reversing its contrast at a frequency of 8 Hz, was presented for a period of 7 min, beginning 4 min before the onset of a 3-min scan. In the baseline condition, subjects fixated a cross-hair from 30 s before until the end of the 3-min scan. The $CMRO_2$ was calculated with the two-compartment weighted integration method (Ohta et al., 1992). The checkerboard minus baseline subtraction yielded statistically significant increases in $CMRO_2$ in the primary (V1) and higher order visual cortices (V4 and V5). The significant $CMRO_2$ increases were detected in these regions in both the group average and in each individual subject.

Introduction

Under normal conditions, brain tissue metabolizes the majority of glucose by oxidation. Thus, at rest and during activation the brain's energy demands are met by oxidation of glucose. Blood flow to the brain has been thought to be tightly coupled to the metabolic requirements of the tissue for oxygen and glucose (Siesjö, 1978). However, Fox and colleagues challenged this view when they reported that uncoupling of cerebral metabolic rate of oxygen ($CMRO_2$) from the blood flow (CBF) and the metabolic rate of glucose (CMR_{glc}) occurs during both somatosensory and visual stimulation (Fox and Raichle, 1986; Fox et al., 1988). By positron emission tomography (PET) of humans, they found CBF and CMR_{glc} to have increased by 30-50% while the $CMRO_2$ had increased only by about 5%. This finding suggested that less oxygen was cleared from the blood during the physiological activation, as compared with a resting state (i.e., net oxygen extraction decreased). Other PET studies have shown CBF changes of 30% during somatosensory stimulation with smaller (13%) increases (Seitz and Roland, 1992) or no change (Kuwabara et al., 1992) of $CMRO_2$.

Biochemical evidence suggests that visual neurons differ in their capacity to sustain oxidative phosphorylation. The staining pattern in primary visual cortex (V1) for the mitochondrial enzyme cytochrome oxidase (COX) (Horton, 1984; Wong-Riley and Carroll, 1984) reflects such specialization.

On this basis, we tested the ability of a visual stimulus, a yellow-blue revers-

ing checkerboard, to raise oxygen consumption in visual cortex. Previously it has been reported that the probability of observing an increase in $CMRO_2$ is greater for a chromatically rich stimulus (Marrett et al., 1995). Due to its high chromatic content as well as the perception of motion induced by the contrast reversal, processing of this stimulus would be expected to occur not only in regions of striate cortex but also in regions of extrastriate cortex. We therefore evaluated the stimulus in terms of its ability to raise oxygen consumption in different regions of visual cortex. For this purpose, we used positron emission tomography (PET) to measure $CMRO_2$ during visual stimulation of the living human brain. We intend to utilize this stimulus for further evaluation of CBF and $CMRO_2$ in patients suffering from disorders of oxidative metabolism.

Materials and Methods

Six healthy normal volunteers (3 men and 3 women) aged 23-33 years (mean= 25±3.9, SD) gave written informed consent to participate in the study approved by the Research Ethics Committee of the Montreal Neurological Institute and Hospital.

PET studies were performed with the Scanditronix PC-2048 15B eight-ring, 15-slice BGO head tomograph with a transverse resolution of 5.8-6.4 mm and an axial resolution of 6.1-7.1 mm (Evans et al., 1991). The images were reconstructed as 128×128 matrices of 2 mm×2 mm pixels using filtered back-projection with an 18 mm FWHM Hanning filter. Reconstruction software included corrections for random and scattered events, detector efficiency variations and dead-time. An orbiting rod transmission source containing about 5 mCi of ^{68}Ge was used for attenuation correction (Evans et al., 1991).

The subjects were positioned in the tomograph with their heads immobilized by means of a customized self-inflating foam headrest. A short indwelling catheter was placed into the left radial artery for blood sampling and blood gas examination. Arterial blood radioactivity was automatically sampled, corrected for delay and dispersion (Vafaee et al., 1996), and calibrated with respect to the tomograph.

At the start of each PET scan, the subjects inhaled 60 mCi of ^{15}O-O_2 in a single breath, and $CMRO_2$ was measured using the single-breath inhalation method (Ohta et al., 1992). In the baseline condition, the subjects were asked to fixate

on a cross-hair in the center of the screen 30 s before the scan and throughout the subsequent 3-min scan. In the activation condition, a circular yellow-blue annular checkerboard (diameter of about 17^0 of visual angle, reversing contrast at a frequency of 8 Hz, and spatial frequency of 1 cycle/deg) was presented for 4 min before the start of the scan and during the following 3-min scan for a total of 7 min. Black drapes were used to create a dark environment around the screen. The baseline and activation scans were each repeated once in the same order as before.

Each subject also underwent a magnetic resonance imaging (MRI) examination on a Philips Gyroscan ACS (1.5 T) superconducting magnet system for structural-functional (MRI-PET) correlation. The MRI image was a T1-weighted, 3D FFE (fast field echo) sequence consisting of 160 contiguous 256×256 sagittal slices of 1 mm thickness. The MR images were transformed into stereotaxic coordinates (Talairach and Tournoux, 1988) by means of an automatic registration program developed at the Montreal Neurological Institute (Collins et al., 1994). The reconstructed PET images were co-registered with the subjects' MRI scans using an automatic registration program based on the Automatic Image Registration algorithm (Woods et al., 1992). To correct for between-scan subject movements, PET-to-PET automatic registration was also performed (Woods et al., 1993). The PET images were then normalized for global $CMRO_2$, averaged across subjects, transformed into stereotaxic coordinates and blurred with a Gaussian filter of

18×18×7.6 mm. Mean subtracted image volumes (stimulation minus baseline) were then obtained and converted into Z-statistic volumes by dividing each voxel mean by the mean standard deviation of the normalized $CMRO_2$ subtraction image obtained by pooling the SD across all intracerebral voxels. Significant focal changes were detected by a method based on 3-D Gaussian random field theory (Worsley et al., 1992). Values equal to or exceeding a criterion of Z=3.5 were deemed statistically significant ($P < 0.00046$, two-tailed, uncorrected). Correcting for multiple comparison, a Z-value of 3.5 yields a false positive rate of 0.85 in 250 resolution elements (each of which has dimensions 18×18×7.6 mm), which approximates the total volume of cortex scanned.

Results

The mean global $CMRO_2$ for all 24 scans performed on the six subjects was 163.7±18.4 (SD) μmol hg^{-1} min^{-1}. There was no significant difference between baseline (159.9±19.6 μmol hg^{-1} min^{-1}) and activation (167.6±20.1 μmol hg^{-1} min^{-1}) values of global $CMRO_2$.

Consistent significant increases in regional $CMRO_2$ were found in the left primary and the right primary/secondary visual cortex (Fig. 1). Oxygen consumption also significantly and unilaterally increased in the right occipito-temporal area (~V5) and in the left fusiform gyrus (~V4) (Table 1).

Discussion

The mechanism linking neuronal activity to the circulation is generally believed to constitute a flow-metabolism couple (Roy and Sherrington, 1890). Recent reports claim a mismatch between changes of blood flow and glucose consumption on the one hand, and oxygen utilization on the other hand, during functional activation of regions of the human brain (Fox and Raichle, 1986; Fox et al., 1988; Seitz and Roland, 1992; Fujita et al., 1992; Ribeiro et al., 1993).

In this paper, we used PET to measure changes in $CMRO_2$ during visual stimulation. The yellow-blue reversing checkerboard used as the stimulus in this study caused significant increases of oxygen consumption in several areas of the visual

cortex. The raised $CMRO_2$ in primary visual cortex is in agreement with previous measurements from this group (Marrett et al., 1995). In the present study we also observed increases of $CMRO_2$ in higher order visual cortices. These measurements of $CMRO_2$ were made after sustained (7 minutes) stimulation of the visual cortex. The observed increases in $CMRO_2$ appear to be stimulus specific since simple photic stimulation with Grass eye goggles, i.e. an array of red LEDs flashing at 8 Hz, failed to induce significant increases of $CMRO_2$ (Fujita et al., 1992; Ribeiro et al., 1993). Since the same method of $CMRO_2$ determination was used in the latter studies, the observed increases in $CMRO_2$ in the visual cortex might be associated with the activation of cytochrome oxidase rich neurons which seem to be involved in color processing.

During the presentation of our chromatic stimulus (yellow-blue checkerboard), $CMRO_2$ rose considerably in the fusiform gyrus. This area lies outside the striate cortex and is an area that was previously demonstrated to show a marked increase of CBF during color stimulation, i.e. V4 (Zeki et al., 1991).

Another area of significant $CMRO_2$ increase was close to the reported site of CBF increases during the presentation of moving stimuli (Zeki et al., 1991; Watson et al., 1991). The location of this area is consistent with the position of the motion area V5 (taking into account its spatial variability) that contains neurons highly selective for motion (Desimone and Ungerleider, 1986; Van Essen et al., 1981). It is worth noticing that, although Zeki and colleagues reported bilateral

increases in rCBF during both the motion and color stimulation, the increase in the right hemisphere was stronger in V5 while, in V4, only the left hemisphere increase reached statistical significance. This result is in line with our observation of a left hemispheric $CMRO_2$ activation in V4 and a right hemispheric focus in V5. The fact that we found strictly unilateral activation might be due, at least in part, to the differential sensitivity of $CMRO_2$ to the stimulus as oposed to CBF.

Finally, contrary to the results of studies which have reported no change of oxygen consumption (Fox and Raichle, 1986; Fox et al., 1988; Ribeiro et al., 1993), we demonstrated that stimulation of visual cortex with a reversing checkerboard pattern for 7 minutes caused a significant increase of $CMRO_2$. The discrepancy between the results of different types of sensorimotor stimulation suggests that the ultimate increase of oxygen consumption depends significantly on the biochemical peculiarities of the neuronal pathway mediating the response of the stimulus (Borowsky and Collins, 1989). For example, in skeletal muscle cells, the content of cytochrome oxidase reflects the maximal level of oxygen consumption habitually required by specific cells (Pette, 1985). This observation suggests that transient increases of energy metabolism above the habitual level of activity cannot, or need never, be accompanied by increased oxygen consumption, e.g., during vibrotactile stimulation of primary sensory cortex or photic stimulation of visual cortex (Ribeiro et al., 1993).

The reduction of oxygen clearance is critical to the interpretation of recent

studies showing a small increase in the magnetic resonance (MR) signal in the brain during neuronal stimulation (Kwong et al., 1992; Ogawa et al., 1992; Frahm et al., 1992). The origin of this signal change is thought to be related to the fact that deoxyhemoglobin is paramagnetic, so that changes in the local deoxyhemoglobin concentration alter the magnetic susceptibility of blood. If the net OEF (oxygen extraction fraction) decreases, so that the local deoxyhemoglobin concentration also decreases, then the MR signal will increase. The advent of functional magnetic resonance imaging (fMRI) using this concept has made it possible to noninvasively investigate the brain work with higher spatial resolution than PET. Studies using several forms of sensory, motor, or cognitive activation have demonstrated focal signal increases in brain structures associated with these tasks (Kwong et al., 1992; Ogawa et al., 1992; Frahm et al., 1992; Engel et al., 1994). However, the quantitative relation between the observed MR effect and changes in local physiological variables such as CBF and $CMRO_2$ is incompletely understood. In particular, because the MRI signal change depends on the relative changes in CBF and $CMRO_2$, any quantitative interpretation of fMRI data requires better understanding of the relationship between flow and metabolism.

In conclusion, we argue prudently that the ability of brain neurons to increase their oxygen use may vary according to the task neurons perform. The observation that the yellow-blue checkerboard gave rise to a significant rise in oxygen consumption may reveal a relationship between the spatio-temporal and chro-

matic structure of the stimulus and the resulting $CMRO_2$. Moreover, we have demonstrated that a colourful visual stimulus in form of a yellow-blue reversing checkerboard gives rise to increased $CMRO_2$ in both striate and extrastriate visual cortices. This stimulus may further be used in CBF and $CMRO_2$ measurements of patients suffering from oxidative metabolic disorders.

Table 1: Coordinates and z-values of cortical regions activated by yellow-blue checkerboard

Region	Brodmann area	coordinates*			z-value**
		x	y	z	
Right primary visual cortex (V1)	17	9	-78	6.5	3.9
Left primary/secondary visual cortex (V1/2)	17/18	-2	-78	16	3.8
Left fusiform gyrus (V4)	19	-23	-54	-8	3.7
Right occipito-temporal area (V5)	19	34	-81	-10	3.6

* Talairach coordinates. ** $p<0.0004$.

Legend to Figure 1:

Figure 1: Averaged PET subtraction images of $CMRO_2$ superimposed upon averaged MRI images. Subtraction of baseline from activation state yielded the focal changes in $CMRO_2$ shown as *Z*-statistic images in three different views (transverse, sagittal, and coronal). Fig. 1A shows the focal $CMRO_2$ changes in the right primary visual cortex (calcarine fissure: area 17) and Fig. 1B the changes in the left dorsal part of V1 and V2. Figures 1C and 1D show Z-statistic images of focal changes of $CMRO_2$ in the extrastriate visual cortex. Fig. 1C shows the focal $CMRO_2$ changes in the left fusiform gyrus (V4) and Fig. 1D those in the right occipito-temporal area (V5).

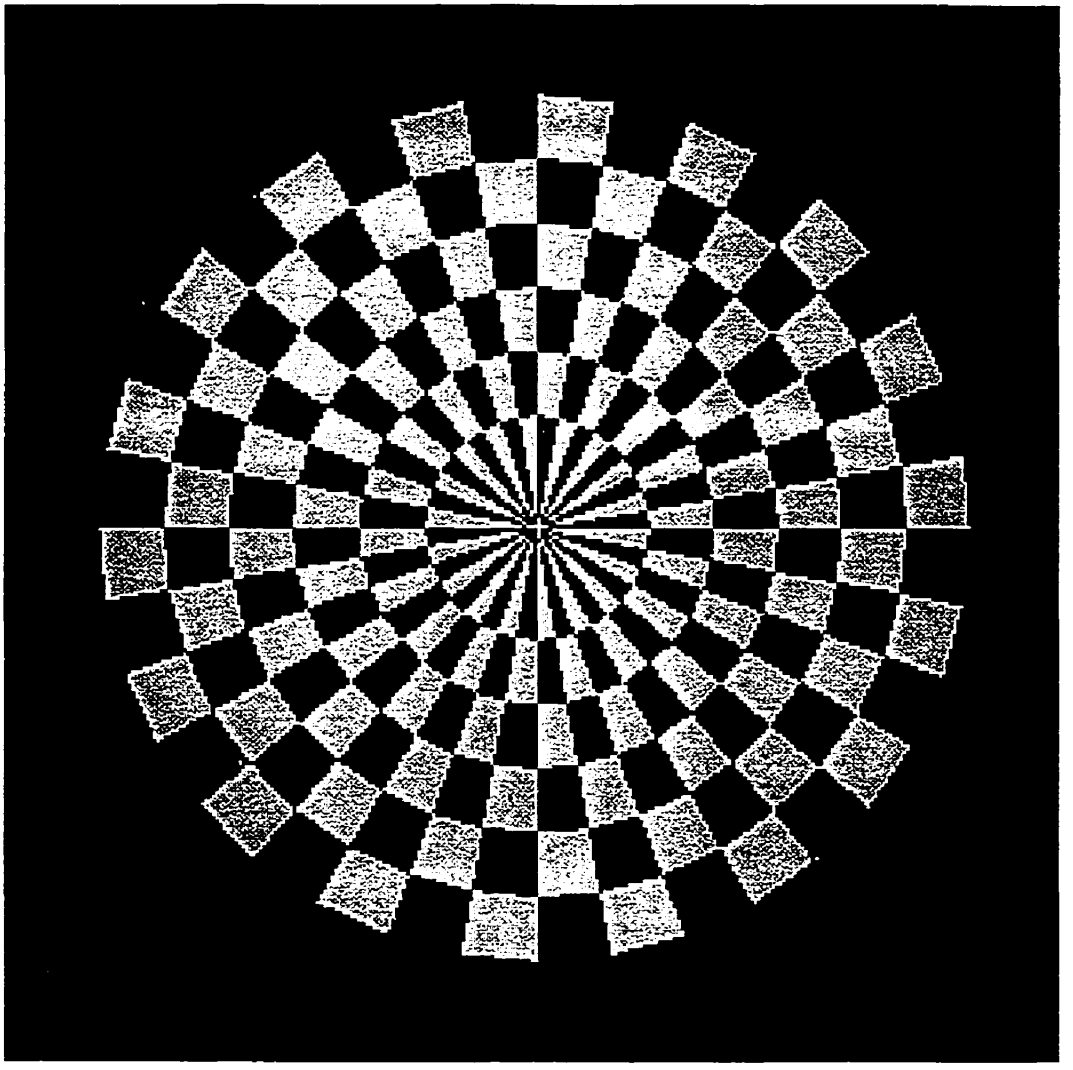

Yellow–blue reversing annular checkerboard

Rationale for the design of the experiment II

Experiment I led to the establishment of a visual paradigm capable of enhancing the oxygen metabolism in the visual cortex as a consequence of the stimulation. We next shifted our interest to the investigation of the relationship between the rate of a sensory stimulus such as that in experiment I, and regional oxygen metabolism in human visual cortex.

There is a substantial body of literature investigating the relationship between stimulation rate and cerebral metabolic rate of glucose (CMR_{glc}) in both the peripheral nervous system (Toga and Collins, 1981) and the central nervous system of rats (Yarowsky et al., 1983). The effect of stimulus rate on cerebral blood flow (CBF) in humans was also studied by several investigators. Studies of human auditory cortex have shown a linear dependence of CBF on the rate of auditory stimulation (Price et al., 1992). As well, it has been reported that different repetition rates of finger and eye movements have led to rate-dependent changes in CBF in the motor cortex (Sadato et al., 1996; Paus et al., 1995). In addition, Fox and Raichle (1984), have shown a stimulus rate dependent regional cerebral blood flow in V1.

However, the issue of the behavior of the oxygen metabolism in the human visual cortex in response to the stimulation rate has never been addressed. We therefore, designed experiment II to investigate this issue by means of PET, and based upon our characterization of the stimulus tested in experiment I.

CHAPTER 3

Frequency-dependent changes in cerebral metabolic rate of oxygen during activation of human visual cortex

M.S. Vafaee, E. Meyer, S. Marrett, T. Paus, A.C. Evans, A. Gjedde

(J Cereb Blood Flow Metab, 19:3:272-277, 1999)

Abstract

To test the hypothesis that brain oxidative metabolism is significantly increased upon adequate stimulation, we varied the presentation of a visual stimulus to determine the frequency at which the metabolic response would be at maximum. We measured regional cerebral metabolic rate of oxygen ($rCMRO_2$) in twelve healthy normal volunteers with the ECAT EXACT HR^+ (CTI/Siemens) 3D whole body positron emission tomograph (PET). In seven successive activating conditions, subjects viewed a blue and yellow annular checkerboard reversing its contrast at frequencies of 0, 1, 4, 8, 16, 32 and 50 Hz. Stimulation began four minutes before and continued throughout the 3-min dynamic scan. In the baseline condition, the subjects began fixating a cross-hair 30 s prior to the scan and continued to do so for the duration of the 3-min scan. At the start of each scan, the subjects inhaled 20 mCi of ^{15}O-O_2 in a single breath. $CMRO_2$ was calculated using a two-compartment, weighted integration method. Normalized PET images were averaged across subjects and co-registered with the subjects' MRI in stereotaxic space. Mean subtracted image volumes (activation minus baseline) of $CMRO_2$ were then obtained and converted to z-statistic volumes. We found a statistically significant focal change of $CMRO_2$ in the striate cortex (x=9; y=-89; z=-1) that reached a maximum at 4 Hz and dropped off sharply at higher stimulus frequencies.

Introduction

The human brain consumes glucose and oxygen to sustain its function. The substrates are continuously supplied via the cerebral circulation, which supplies 20% of the cardiac output. The mechanism linking neuronal activity to the circulation is generally believed to constitute a flow-metabolism couple. The purpose of this couple is thought to be to satisfy the principle of Roy and Sherrington (Roy and Sherrington, 1890) which has been interpreted to mean that cerebral blood flow changes must subserve a tight coupling between cellular energy requirements and the supplies of glucose and oxygen to the brain (Gjedde, 1997). The homeostatic mechanism maintains a constant concentration of adenosine triphospate (ATP), the compound that ties the processes that deplete the energy potential of brain tissue to those that restore it. A number of investigators have demonstrated that cerebral blood flow (CBF) in the brain is tightly coupled to the metabolic requirements of tissue for glucose and oxygen, i.e., cerebral metabolic rates of glucose (CMR_{glc}) and oxygen ($CMRO_2$) (Siesjö, 1978; Yarowsky and Ingvar, 1981).

More recent studies reported a mismatch between changes of CBF and oxygen utilization during functional activation of the human brain despite a match between changes of regional glucose consumption and CBF (Fox and Raichle, 1986; Fox et al., 1988; Fujita et al., 1992 and 1993; Ribeiro et al., 1993). These findings constitute a significant departure from the original principle formulated by Roy and Sherrington. However, in this laboratory we have observed significant

increases of $CMRO_2$ in the striate cortex in response to a visual stimulation (Marrett et al., 1995; Vafaee et al., 1996 and 1998; Marrett and Gjedde, 1997) along with a commensurate elevation of CBF. In these studies, the $CMRO_2$ response to a single stimulation frequency namely 8 Hz which had provided a maximum response in previous CBF studies (Fox and Raichle, 1984 and 1985), was compared with a resting baseline. In the present experiment, we examined changes in $CMRO_2$ as a function of stimulus frequency (tuning curve).

Knowledge of the $CMRO_2$ response to the rate of stimulation is required to evaluate the so-called Oxidative Index (OI), defined as the $CMRO_2$/CBF ratio. This index yields new information about the degree of oxidative breakdown of glycolysis prevailing in specific areas of the brain during physiological stimulation. The goal of the present experiment was to determine the frequency dependence of $CMRO_2$ changes by means of a previously tested visual stimulus, a yellow-blue contrast reversing checkerboard. We have already shown that this stimulus was capable of giving rise to changes of $CMRO_2$ in the visual cortex (Marrett et al., 1995; Vafaee et al., 1996 and 1998; Marrett and Gjedde, 1997).

Materials and Methods

Twelve healthy normal volunteers (6 males and 6 females), aged between 22 and 32 years (mean$\pm$SD : 25$\pm$3.5 years), were studied for this protocol approved

by the Research Ethics Committee of the Montreal Neurological Institute and Hospital. Informed written consent was obtained from each volunteer.

PET measurement

PET studies were performed on the ECAT EXACT HR$^+$ (CTI/Siemens) whole-body tomograph, operating in a 3D acquisition mode, with a transverse resolution of 4.5-5.8 mm and an axial resolution of 4.9-8.8 mm (Adam et al., 1997). The images were reconstructed as 128×128 matrices of 2 mm×2 mm pixels using filtered back-projection with an 8 mm Hanning filter (FWHM). Reconstructed images were corrected for random and scattered events, detector efficiency variations and dead-time. Three orbiting rod transmission sources, each containing about 5 mCi of ^{68}Ge, were used for attenuation correction.

The subjects were positioned in the tomograph with their heads immobilized by means of a customized headholder (Vac-Lock; MED-TECH). A short indwelling catheter was placed into the left radial artery for blood sampling and blood gas examination. Arterial blood radioactivity was automatically sampled, corrected for delay and dispersion (Vafaee et al. 1996), and calibrated with respect to the tomograph using samples obtained manually during the last sixty seconds of each 3-min scan. At the start of each scan, the subjects inhaled 20 mCi of ^{15}O-O_2 in a single breath. $CMRO_2$ was calculated using the two compartment, weighted integration method (Ohta et al., 1992). Each subject also underwent a magnetic

resonance imaging (MRI) examination on a Philips Gyroscan ACS (1.5 T) superconducting magnet system for structural-functional (MRI-PET) correlation. The MRI image was a T1-weighted, 3D FFE (fast field echo) sequence consisting of 160 256×256 sagittal slices of 1mm thickness.

Stimulus conditions

The stimulus was generated with a Silicon Graphics (SGI) workstation and presented via a 21-inch NEC monitor (MultiSync XP21) with a synchronization range of 31 to 89 kHz (horizontal) and 55 to 160 Hz (vertical), and a temporal resolution of 55 to 83 Hz. It consisted of a yellow-blue annular checkerboard with an outer diameter of 13.5 cm and an inner diameter of 0.5 cm. It contained six concentric rings, each ring consisting of a total of 36 segments of equal size, alternating in intensity (yellow and blue). The dimensions of the outermost segments were 8 mm peripherally and 12 mm axially. A cross-hair (0.5 cm) was located at the center of the circle. The stimulus was presented at about 17^0 of visual angle (40-45 cm from the eyes) and its contrast was reversing at specified frequencies. In the baseline condition, the subjects were asked to fixate on a cross-hair in the center of the screen 30 s before the scan, and throughout the subsequent 3-min scan. In seven successive activation conditions, the subjects were shown a blue-yellow annular checkerboard reversing its contrast at frequencies of 0, 1, 4, 8, 16, 32 and 50 Hz. Six of the subjects were shown the stimulus in ascending order

(baseline, 0, 1, 4, 8, 16, 32 and 50 Hz) while the other six were shown the stimulus in descending order (baseline, 50, 32, 16, 8, 4, 1 and 0 Hz). Stimulation began 4 minutes before the start of the dynamic PET scan, and continued throughout the following 3-min scan for a total of 7 min. There was a minimum of 15 minutes time gap between each scan. Black drapes were used to create a dark environment around the screen.

Data analysis

MR images were transformed into stereotaxic coordinates (Talairach and Tournoux, 1988) by means of an automatic registration algorithm (Collins et al., 1994). The reconstructed PET images were co-registered with the subjects' MRI scans using an automatic registration program based on the Automatic Image Registration algorithm (Woods et al., 1992). For this purpose, the sum of the PET images across all frames was calculated for each scan. Then, the MRI image was aligned with the summed PET image. To correct for between-scan subject movements, automatic PET-to-PET registration was also performed (Woods et al., 1993). This method uses the first PET scan (summed across frames) as the registration target for each subsequent summed PET scan. The global cerebral metabolic rates of oxygen ($CMRO_2$) were determined for each subject by means of a binarized brain mask which filters out all extracerebral voxels. This mask was created by thresholding and manually editing the average MRI of 305 normal brains scanned at the

Montreal Neurological Institute. The global $CMRO_2$ for each subject was then determined by averaging the values of all intracerebral voxels. The reconstructed PET images were then normalized for global $CMRO_2$ and averaged across subjects, transformed into stereotaxic coordinates and blurred with a Gaussian filter of 22 mm×22 mm×22 mm×. Mean subtracted image volumes (stimulation minus baseline) were obtained and converted to z-statistic volumes by dividing each voxel by the mean standard deviation of the normalized subtraction image obtained by pooling the SD across all intracerebral voxels. Significant focal changes of $CMRO_2$ were identified by a method based on 3-D Gaussian random field theory (Worsley et al., 1996). Values equal to or exceeding a criterion of z=3.5 were deemed statistically significant ($p < 0.00046$, two-tailed, uncorrected). Correcting for multiple comparison, a z-value of 3.5 yields a false positive rate of 0.26 in 70 resolution elements, each of which has dimensions 22×22×22 mm^3. This approximates the total volume of brain scanned ($2.2\times2.2\times2.2\times70=750cm^3$).

Results

The mean global $CMRO_2$ values of the twelve subjects at the seven stimulus frequencies are shown in Fig. 1. A one-factor ANOVA showed that there was no significant effect of scanning condition on $CMRO_2$ ($F=0.15$; $p>0.5$).

In contrast, regional $CMRO_2$ in primary visual cortex (Fig. 2) varied as a

function of stimulus frequency. As shown in Fig. 3, $CMRO_2$ in primary visual cortex increased as the stimulus frequency increased, peaking at 4 Hz, and then dropped off sharply at higher frequencies. Table 1 shows the z-values and p-values for significant peaks obtained for different frequencies. A one-factor ANOVA performed on the absolute regional $CMRO_2$ values derived from a region of interest (primary visual cortex) for all frequencies resulted in F=3.55 and $p<0.05$, thus confirming that there is a significant difference between those values. In addition, post-hoc pairwise comparisons were performed on the absolute $CMRO_2$ values using a paired t-test. As a result, a statistically significant difference was found between the values of 4 and 1 Hz ($p<0.05$). The test also showed that there is no significant difference between the values of 0 and 8 Hz ($p=0.7$) while there were significant differences between the $CMRO_2$ values for these frequencies and those at 1 Hz ($p<0.005$). Moreover, the test showed that there were no significant differences between the $CMRO_2$ values of 16, 32 and 50 Hz ($p=0.98$).

We ascertained that the order of presentation of the stimulus did not alter the final values of $CMRO_2$ (global and regional) by performing a two-factor ANOVA. The test showed that there was no statistically significant difference between the $CMRO_2$ values when stimulus frequency was presented in different orders (F=0.38; $p>0.5$).

Discussion

A direct relationship between stimulation rate and cerebral metabolic rate of glucose (CMR_{glc}) has been reported in both the peripheral nervous system (Toga and Collins, 1981) and the central nervous system of rats (Yarowsky et al., 1983). The effect of stimulus rate on cerebral blood flow (CBF) in humans was also studied by several investigators. Studies of human auditory cortex have shown a linear dependence of CBF on the rate of auditory stimulation (Price et al., 1992). In addition, in the motor system, different repetition rates of finger and eye movements have led to rate-dependent changes in CBF (Sadato et al., 1996; Paus et al., 1995). In this laboratory, we have also observed a linear relationship between the direct stimulation of the human cerebral cortex by means of transcranial magnetic stimulation (TMS) and rCBF (Paus et al., 1997). Moreover, the relationship between stimulation rate and CBF change in human visual cortex has been investigated using positron emission tomography (Fox and Raichle, 1984 and 1985).

The purpose of this study was to determine which relation, if any, existed between frequency as an indicator of neuronal work and $rCMRO_2$ as an index of oxidative metabolism. In essence, we tested the hypothesis that oxidative metabolism must be elevated when activated by an adequate stimulus, "adequate" classically referring to the stimulus to which the system responds maximally.

Biochemical evidence suggests that visual neurons differ in their capacity to sustain oxidative phosphorylation. The staining pattern in primary visual cor-

tex (V1) for the mitochondrial enzyme cytochrome oxidase (COX) (Horton, 1984; Wong-Riley and Carroll, 1984) reflects such a specialization. This pattern reveals an organization of neurons in the superficial layers III and II into the so-called "blobs" and "inter-blobs". We showed previously that following the activation of visual cortex with a chromatically rich stimulus, i.e. a yellow-blue reversing checkerboard, $CMRO_2$ rose markedly in primary visual cortex (Marrett et al. 1995; Vafaee et al., 1996 and 1998: Marrett and Gjedde, 1997). The high abundance in the visual cortex of color-sensitive neurons rich in COX was a possible explanation for this finding. These measurements of $CMRO_2$ were made after sustained (7 minutes) stimulation of the visual cortex. The observed increases in $CMRO_2$ appeared to be stimulus specific since simple photic stimulation with Grass eye goggles, i.e. an array of red LEDs flashing at 8 Hz, failed to induce significant increases of $CMRO_2$ (Fujita et al., 1992, 1993; Ribeiro et al., 1993). Since the same method of $CMRO_2$ determination was used in the latter studies, the observed increases in $CMRO_2$ in the visual cortex might be associated with the ability of the chromatically rich stimulus to activate the cytochrome oxidase rich neurons (blobs) which seem to be involved in color processing.

It has been reported that the response of retinal ganglion cells directly depends on the temporal frequency of the flicker (Henkes and Van Der Tweel, 1964; Schickman, 1981). The term flicker was referred to as a pattern of illumination on the retina, some portion of it being turned on and off or having its intensity

modulated with time. Bartley, in 1937, studied the retinal reponse via optic nerve discharges and found that, as the interval between successive photic pulses was shortened, the latency of discharges was lengthened (Bartley, 1937b and 1968). This continued up to a certain rate, then, as the intervals between pulses were further shortened, the latency began to decrease. Bartley assumed that this phenomenon was evidence for the receptor-bipolar-ganglion cell chains being able to follow the input rate only up to certain limit. Other investigators have also demonstrated that, following electric and photic stimulation of postretinal visual structures, evoked potentials of the visual system became a function of temporal frequency of stimulation (Bartley, 1968; Movshon et al., 1978) which, in humans, peaked around the alpha-rhythm activity of 8-10 Hz. The frequency-dependent changes of blood flow in visual cortex reported by Fox and Raichle are in agreement with the fact that cerebral blood flow is an index of neuronal activity, and their finding that CBF peaks around 8 Hz is a confirmation for the findings discussed above.

Our results show that, for the present stimulus, $CMRO_2$ in the visual cortex varies as a function of stimulus frequency. Unlike rCBF, which has been observed to peak at 8 Hz (Fox and Raichle, 1984 and 1985), $rCMRO_2$, in this study, reached its peak at 4 Hz and dropped off at higher frequencies. Based on our findings, we speculate that two limitations may operate in the tissue. A primary limitation (physiologic) is imposed by the finite oxygen diffusibility in the brain tissue (Kas-

sissia et al., 1995). This limitation is a result of the barrier-limited oxygen transfer to brain across cerebral capillaries. From human studies showing increased blood flow during stimulation of visual cortex (Fox et al. 1985; Marrett et al., 1997), we hypothesize that this limitation is overcome whenever blood flow increases sufficiently to raise the average oxygen tension in capillary blood. However, previous studies have also shown that, even when the limit to increased oxygen delivery has been lifted by an increase of blood flow, oxygen consumption does not always rise under conditions accompanied by increased blood flow. We speculate that this secondary limitation (enzymatic) represents a cellular mechanism that causes the brain not to fully sustain the increase of $CMRO_2$ made possible by the blood flow increase. The current results suggest that such a secondary limitation could be overcome by increasing the stimulus load. In this context the term stimulus "load" refers to the integration of the stimulus effects on the system as a function of time and intensity. We, therefore, hypothesize that a blood flow increase accompanying the stimulus frequency of 4 Hz permits the $CMRO_2$ to increase to the observed value. When the frequency of the stimulus increases above 4 Hz, neuronal work no longer requires the $CMRO_2$ to rise. Thus, we claim that the two limitations appear to operate in the tissue are a limitation which is lifted in proportion to stimulus load, the variable which integrates length, strength, and kind of stimulation applied, following a basic oxygen diffusibility limitation which is lifted when blood flow is raised.

It should be noted that we had previously reported a significant $CMRO_2$ change at 8 Hz with the same visual stimulus (Vafaee et al. 1996 and 1998). That study, however, had been carried out using a single stimulation frequency (8 Hz) unlike the present experiment which was especially designed to explore the frequency response (tuning curve) to the same visual stimulus used before. Furthermore, the previous study was performed on an older 2D acquisition tomograph (Scanditronix PC-2048 15B) while, for the present study, a state-of-the-art 3D machine (ECAT EXACT HR^+ CTI/Siemens) with a five to seven times larger sensitivity was used. Therefore, the Gaussian filter, which was employed to enhance the signal-to-noise ratio of an image (due to low count rates), was not the same for the two studies, given the entirely different noise characteristics of the two machines (2D vs. 3D). As a consequence, the $CMRO_2$ change at 8 Hz in the present study failed to be significant although the activation peaks were apparent upon visual inspection.

In conclusion, the ability of brain neurons to increase oxygen use may depend on the specific task the neurons perform, and the stimulus load imposed on the brain tissue must exceed a certain threshold before glycolysis is augmented by increased oxidative metabolism.

Legends to Figures

Figure 1: Change in global $CMRO_2$ ($\pm$SD) as a function of checker board contrast reversal frequency.

Figure 2: Averaged PET subtraction images of $CMRO_2$ superimposed upon averaged MRI images. Subtraction of control from activation state yielded the focal changes in $CMRO_2$ shown as z-statistic images. Figure 2A shows the focal $CMRO_2$ changes in primary visual cortex (occipital pole) for a frequency of 4 Hz, and Figure 2B shows a PET $CMRO_2$ image superimposed on averaged, rendered MRI image (4 Hz).

Figure 3: Change in $rCMRO_2$ ($\pm$SD) in primary visual cortex as a function of checkerboard contrast reversal frequency.

Table 1: Z-values and corresponding *p*-values of significant activation peaks in primary visual cortex (stimulation - baseline) in response to stimulation by yellow-blue checkerboard (x=9; y=-89; z=-1).

Reversal rate (Hz)	z-value	*p*-value
0	1.9	0.07
1	3.5	0.005
4	4.6	0.0004
8	2.0	0.06
16	0.9	0.36
32	0.7	0.48
50	0.8	0.42

Figure 1:

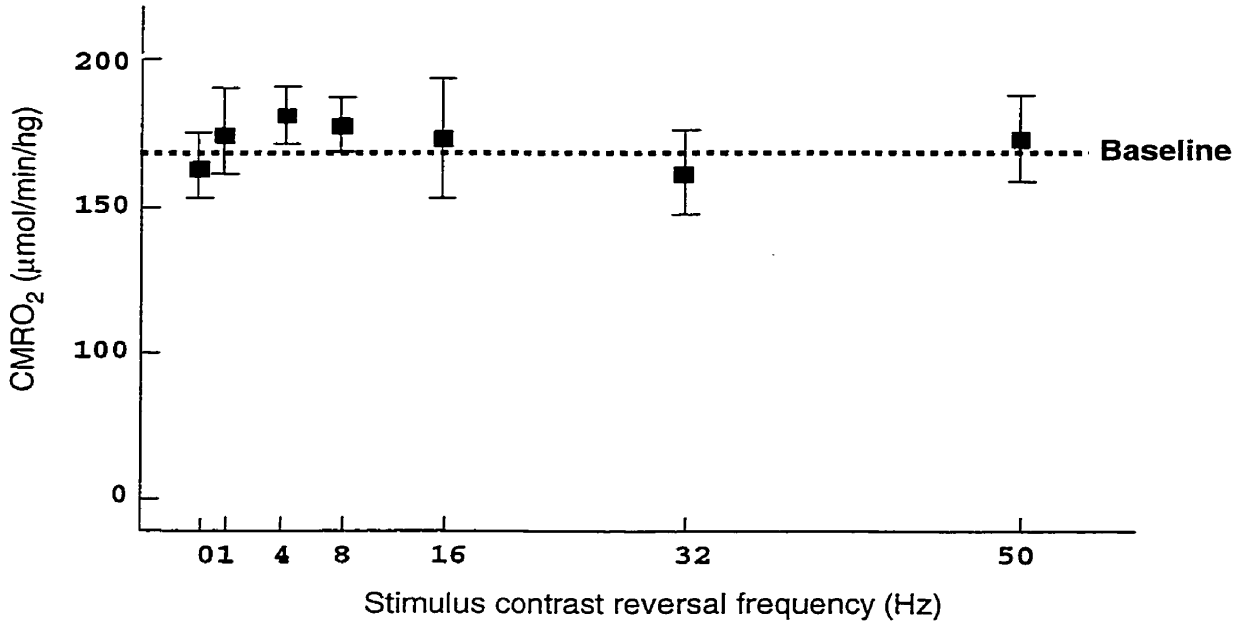
200
150
100
0
$CMRO_2$ (µmol/min/hg)
Baseline
01
4
8
16
32
50
Stimulus contrast reversal frequency (Hz)

Figure 2:

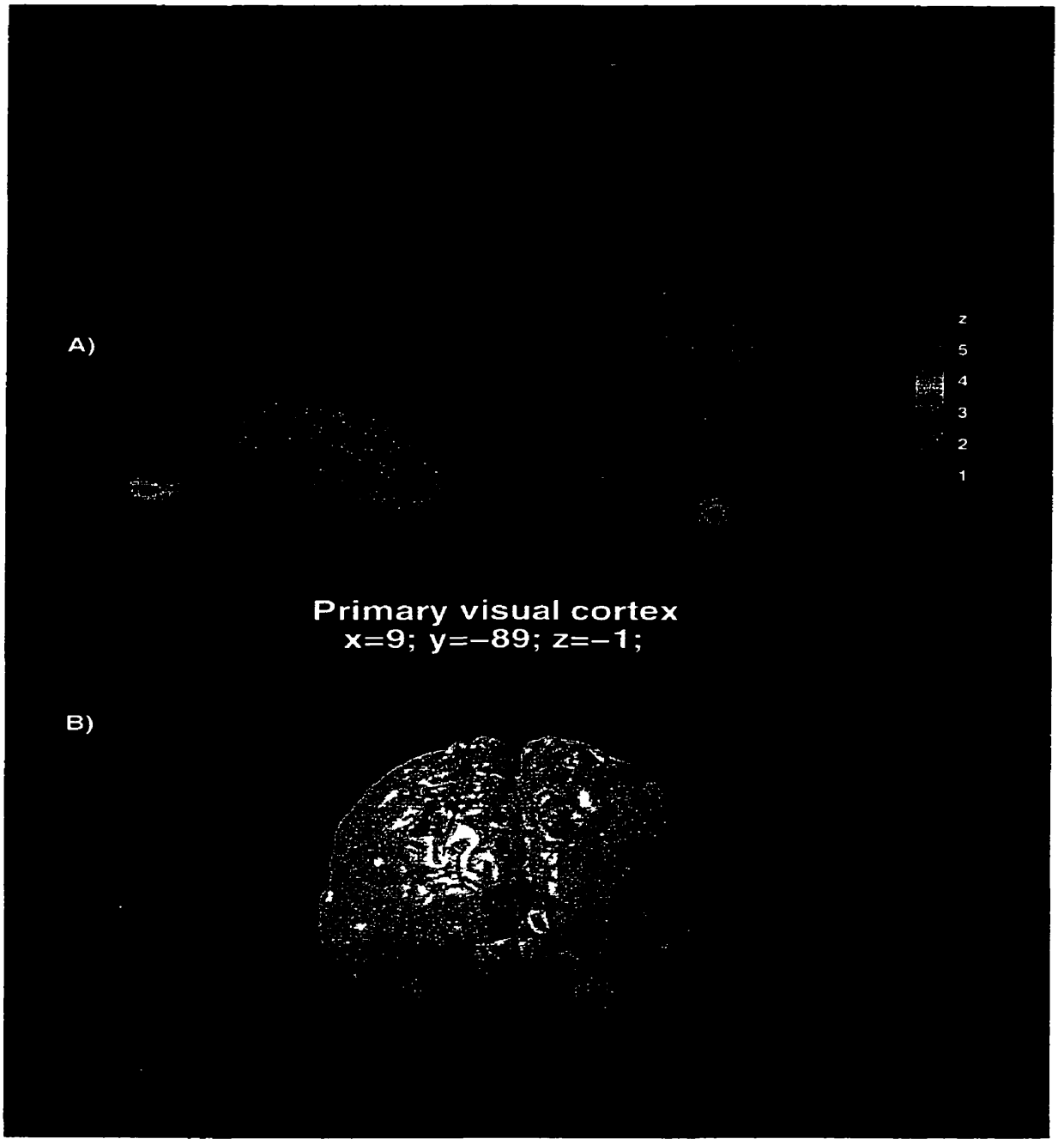

Figure 3:

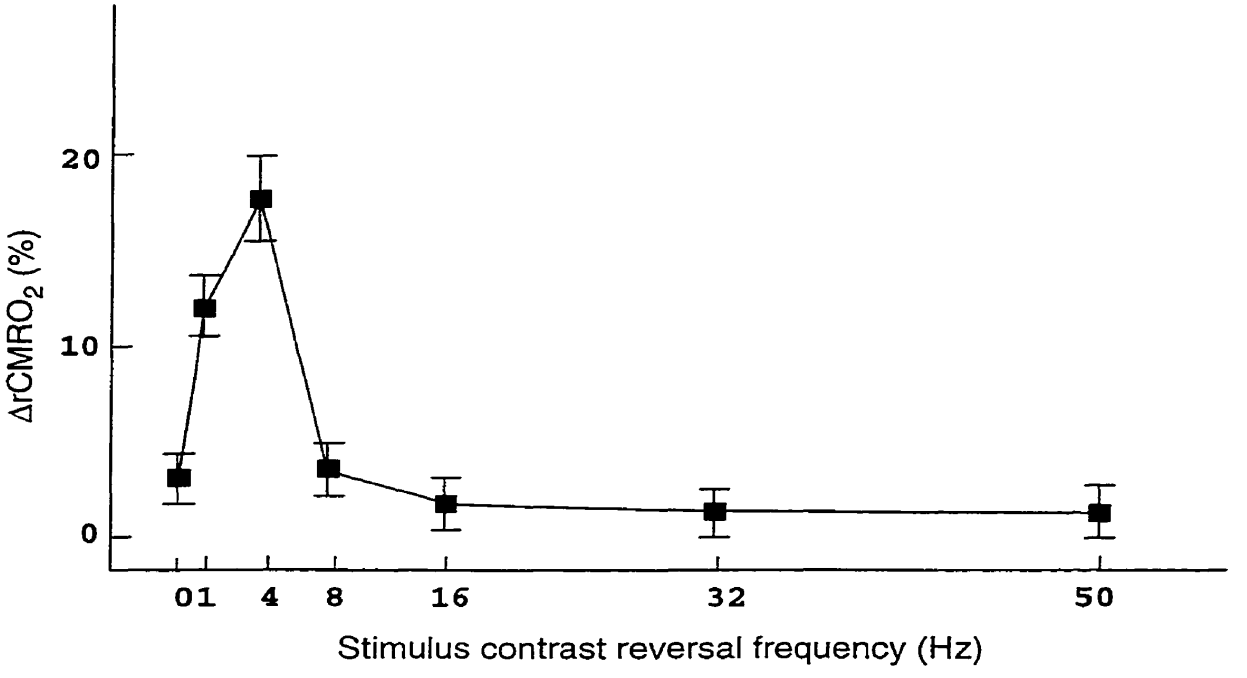
20
10
0
ΔrCMRO2 (%)
01
4
8
16
32
50
Stimulus contrast reversal frequency (Hz)

Rationale for the design of the experiment III

Following experiments I and II in which we studied the behavior of the oxygen consumption in the visual cortex as a consequence of stimulation with specially designed stimulus, we wanted to extend further our investigation by studying the behavior of the oxidative breakdown of glucose in the visual cortex. This could be achieved by measuring the Oxidative Index (OI), defined as the ratio of the $CMRO_2/CBF$. This index will also yield information regarding blood-oxygenation-level-dependent MR signal (BOLD). Moreover, we intended to test a model which accounts for the discrepant changes of oxygen consumption and blood flow during the neuronal activation. For this purpose, we slightly changed the design of the experiment II and measured $CMRO_2$ in the baseline condition and three different activation states (1, 4, and 8 Hz) as well as CBF.

CHAPTER 4

Increase of oxygen consumption in visual cortex consistent with model of oxygen delivery

M.S. Vafaee, and A. Gjedde

(Submitted to the J Cereb Blood Flow Metab)

Abstract

The changes of the cerebral metabolic rate of oxygen ($CMRO_2$) and cerebral blood flow (CBF) in response to excitation can be evaluated by calculation of an Oxidative Index (OI), equal to the $CMRO_2$/CBF ratio. This index yields information about the degree of flow-metabolism coupling prevailing in specific areas of the brain during physiological stimulation, and predicts the magnitude of the expected BOLD (blood oxygenation level dependent) phenomenon. To evaluate the changes of the OI in response to visual stimulation, we studied the relationships between the flicker rate of the visual stimulus, and the magnitudes of CBF, and $CMRO_2$ in the human brain. We measured cerebral blood flow and cerebral metabolic rate of oxygen in twelve healthy normal volunteers with positron emission tomography (PET). Subjects viewed a yellow-blue annular checkerboard reversing contrast at a frequency of 1, 4, or 8 Hz. Stimulation began four minutes before and continued throughout the 3-min dynamic scan. In the baseline condition, the subjects fixated a cross-hair from 30 s before until the end of the 3-min scan. The magnitude of CBF in the primary visual cortex increased as a function of the checkerboard contrast reversal rate, and was maximized at the flicker frequency of 8 Hz (Z=16.0), while the magnitude of $CMRO_2$ peaked at 4 Hz (Z=4.0). As a consequence, the OI was lower at 8 Hz than at 1 and 4 Hz, in contrast to the oxidative metabolic rate which had its maximum at 4 Hz.

Introduction

The human brain consumes glucose and oxygen in stoichiometric proportion. The substrates are continuously supplied via the cerebral circulation and the mechanism linking neuronal activity to the circulation is generally believed to constitute a flow-metabolism couple. This couple is commonly said to satisfy the principle of Roy and Sherrington (Roy and Sherrington, 1890) which is usually interpreted to mean that changes of cerebral blood flow subserve a tight coupling between cellular energy requirements and the supplies of glucose and oxygen to the brain (Gjedde, 1997). Several studies have revealed significant increases of $CMRO_2$ in the striate cortex in response to a visual stimulation (Marrett and Gjedde, 1997; Vafaee et al., 1998; Vafaee et al., 1999). However, other studies reported an unexpected mismatch between changes of CBF and $CMRO_2$ during certain kinds of stimulation believed to represent functional activation of the human brain (Fox and Raichle, 1986, 1988; Fujita et al., 1992 and 1993; Ribeiro et al., 1993; Ohta et al., 1999; Fujita et al. 1999). The discrepancy between changes of blood flow and oxygen and glucose consumption during different kinds of stimulation suggests that the mechanism underlying the flow-metabolism couple is poorly understood. We assume that the increased blood flow reflects a degree of metabolic activation. Oxygen transport from blood to brain tissue is significantly limited by hemoglobin binding and possibly by other factors as well, including a specific resistance at the endothelium of brain capillaries (Gjedde et al. 1991; Kassissia et al. 1995). We

(Gjedde et al. 1991) proposed that, in the absence of recruitment, increased blood flow would be required to raise oxygen delivery and formulated a model of the relationship between blood flow and oxygen delivery (1997). According to this model, oxygen consumption depends exclusively on the delivery of oxygen when the tension of oxygen in mitochondria is negligible compared to the average capillary tension. The mean oxygen tension in the capillary then drives the oxygen delivery and hence the oxygen consumption. When more oxygen is needed, the oxygen extraction must decline to raise the average capillary oxygen tension to the magnitude required to drive the needed oxygen into the tissue (Widen, 1991). This assumes that there is little recruitment of capillaries capable of reducing the diffusion distance in the tissue or increasing the intrinsic permeability of the capillary endothelial wall (Kuschinsky and Paulson, 1992; Connett et al., 1985; Ohira and Tabata, 1992).

The purpose of this study was to test the hypothesis that the decline of the oxidative index, indicative of the BOLD phenomenon, correctly predicts the degree of metabolic activation of brain tissue. According to the model, at steady-state, the oxygen consumption is given by:

$$R = FEC_a \tag{1}$$

where R is the net oxygen consumption, F blood flow, E the unidirectional oxygen extraction fraction, equal to the net oxygen extraction fraction when the tissue

oxygen tension is negligible, and C_a the arterial oxygen concentration. The unidirectional delivery of oxygen is a function of the average capillary oxygen tension:

$$J = LP_{cap} \tag{2}$$

where J is the influx of oxygen, L (in units of μmol·hg^{-1}·min^{-1}·mmHg^{-1}), the average tissue conductivity of oxygen transport between the capillary lumen and the mitochondria and P_{cap} the average capillary oxygen tension. The mitochondrial oxygen tension derived from the tissue conductivity of oxygen (L) is:

$$P_{brain} = P_{cap} - \frac{R}{L} \tag{3}$$

where P_{brain} is the oxygen tension at the site of oxygen consumption. The net extraction defines the average capillary hemoglobin saturation with oxygen, assuming even delivery of the oxygen along the capillary length:

$$S_{cap} = 1 - \frac{E}{2} \tag{4}$$

where S_{cap} is the mean capillary hemoglobin oxygen saturation. The net extraction also defines the mean venous hemoglobin oxygen saturation:

$$S_{ven} = 1 - E \tag{5}$$

where S_{ven} is the venous hemoglobin oxygen saturation. The oxygen tension and hemoglobin saturation with oxygen are related by the Hill equation of the oxygen dissociation curve:

$$S = \frac{1}{1 + [\frac{P_{50}}{P_{O_2}}]^h} \tag{6}$$

where P_{50} is the hemoglobin half-saturation oxygen tension and h is the Hill-coefficient of the oxygen dissociation curve. The solution to the above relationships is:

$$R = LP_{50}[(\frac{2}{E} - 1)^{1/h} - P_{brain}] \tag{7}$$

Defining the fraction η as the ratio between P_{brain} and P_{ven}, the venous oxygen tension, the brain oxygen consumption is also:

$$R = LP_{50}[(\frac{2}{E} - 1)^{1/h} - \eta(\frac{1}{E} - 1)^{1/h}] \tag{8}$$

where η is a venous "equilibration index". When this index is nil, the mitochondrial oxygen tension is zero at the far end of the diffusion path and the oxygen consumption equals the oxygen delivery, i.e.:

$$L = \frac{R}{P_{50}(\frac{2}{E} - 1)^{1/h}} \tag{9}$$

When R and E are known, and η is assumed to be nil, L can be calculated from equation (9). When R, E, and L are known, η can be calculated from equation (8) as follows:

$$\eta = \frac{LP_{50}(\frac{2}{E} - 1)^{1/h} - R}{LP_{50}(\frac{1}{E} - 1)^{1/h}} \tag{10}$$

The goal of the present experiment was to determine the significance of the flicker frequency on changes of $CMRO_2$ and CBF, using the previously tested yellow-blue contrast-reversing checkerboard. This enabled us to evaluate the Oxidative Index (OI), defined as the $CMRO_2$/CBF ratio. As an index of the oxidative

breakdown of glucose prevailing in specific areas of the brain during physiological stimulation, this index predicts the BOLD phenomenon for a given stimulus. When F, L, E, and η are known, the OI can be shown to depend on several factors in addition to F and E, including P_{50} and h which are sensitive to numerous physiological influences.

$$OI = \frac{LP_{50}}{F}\left[\left(\frac{2}{E}-1\right)^{1/h} - \eta\left(\frac{1}{E}-1\right)^{1/h}\right] \tag{11}$$

Materials and Methods

Twelve healthy normal volunteers (6 males and 6 females), aged between 19 and 28 years (mean 23±3 (SD) years), were studied for this protocol approved by the Research Ethics Committee of the Montreal Neurological Institute and Hospital. Informed written consent was obtained from each volunteer.

PET Measurements

PET studies were performed on the ECAT EXACT HR$^+$ (CTI/Siemens) whole-body tomograph, operating in a 3D acquisition mode, with a transverse resolution of 4.5-5.8 mm and an axial resolution of 4.9-8.8 mm (Adam et al., 1997). The images were reconstructed as 128×128 matrices of 2 mm×2 mm pixels using

filtered back-projection with an 8 mm Hanning filter (FWHM). Reconstructed images were corrected for random and scattered events, detector efficiency variations and dead-time. Three orbiting rod transmission sources, each containing about 5 mCi of ^{68}Ge, were used for attenuation correction.

The subjects were positioned in the tomograph with their heads immobilized by means of a customized headholder (Vac-Lock; MED-TECH). A short indwelling catheter was placed into the left radial artery for blood sampling and blood gas examination. Arterial blood radioactivity was automatically sampled, corrected for delay and dispersion (Vafaee et al., 1996), and calibrated with respect to the tomograph using samples obtained manually during the last sixty seconds of each 3-min scan. At the start of each $CMRO_2$ scan, the subjects inhaled 20 mCi of ^{15}O-O_2 in a single breath, while at the start of each CBF scan, they were injected 10 mCi of $H_2{}^{15}O$ intravenously. $CMRO_2$ and CBF were calculated using the two compartment, weighted integration method (Ohta et al., 1992, 1996). Each subject also underwent a magnetic resonance imaging (MRI) examination on a Philips Gyroscan ACS (1.5 T) superconducting magnet system for structural-functional (MRI-PET) correlation. The MRI image was a T1-weighted, 3D fast-field echo sequence consisting of 160 256×256 sagittal slices of 1mm thickness.

Stimulus Conditions

The stimulus was generated with a Silicon Graphics (SGI) workstation and

presented through a 21-inch NEC monitor (MultiSync XP21) with a synchronization range of 31 to 89 kHz horizontal, 55 to 160 Hz vertical, and a temporal resolution of 55 to 83 Hz. It consisted of a yellow-blue annular checkerboard with a diameter of about 17^0 of visual angle (the detailed explanation of the stimulus was discussed in Vafaee et al., 1998b). In the baseline condition, the subjects were asked to fixate on a cross-hair in the center of the screen 30 s before the scan, and throughout the subsequent 3-min scan. In three successive activation conditions, the subjects were shown a blue-yellow annular checkerboard reversing its contrast at frequencies of 1, 4, and 8 Hz. The order of baseline and stimulus presentation was randomized. Stimulation began 4 minutes before the start of the dynamic PET scan, and continued throughout the following 3-min scan for a total of 7 min. There was a time gap of at least 15 minutes between each scan. Black drapes were used to create a dark environment around the screen.

Data Analysis

MR images were transformed into stereotaxic coordinates (Talairach and Tournoux, 1988) by means of an automatic registration algorithm (Collins et al., 1994). The reconstructed PET images were co-registered with the subjects' MRI scans using an automatic registration program based on the Automatic Image Registration algorithm (Woods et al., 1992). For this purpose, the sum of the PET images across all frames was calculated for each scan. Then, the MRI image was aligned with

the summed PET image. To correct for between-scan subject movements, PET-to-PET automatic registration was also performed (Woods et al., 1993). This method uses the first PET scan (summed across frames) as the registration target for each subsequent summed PET scan. The global cerebral metabolic rates of oxygen ($CMRO_2$) were determined for each subject by means of a binarized brain mask which filters out all extracerebral voxels. This mask was created by thresholding and manually editing the average MRI of 305 normal brains scanned at the Montreal Neurological Institute. The global $CMRO_2$ for each subject was then determined by averaging the values of all intracerebral voxels. The reconstructed PET images were then normalized for global $CMRO_2$ and averaged across subjects. Mean subtracted image volumes (stimulation minus baseline) were obtained and converted to z-statistic volumes by dividing each voxel by the mean standard deviation of the normalized subtraction image obtained by pooling the SD across all intracerebral voxels. Significant focal changes of $CMRO_2$ were identified by a method based on 3-D Gaussian random field theory (Worsley et al., 1996). Values equal to or exceeding a criterion of Z=3.5 were deemed statistically significant ($P < 0.00046$, two-tailed, uncorrected). Correcting for multiple comparison, a Z-value of 3.5 yields a false positive rate of 0.26 in 70 resolution elements, each of which has dimensions 22×22×22 mm. This approximates the total volume of cortex scanned ($2.2cm \times 2.2cm \times 2.2cm \times 70 = 750cm^3$). The $CMRO_2$ and CBF (primary visual cortex) for each subject were also determined by manually drawn

ROIs (region of interests) on PET images (registered on corresponding MRIs) in Talairach space.

Results

The global CBF and $CMRO_2$ values were determined for each subject. The mean global CBF and $CMRO_2$ values of the twelve subjects at the three stimulus frequencies and the baseline (Table 1) were analyzed for possible variances. An ANOVA test showed that there was no significant effect of scanning condition on CBF (F=0.8; $P>0.5$) and $CMRO_2$ (F=0.015; $P>0.5$).

In contrast, regional CBF and $CMRO_2$ in primary visual cortex (x=10; y=-89; z=-3) (Fig. 1) varied as a function of stimulus frequency. As shown in Fig. 2, the magnitude of CBF in the primary visual cortex increased as a function of checker-board contrast reversal rate, and peaked at 8 Hz (Z=16.0), while the magnitude of $CMRO_2$ in primary visual cortex increased as the stimulus frequency increased, peaked at 4 Hz (Z=4.0), and then dropped off at 8 Hz (Z=2.0) (Fig. 3). As a consequence, the magnitude of the OI was lower at 8 Hz than at 1 or 4 Hz (Fig. 4). A one-factor ANOVA test on the absolute regional CBF and $CMRO_2$ values derived from a region of interest for all three frequencies confirmed significant differences ($P<0.05$) among the values at 1, 4 and 8 Hz.

The magnitude of L was calculated according to equation (9) for baseline, 1 and 4 Hz because the baseline value of L did not satisfy the equation for $\eta=0$. For

8 Hz, L was calculated from the mean $\Delta L/\Delta$CBF ratio for 1 and 4 Hz. With this L, the venous equilibration index η was calculated from equation 10 (as listed in Table 2). Table 2 shows that L increased at both 1 and 4 Hz, indicating recruitment. At 8 Hz, the rise of η predicted that the tissue oxygen tension increased, implying an excessive increase of blood flow.

Discussion

It has been claimed that the rate of oxidative phosphorylation cannot instantaneously keep pace with the sevenfold increase of the rate of pyruvate production seen under the most extreme circumstances of glycolytic stimulation in the mammalian brain (Van den Berg and Bruntink, 1983). According to this claim, pyruvate and hence lactate must both rise, at least until oxidative phosphorylation eventually matches the metabolic requirement of the tissue. Recent measurements of oxygen consumption made during sensory and visual stimualtion of human cerebral cortex generally revealed little change of oxygen consumption during brief cortical stimulation (Fox and Raichle 1986; Seitz and Roland, 1992; Fox et al, 1988; Ribeiro et al. 1993). Yet, for reasons mainly in doubt, blood flow increased markedly.

A model of blood-brain transfer of oxygen was formulated to account for the discrepant changes of oxygen consumption and blood flow during neuronal excitation (Gjedde, 1997). A slightly different model was presented by Buxton and Frank (1997) who treated oxygen delivery to brain as a special case of the Crone model of blood-brain transfer (Crone, 1963).

Previously, it was shown that stimulation frequency is a significant determinant of regional cerebral blood flow (rCBF) in the visual cortex (Fox and Raichle, 1985), as well as in auditory and motor cortex (Price et al., 1992; Sadato et al., 1996). Recently, we also showed frequency-dependent changes of regional cere-

bral metabolic rate of oxygen ($rCMRO_2$) in visual cortex by means of positron emission tomography (Vafaee et al., 1999). The purpose of the present study was to test the use of the oxidative index (OI), defined as the $CMRO_2/CBF$ ratio, as an index of oxidative metabolism during stimulation of neuronal work. This use requires that the mitochondrial oxygen tension in cerebral tissue, indicated by the magnitude of the coefficient η, as well as a number of other factors, summarized in equation (11), be constant. For this purpose, we used the yellow-blue reversing checkerboard stimulus which has previously been shown to lead to a marked increase of $CMRO_2$ in primary visual cortex (Marrett and Gjedde, 1997; Vafaee et al., 1998). The results confirmed that the magnitude of $CMRO_2$ measured at 4 min of stimulation, does not vary as a simple function of stimulus frequency. Unlike rCBF, which was still rising at 8 Hz, $rCMRO_2$ in this study reached a peak at 4 Hz and dropped off at 8 Hz (Fig. 3). The consequence of the results was that the oxygen tension in the tissue was shown to remain negligible at 1 and 4 Hz, while it increased at 8 Hz, indicating that the OI (and hence the BOLD phenomenon) is not a faithful index of neuronal work.

The implications of our results are twofold. First, we have confirmed that oxidative metabolism is elevated when activated by an adequate stimulus, "adequate" classically referring to the stimulus to which the system responds maximally (Vafaee et al., 1999).

The model used to account for oxygen delivery is based on the claim that oxy-

gen transfer to brain across cerebral capillaries occurs in a barrier-limited fashion (Kassissia et al., 1995). It is overcome whenever blood flow increases sufficiently to raise the average oxygen tension in capillary blood. When the barrier to increased oxygen delivery is lifted by the increase of blood flow, the increased blood flow is accompanied by increased oxygen consumption under some conditions. Neither constant L nor constant or negligible η satisfied the model in all 4 situations. According to the model, when the mitochondrial oxygen tension is negligible at the far end of the diffusion path, the predicted relationship satisfies the equation (9). This equation describes a straight line with a zero ordinate intercept. When equation (9) was applied to the existing data and solved for L, the diffusibility of oxygen was calculated for the conditions 1 and 4 Hz (Table 2). Using the average diffusibility increase to predict the magnitude of η during visual stimulation at 8 Hz, we conclude that neither constant L nor constant η satisfied the model. The model was consistent with the measured oxygen consumption when L was allowed to rise as an indication of recruitment.

Second, the results were in agreement with the model at 8 Hz stimulation only if η, the venous equilibration index was allowed to rise. We speculate that a cellular mechanism acted as a second rate-limiting factor, preventing the cells from fully sustaining the increase of $CMRO_2$ allowed by the blood flow increase. This secondary block is perhaps overcome only by an adequate stimulus "load" which refers to the sum of the stimulus effects on the system as a function of time and

intensity.

As shown in Fig. 3. the oxygen consumption curve drawn on the basis of the CBF tuning curve (Fig. 2) for η=0, predicts a further $CMRO_2$ enhancement at a flicker frequency of 8 Hz. Thus, at frequencies of 1 and 4 Hz, the magnitude of $CMRO_2$ can be predicted from the model with η=0, while a higher than negligible level of oxygen resulted at 8 Hz. At 4 Hz, we claim that the excess of blood flow (perhaps because of capillary recruitment) assisted the $CMRO_2$ enhancement. As the frequency of the stimulus increased further, tissue factors prevented $CMRO_2$ from increasing as predicted. Although enough blood is supplied to the brain, the stimulus load must exceed a threshold for oxidative phosphorylation to rise. In conclusion, two blocks appear to limit oxygen consumption, a tissue block which is lifted in proportion to the stimulus adequacy, the variable which integrates length, strength, and kind of stimulation applied, and an oxygen diffusibility block which is lifted when blood flow rises. The poor correlation at 8 Hz may also signify activation of other neurons supplied by a separate vascular bed with a lower capillary density and hence lower oxygen diffusibility. This differential response suggests that capillary density and oxygen diffusibility may be coupled to the steady-state oxygen demand for given populations of neurons.

We conclude that, changes of blood flow are less specifically coupled to an adequate stimulation of the visual cortex than are changes of oxygen consumption. Under some circumstances, this discrepancy can cause the oxidative index

and hence the blood-oxygenation-level-dependent signal to be a poor index of the physiological stimulation of a sensory system.

Legends to Figures

Figure 1: Averaged PET subtraction images of CBF and $CMRO_2$ superimposed upon averaged MRI images. Subtraction of control from activation state yielded the focal changes in CBF and $CMRO_2$ shown as z-statistic images. Figure 1A shows the focal CBF changes in primary visual cortex (occipital pole) for a frequency of 8 Hz , and Figure 1B shows the $CMRO_2$ changes in primary visual cortex (occipital pole) for a frequency of 4 Hz.

Figure 2: Measured cerebral blood flow in primary visual cortex as a function of checkerboard contrast reversal rate.

Figure 3: Measured and predicted (oxygen delivery model) cerebral oxygen consumption in primary visual cortex as a function of checkerboard contrast reversal rate.

Figure 4: Percentage changes of CBF, $CMRO_2$, and OI in primary visual cortex as a function of checkerboard contrast reversal rate.

Table 1: Average global CBF and $CMRO_2$ values as a function of checkerboard contrast reversal rate measured in twelve subjects.

Scan condition	CBF ($ml \cdot hg^{-1} \cdot min^{-1}$)	$CMRO_2$ ($\mu mol \cdot hg^{-1} \cdot min^{-1}$)
Baseline	$33 \pm 5^{\dagger}$	$181 \pm 12^{\dagger}$
1 Hz	36 ± 5	182 ± 13
4 Hz	36 ± 3	179 ± 19
8 Hz	35 ± 5	180 ± 12

†standard deviation

Table 2: CBF (ml·hg^{-1}·min^{-1}), $CMRO_2$ (μmol·hg^{-1}·min^{-1}), E_{O2}, P_{cap} (mm·Hg), L (μmol·hg^{-1}·min^{-1}·mmHg^{-1}), and η in visual cortex as a function of checkerboard contrast reversal rate. The tissue conductivity of oxygen (L) was calculated using Equation 9 (except for 8 Hz) and η (the ratio between P_{brain} and P_{ven}) was calculated from the value of L. CBF and $CMRO_2$ values were observed values for the primary visual cortex.

Scan condition	CBF	$CMRO_2$	E_{O2}	P_{cap}	L	η
Baseline	50±5.0†	280±12†	0.43±0.07 †	41	6.83	0.0
1 Hz	66±6.5	308±15	0.38±0.08	43.3	7.11	0.0
4 Hz	69±7.5	322±17	0.38±0.09	43.3	7.44	0.0
8 Hz	71±8.0	294±10	0.34±0.07	45.4	7.37‡	0.167

†standard deviation:

‡calculated from average $\Delta L/\Delta$CBF at 1 and 4 Hz:

Figure 1:

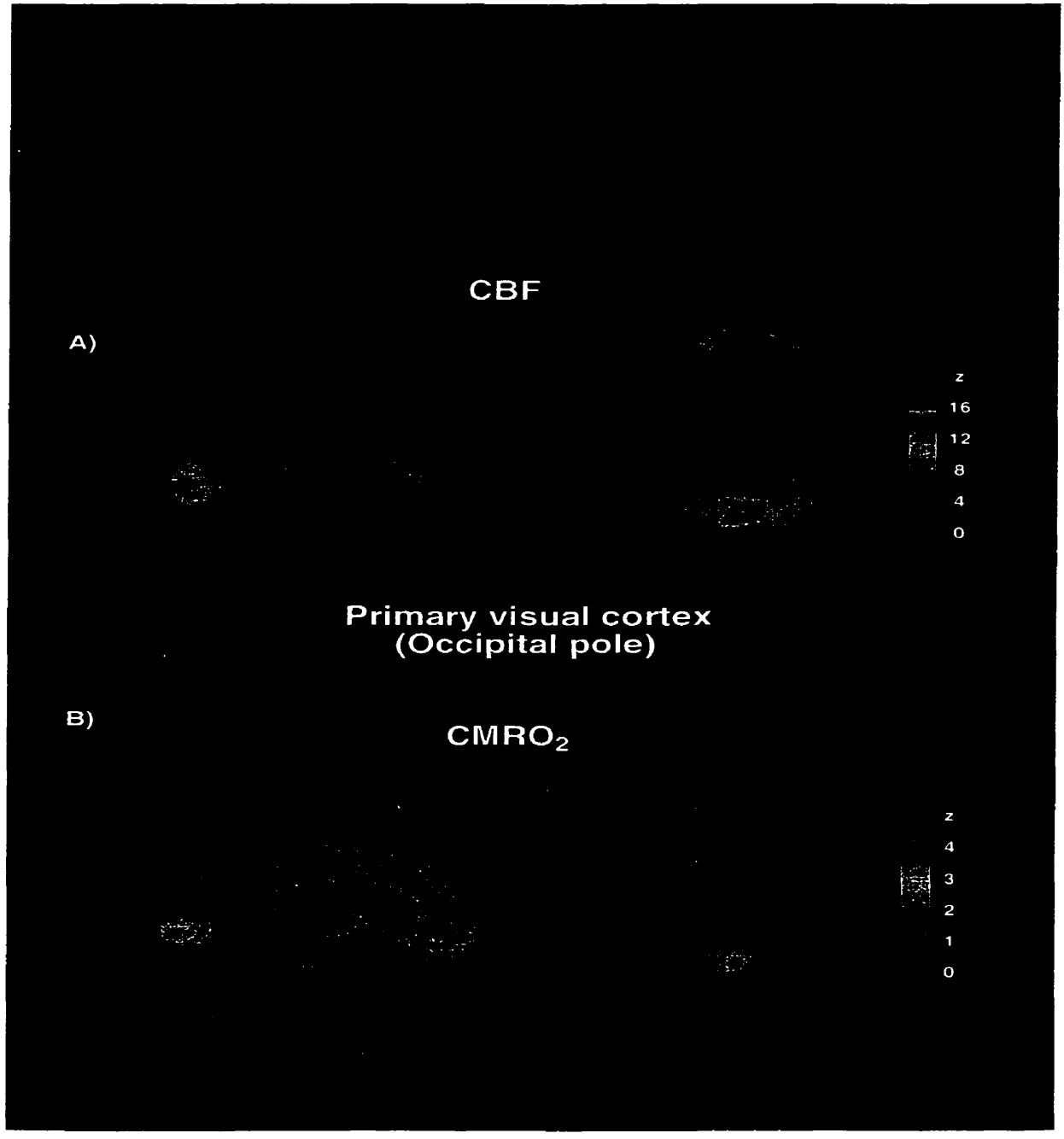
CBF
A)
z
16
12
8
4
0
Primary visual cortex
(Occipital pole)
B)
CMRO2
z
4
3
2
1
0

Figure 2:

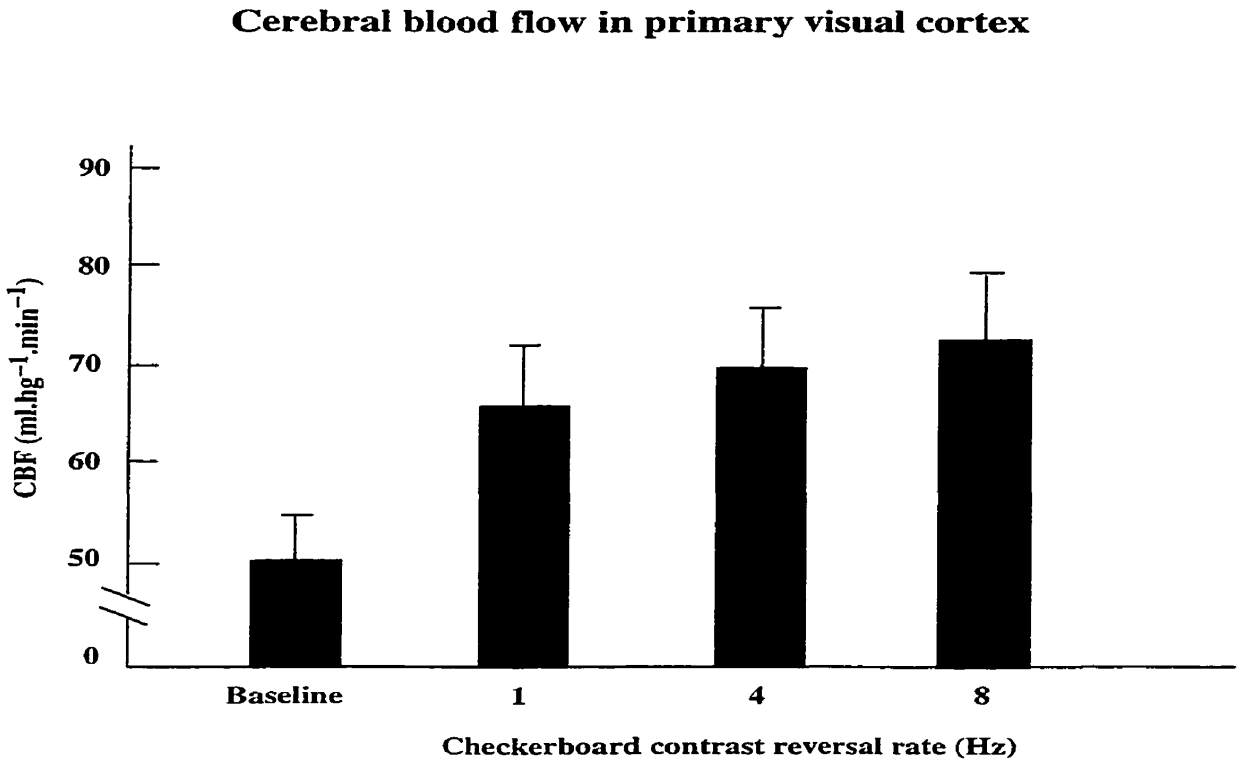
Cerebral blood flow in primary visual cortex
90
80
70
60
50
0
CBF (ml.hg^{-1}.min^{-1})
Baseline
1
4
8
Checkerboard contrast reversal rate (Hz)

Figure 3:

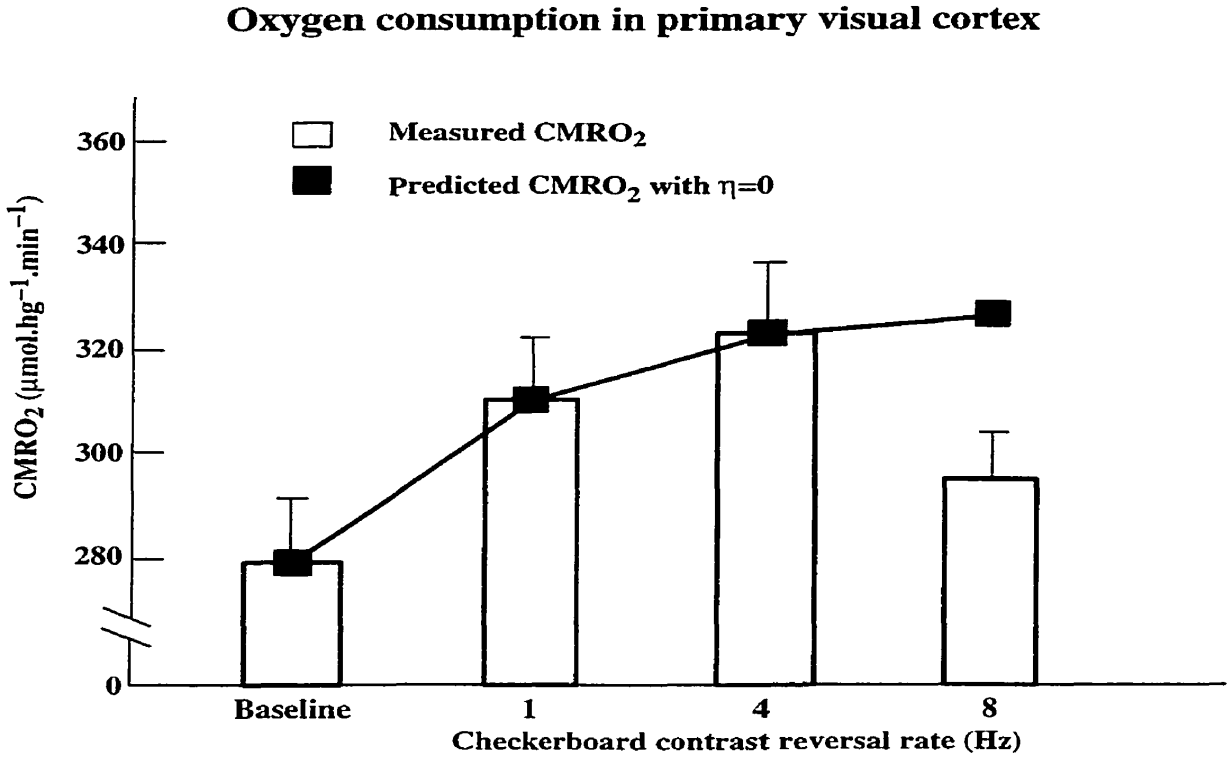
Oxygen consumption in primary visual cortex
Measured CMRO2
Predicted CMRO2 with η=0
CMRO2 (μmol.hg-1.min-1)
360
340
320
300
280
0
Baseline
1
4
8
Checkerboard contrast reversal rate (Hz)

Figure 4:

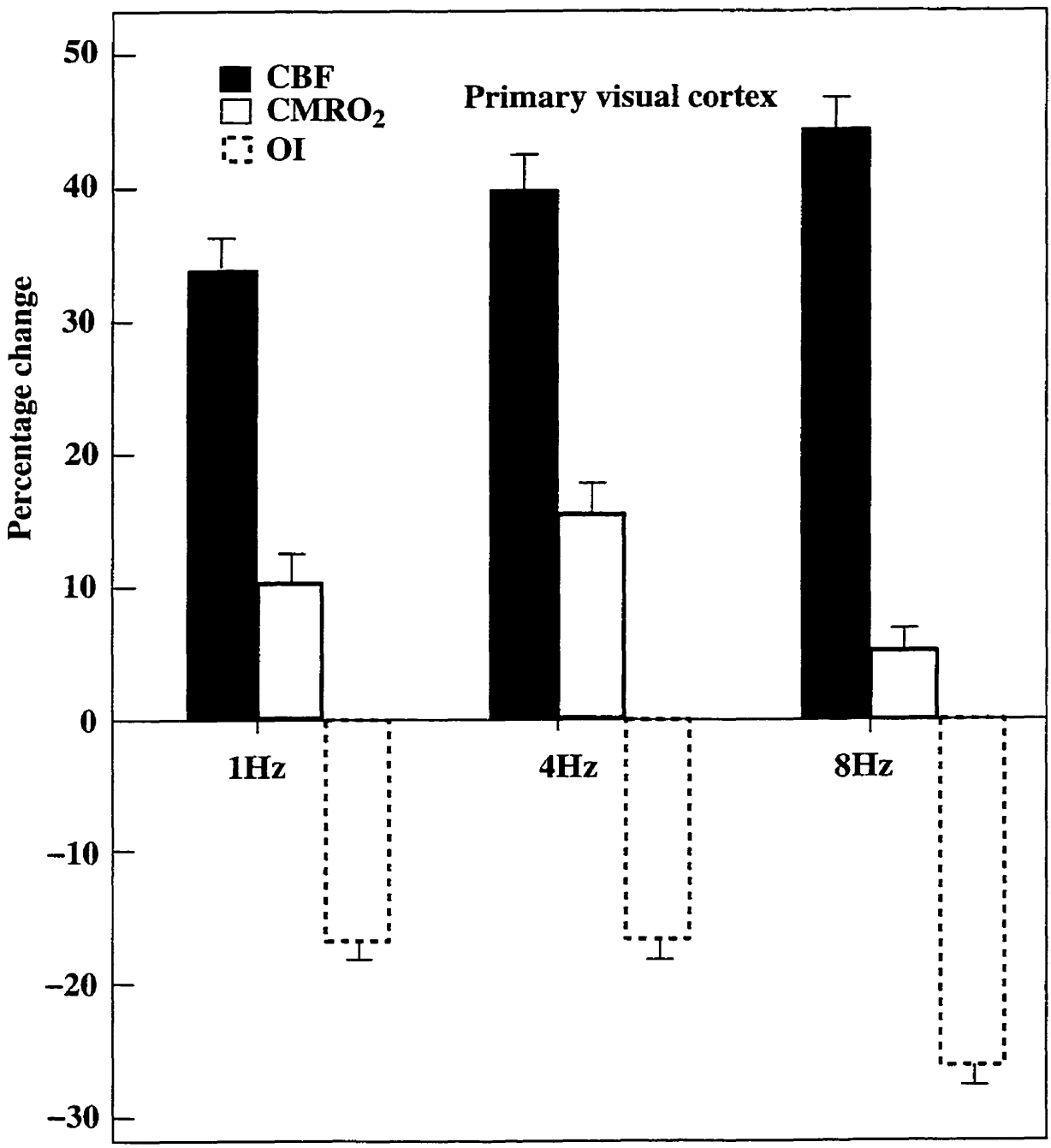
CBF
CMRO2
OI
Primary visual cortex
Percentage change
50
40
30
20
10
0
-10
-20
-30
1Hz
4Hz
8Hz

Rationale for the design of the experiment IV

In experiments I, II, and III, we studied closely the behaviors of cerebral blood flow and cerebral oxygen consumption in visual cortex of normal subjects following stimulation with yellow-blue checkerboard. This allowed us to collect a reliable data set for normal volunteers. We then intended to perform the same nature of experiments on some patients presenting at the MNH with mitochondrial disease and consequently, abnormal oxidative metabolism in order to test the hypothesis that abnormal blood flow and oxygen metabolism changes may be involved in the pathophysiology of these diseases. It is hoped that these investigations would eventually be informative of the pathophysiology of defects in mitochondrial metabolism.

CHAPTER 5

Cerebral Metabolic Rate of Oxygen ($CMRO_2$) and Cerebral Blood Flow (CBF) in Mitochondrial Encephalomyopathy: A PET study

M.S. Vafaee. E. Meyer. A.C. Evans, A. Gjedde

(In preparation for the Annals of Neurology)

Abstract

To test the hypothesis that increased blood flow may be required to allow oxygen consumption to increase in brain tissue, we measured changes of blood flow and oxygen consumption in mitochondrial disease during neuronal stimulation. Mutations in mitochondrial DNA (mtDNA) impair oxidative phosphorylation of ADP and are responsible for a wide variety of neurological diseases. Chronic Progressive External Ophthalmoplegia (CPEO) is a mitochondrial disease associated with large-scale deletions in mtDNA or less commonly by point mutations in tRNA genes. We used positron emission tomography (PET) to measure $CMRO_2$ and CBF in two patients with CPEO and compared the results with those obtained in normal control subjects to investigate the relationship between mitochondrial encephalomyopathies and defective oxidative metabolism. Dynamic PET studies mapped both CBF and $CMRO_2$. In the activation conditions, patients were shown a blue and yellow annular checkerboard reversing contrast at frequencies of 4 and 8 Hz. In the baseline condition, they were asked to fixate on a cross-hair in the center of the monitor screen. CBF and $CMRO_2$ were calculated using the two-compartment, weighted integration method. Global CBF of the patients was within normal values (40 ± 5). In the activation states, unlike normal subjects who had pronounced increases of CBF in the pericalcarine visual cortex, Patient #1 had only a mild increase of CBF while Patient #2 had no CBF increase. Global $CMRO_2$ of Patient #1 was within the normal range (195 ± 5) while that of Patient

#2 was below normal. In the activation states, healthy subjects showed a pronounced increase of $CMRO_2$ in the pericalcarine visual cortex at 4 Hz and a further slight increase at 8 Hz while no patient had a significant change in $CMRO_2$ during activation. This study shows that patients with mitochondrial encephalomyopathy may have measurably abnormal cerebral oxidative metabolism resulting in negligible increase of $CMRO_2$, possibly related to the minimal increase of CBF upon neuronal activation.

Introduction

ATP is the immediate source of chemical energy for tissue. During intense short-term exercise, ATP is first provided by breakdown of creatine phosphate (reservoir for high energy phosphate) and then by the conversion of glycogen to lactate by glycolysis which only provides 3 molecules of ATP per glucose unit of glycogen metabolised. During sustained moderate exercise, ATP is provided more efficiently by the oxidation of various metabolic fuels of which glucose is the most important in the brain. This process, oxidative phosphorylation, utilizes molecular oxygen (O_2) as the oxidant and occurs in mitochondria. The primary function of mitochodrial is to supply ATP for cellular work through oxidative phosphorylation.

Mitochondria have their own genome and each contains 2-10 double stranded circular DNA molecules, about 16.56 kilobases (kb). Mitochondrial DNA has been completely sequenced (Andersen et al., 1981). The mitochondrial genome contributes about 1% of total cellular DNA. Human mtDNA differs from nuclear DNA in its genetic code and also because it contains no introns and in fact very few noncoding sequences (Harding, 1991). MtDNA encodes two ribosomal RNAs (rRNAs), 22 transfer RNAs (tRNAs), and 13 of the 80 subunits of the mitochondrial respiratory chain and oxidative phosphorylation system (Wallace, 1992). Complex I, the main entrance of the electron transport chain, consists of approximately 41 polypeptides, seven encoded by the mtDNA (NADH dehydro-

genase, ND); Complex II, another entrance to electron transport chain, consists of four polypeptides, all nuclear; Complex III (cytochrome-c-reductase) of about 10 polypetides, one (cytochrome b, cytb) encoded by the mtDNA; Complex IV (cytochrome-c-oxidase) of 13 polypeptides, three (COI, COII, and COIII) encoded by the mtDNA; Complex V (ATP synthase) of 12 polypeptides, two (ATPase6 and 8) encoded by the mtDNA (Andersen et al., 1981; Wallace, 1992). MtDNA is transmitted exclusively through females in mammals (Giles et al., 1980).

The concept of mitochondrial disease was introduced in 1962 when Luft et al. described loose coupling of muscle mitochondria in a patient with nonthyroidal hypermetabolism. What makes mitochondrial disease uniquely interesting from a genetic point of view is the fact that mitochondria contain their own DNA and are capable of synthesizing a small but vital set of proteins, all of them components of the respiratory chain complexes. Genetic classification has been proposed dividing mitochondrial diseases into four groups (Grossman and Shoubridge, 1996): (1) Large-scale rearrangements (deletions, duplications); (2) point mutations in rRNA or tRNA genes; (3) point mutations or small deletions in protein-coding genes; and (4) nuclear gene defects resulting in abnormalities in mtDNA (multiple deletion, mtDNA depletion syndrome).

Single large-scale deletions in mtDNA have been found in patients with Kearns-Sayer syndrome (KSS) (Holt et al, 1989; Moraes et al., 1989), progressive external ophthalmoplegia (PEO) (Holt et al, 1989; Moraes et al., 1989) and Pearson's syn-

drome (PS) (McShane et al., 1991).

KSS is a complex neurological syndrome in which the core clinical phenotype includes PEO, progressive, asymmetric, nonfluctuating paresis of multiple extraocular muscles bilaterally plus heart block (Karpati and Shoubridge, 1993).

The most common mtNDA deletion involves 4977 base pairs and is found about 40% of patients (Schon et al., 1989). About 20% of the patients do not have detectable deletions (Moraes et al., 1991). Two patients with KSS were shown to have an mtDNA duplication (Poulton et al., 1989).

PEO is a sporadic syndrome with abnormal ocular motility very similar to KSS. Other minor manifestations ("ophthalmoplegia plus") may be present (Karpati and Shoubridge, 1993). The mtDNA defect is indistinguishable from that of KSS however, the relative proportion of mtDNA deletions in nonmuscle tissues usually is extremely low. About 50% of the patients with PEO have detectable mtDNA deletions (Moraes et al., 1989). A significant proportion of those patients who are negative for deletions have been shown to carry the 3243 point mutation in $tRNA^{leu(UUR)}$ that is associated commonly with MELAS (mitochondrial encephalomyopathy with lactic acidosis and stroke-like episodes) (Ciacci et al., 1992).

Positron emission tomography (PET) provides a quantitative tracer method to measure tissue energy metabolim in intact tissues in vivo (Phelps et al., 1986). In the past it has been used in the past to study the cerebral oxygen and glu-

cose metabolic rates in patients with mitochondrial encephalomyopathy including central nervous system (CNS) disease (Frackowiak et al., 1988) and myoclonus epilepy with ragged-red fibers (MERRF) (Berkovic et al., 1989).

The goal of this study was to measure CBF and $CMRO_2$ both at rest and during physiological stimulation in two patients diagnosed with Chronic Progressive External Ophthalmoplegia (CPEO) and compare the results with those obtained from a series of normal subjects using the same methods in order to test the hypothesis that insufficient blood flow change may be implicated in the pathophysiology of mitochondrial disorders.

Materials and Methods

Two patients with CPEO were studied. The first patient was a 47 year old female diagnosed with an mtDNA deletion. The second patient was a 59 year old male who presented with proximal limb muscle weakness and a chronic progressive external ophthalmoplegia syndrome (Fu et al., 1996), in whom a mtDNA point mutation was detected in the $tRNA^{Leu}$ gene (G to A at position 12315).

PET measurement

PET studies were performed on the ECAT EXACT HR^+ (CTI/Siemens) whole-body tomograph, operating in a 3D acquisition mode, with a transverse resolution of 4.5-5.8 mm and an axial resolution of 4.9-8.8 mm (Adam et al., 1997). The images were reconstructed as 128×128 matrices of 2 mm$\times$2 mm pixels using filtered back-projection with an 8 mm Hanning filter (FWHM). Reconstructed images were corrected for random and scattered events, detector efficiency variations and dead-time. Three orbiting rod transmission sources, each containing about 5 mCi of ^{68}Ge, were used for attenuation correction.

The patients were positioned in the tomograph with their heads immobilized by means of a customized headholder (Vac-Lock; MED-TECH). A short indwelling catheter was placed into the left radial artery for blood sampling and blood gas examination. Arterial blood radioactivity was automatically sampled, corrected for delay and dispersion (Vafaee et al., 1996), and calibrated with respect to the

tomograph using samples obtained manually during the last sixty seconds of each 3-min scan. At the start of each $CMRO_2$ scan, the patients inhaled 20 mCi of ^{15}O-O_2 in a single breath while at the start of each CBF scan, they were injected with 10 mCi of $H_2{}^{15}O$ intravenously. $CMRO_2$ and CBF were calculated using the two compartment, weighted integration method (Ohta et al., 1992 and 1996). Each patient also underwent a magnetic resonance imaging (MRI) examination on a Philips Gyroscan ACS (1.5 T) superconducting magnet system for structural-functional (MRI-PET) correlation. The MRI image was a T1-weighted, 3D FFE (fast field echo) sequence consisting of 160 256×256 sagittal slices of 1mm thickness.

Stimulus conditions

The stimulus was generated on a Silicon Graphics (SGI) workstation and presented through a 21-inch NEC monitor (MultiSync XP21) with a synchronization range of 31 to 89 kHz (horizontal) and 55 to 160 Hz (vertical), and a temporal resolution of 55 to 83 Hz. It consisted of a yellow-blue annular checkerboard with a diameter of about 17^0 of visual angle (for detailed explanation of the stimulus refer to Vafaee et al. 1998b). In the baseline condition, the patients were asked to fixate on a cross-hair in the center of the screen 30 s before the scan, and throughout the subsequent 3-min scan. In two successive activation conditions, the patients were shown the checkerboard reversing its contrast at frequencies of

4, and 8 Hz. Stimulation began 4 minutes before the start of the dynamic PET scan, and continued throughout the following 3-min scan for a total of 7 min. There was a time gap of at least 15 minutes between each scan. Black drapes were used to create a dark environment around the screen.

Data analysis

MR images were transformed into stereotaxic coordinates (Talairach and Tournoux, 1988) by means of an automatic registration algorithm (Collins et al., 1994). The reconstructed PET images were co-registered with the subjects' MRI scans using an automatic registration program based on the Automatic Image Registration algorithm (Woods et al., 1993). For this purpose, the sum of the PET images across all frames was calculated for each scan. Then, the MRI image was aligned with the summed PET image. The global cerebral metabolic rates of oxygen ($CMRO_2$) were determined for each subject by means of a binarized brain mask which filters out all extracerebral voxels. This mask was created by thresholding and manually editing the average MRI of 305 normal brains scanned at the Montreal Neurological Institute. The global $CMRO_2$ for each patient was then determined by averaging the values of all intracerebral voxels. The regional cerebral metabolic rates of oxygen ($CMRO_2$) for each patient (pericalcarine visual cortex) were also determined by manually drawn ROIs (regions of interest) on PET images (registered on corresponding MRIs) in Talairach space. Both global

and regional $CMRO_2$ and CBF values were then compared to average values obtained from twelve normal subjects at rest and during visual stimulation (Vafaee et al., 1998c).

Results

As shown in Fig. 1, global CBF values of the patients were within normal limits (40±5) both at baseline and in the activation conditions. In the activation states, unlike normals who showed pronounced increases of CBF with stimulus frequency in the pericalcarine visual cortex (40% at 4 Hz; 45% at 8 Hz), Patient #1 only showed a mild increase of CBF (6% at 4 Hz; 16% at 8 Hz), while Patient #2 showed no CBF increase at all (Fig. 2). Global $CMRO_2$ of Patient #1 was within normal range, while that of Patient #2 was below normal (Fig. 3). Although global $CMRO_2$ of both patients and normals did not change significantly between baseline and activation states, global $CMRO_2$ values of Patient #2 were significantly lower in each state compared to those of normals. In the activation states, healthy subjects showed a pronounced increase of $CMRO_2$ in the pericalcarine visual cortex at 4 Hz (15%), and a slight increase at 8 Hz (5%) compared to baseline, while no patient showed a significant changes of $CMRO_2$ during activation (Fig. 4).

Discussion

Mitochondrial DNA deletions have been found to cause the majority of cases of ocular myopathy and Pearson Syndrome (Wallace et al., 1990, Holt et al., 1988). Ocular myopathy patients manifest a continuous range of symptoms from ophthalmoplegia, ptosis, and mitochondrial myopathy (chronic progressive external ophthalmoplegia, CPEO), to retinitis pigmentosa, lactic acidosis, neurosensory hearing loss, ataxia, heart conduction defects, elevated CSF protein, and dementia (Kearns-Sayer Syndrome, KSS) (Wallace, 1992).

KSS has been recognized as being a "mitochondrial disease" for a long time but unequivocal evidence for a primary role of mitochondria in the etiology was obtained by demonstrating major deletions in mtDNA (Holt et al., 1988; Zeviani et al., 1988). The most common mDNA deletion involves 4,977 base pairs and is found in about 40% of patients (Schon et al, 1989). About 20% of the patients do not have detectable deletions (Moraes et al., 1991). The proportion of mtDNA deletion mutants varies between about 20% and 80% in muscle, and their presence is detected easily by Southern blot analysis (Karpati and Shoubridge, 1993).

PEO is a sporadic syndrome with abnormal ocular motility very similar to KSS. It is characterized by ophthalmoplegia, ptosis, and proximal limb and respiratory muscle weakness, cataracts, and hearing loss. About 50% of all patients with PEO have mtDNA deletions (Moraes et al., 1989). Biochemical studies of muscle have shown combined defects of the respiratory chain of varying severity

in one family (Servidei et al., 1991)), complex I deficiency (Cormier et al., 1991).

The two patients of the current study had been clinically diagnosed with CPEO. Patient #1 had been diagnosed with 4 kb deletion in mtDNA. Based on neuropathological reports, Patient #2 demonstrated severe cytochrome oxidase deficiency presumably due to translation defects affecting all of the respiratory chain complexes encoded by mtDNA. Although CBF of both patients globally appeared to be normal (Fig. 1). in the activation states both patients showed different blood flow responses compared to those of normals. As shown in Fig. 2, CBF in normals was enhanced significantly by increasing the frequency of the stimulus. In the case of Patient #1, although the occipital CBF value in the baseline condition was slightly lower than in normals, increasing the frequency of the stimulus resulted in a slight enhancement of CBF at 8 Hz (%16) without any pronounced change at 4 Hz (%6). The CBF change of Patient #2 appeared to be less sensitive to the stimulus frequency, as the already low CBF in the baseline condition remained unchanged regardless of the frequency of the stimulus.

We also measured oxygen consumption in these patients as an index of oxidative metabolism and compared it with normal values. As shown in Fig. 3, $CMRO_2$ of Patient #1 globally appeared to be normal, while Patient #2 demonstrated a dramatic, and statistically significant, decline of global $CMRO_2$ in both baseline and activation states. Moreover, in the activation states, unlike normals who showed a significant $CMRO_2$ increase at 4 Hz and a slight increase at 8 Hz

(Vafaee et al., 1999), $CMRO_2$ of both patients remained unchanged in response to the stimulus frequency, with Patient #2 consistently demonstrating lower values.

The data from this study can be interpreted in several ways. From the physiological point of view, both patients demonstrated normal values of CBF globally when compared to control subjects in spite of the fact that Patient #1 showed a reduced sensitivity of CBF to stimulation of the visual cortex and Patient #2 showed no response to the stimulation at all. When compared to the normals, the $CMRO_2$ change was less straightforward than that of CBF. Although both patients showed no regional $CMRO_2$ response to the visual stimulation, Patient 1# had normal global $CMRO_2$ while the values for Patient #2 were significantly lower than in normals. The observation that both patients consistently demonstrated lower $CMRO_2$ values implies a disturbance in the normal coupling between perfusion and energy metabolism in these patients. This observation is consistent with the fact that the energy-generating pathway subserving oxidative phosphorylation, consists of enzyme complexes assembled from subunits derived from both mDNA and nDNA. Defective mtDNA could therefore result in an impairment of energy metabolism. On the other hand, if oxidative phosphorylation is impaired due to a primary defect of mitochondrial function, excess of ADP and/or $NADH^+$ will stimulate glycolysis via the anaerobic pathway, leading to excess production of lactate. This hypothesis was partially supported in these patients as the serum lactate level of patient 1 was within normal values (1.7 mM) while that of patient

2 was higher than normal (2.4 mM).

Although both patients had been diagnosed with the CPEO syndrome from the neurological point of view, there were striking differences between them. As mentioned above, Patient #2 consistently showed lower CBF values in comparison to Patient #1 without demonstrating any sensitivity to the stimulus frequency. Moreover, Patient #1 had normal global $CMRO_2$ values while those of Patient #2 were significantly lower. These differences between the two patients could also be attributed to the severity and duration of the disease. Patient 1 (47 year old female) had been diagnosed with the CPEO syndrome 20-27 years ago while Patient #2 (59 year old male) had been suffering from CPEO for 30-40 years. In addition, the higher lactate level of Patient #2, compared to Patient #1, is consistent with our finding that more progressive mitochondrial disease would cause the patients to tend to supplement the oxidative energy production by anaerobic glycolysis.

Based on the results, we speculate that the capacity of brain cells for oxygen consumption and consequently for oxidative metabolism is different in mitochondrial disorders compared to normals. The statistically low occipital $CMRO_2$ values of Patient #2, suggests that this region is working at $V_{O2_{max}}$. On the other hand, normal global and lower occipital $CMRO_2$ values of Patient #1 suggests that cerebral cortex in this patient is working at a level somewhere below $V_{O2_{max}}$. Moreover, the comparison of the CBF and $CMRO_2$ values of the two patients does

not reject the hypothesis that blood flow and oxygen consumption are uncoupled in these patients.

The heterogeneity of physiological and molecular findings in patients with similar underlying neurological deficits is puzzling. The major changes in energy metabolism do not reject the hypothesis that defective mtDNA leading to OXPHOS diseases result in depression of oxygen consumption. This means that PET can be used to measure pathological changes of the coupling between CBF, $CMRO_2$, and $CMRO_{glc}$ which may help to establish the stage and severity of OXPHOS disorders. The absent response of CBF and $CMRO_2$ to physiological stimulation is consistent with our hypothesis that increased blood flow, possibly elicited by a signal from "needy" neurons i.e neurons that need more oxygen, is required to allow increases of oxygen consumption (Gjedde, 1997; Vafaee et al., 1999).

Legends to Figures

Figure 1: Comparison of global $\dot{C}BF$ values in the baseline and activation states (4 and 8 Hz) in two patients and twelve controls (mean±two standard deviations).

Figure 2: Comparison of occipital CBF values in the baseline and activation states (4 and 8 Hz) in two patients and twelve controls (mean±two standard deviations).

Figure 3: Comparison of global $CMRO_2$ values in the baseline and activation states (4 and 8 Hz) in two patients and twelve controls (mean±two standard deviations).

Figure 4: Comparison of occipital $CMRO_2$ values in the baseline and activation states (4 and 8 Hz) in two patients and twelve controls (mean±two standard deviations).

Figure 1:

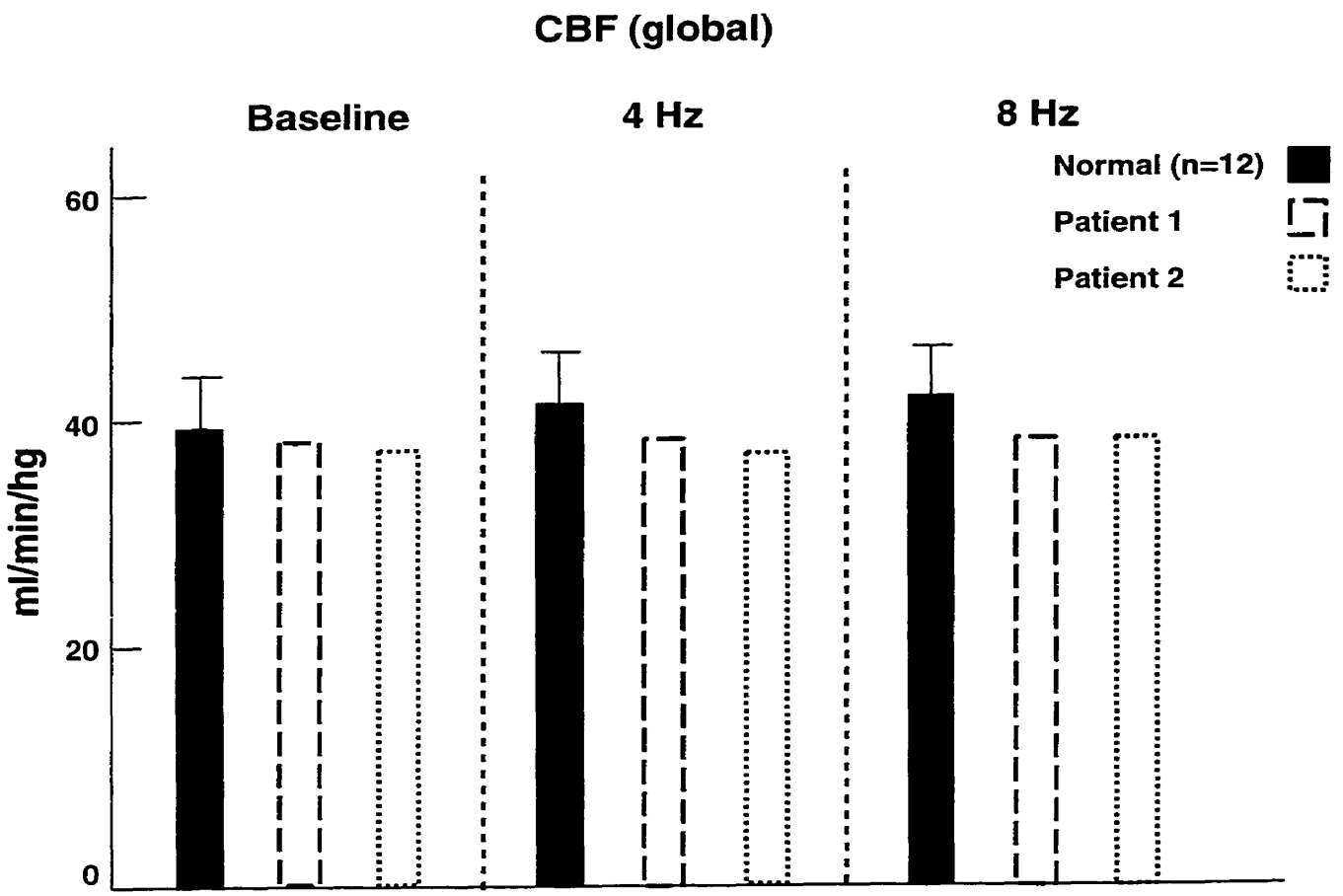
CBF (global)
Baseline
4 Hz
8 Hz
Normal (n=12)
Patient 1
Patient 2
60
40
20
0
ml/min/hg

Figure 2:

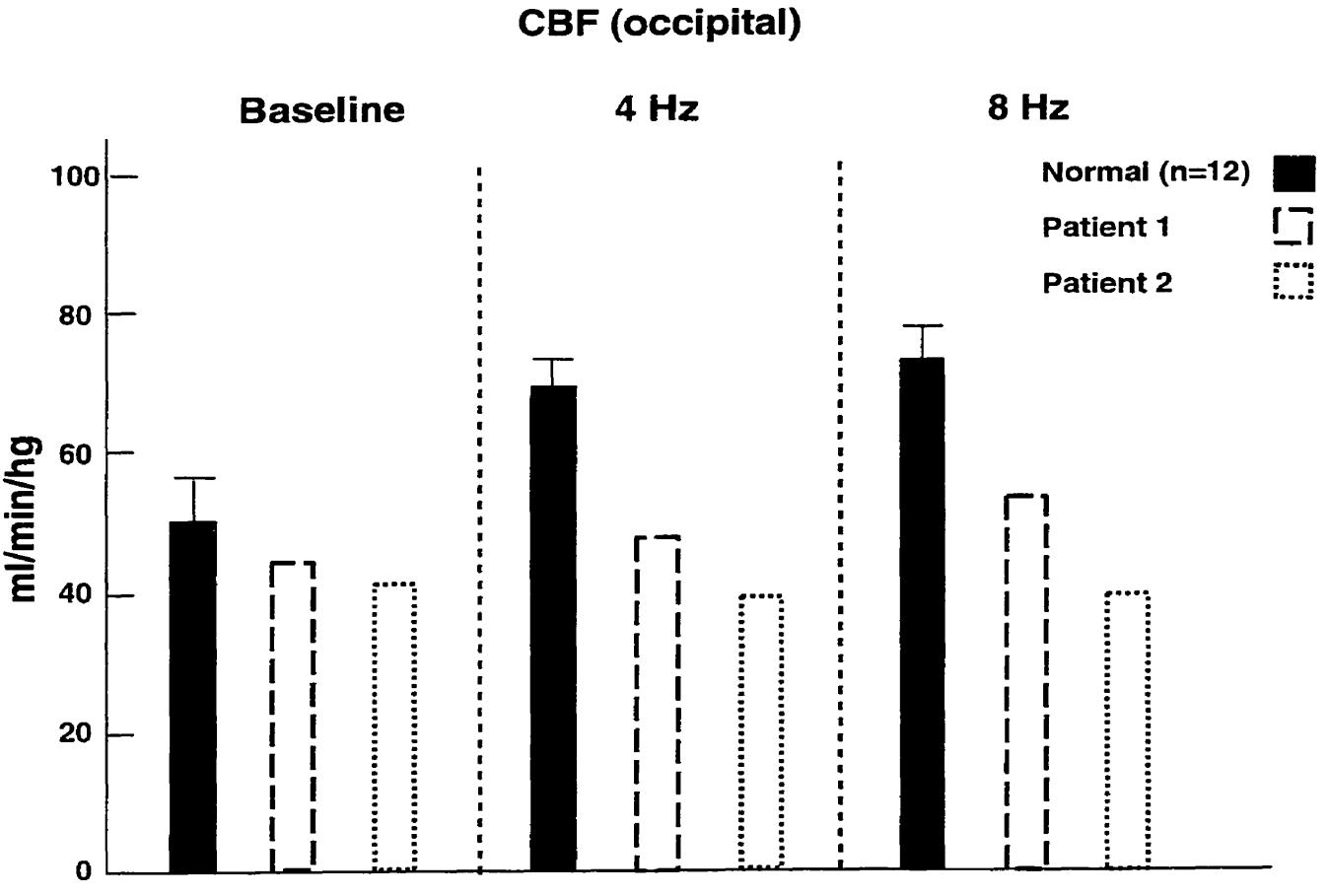
CBF (occipital)
Baseline
4 Hz
8 Hz
Normal (n=12)
Patient 1
Patient 2
ml/min/hg
100
80
60
40
20
0

Figure 3:

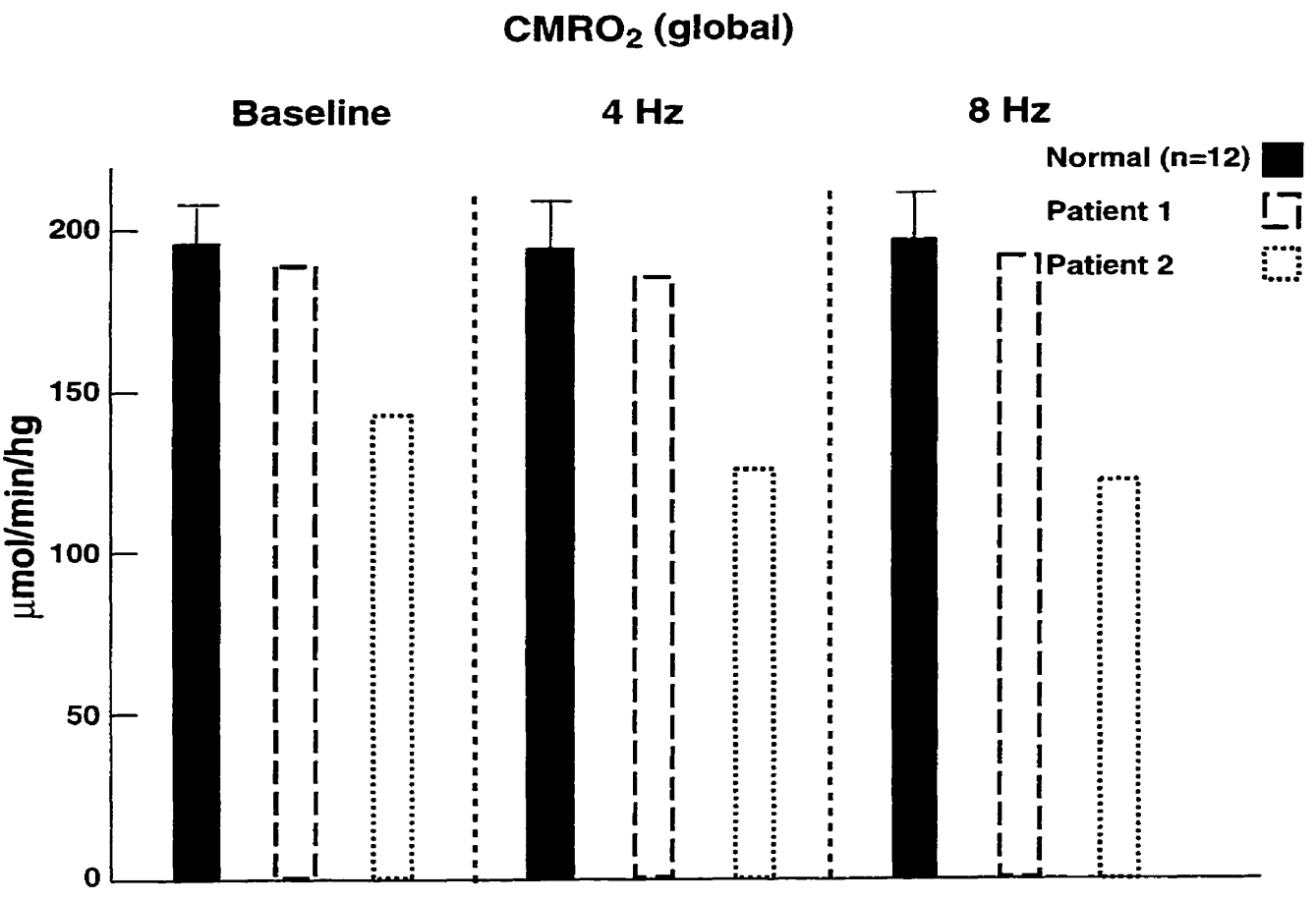
CMRO2 (global)
Baseline
4 Hz
8 Hz
Normal (n=12)
Patient 1
Patient 2
µmol/min/hg
200
150
100
50
0

Figure 4:

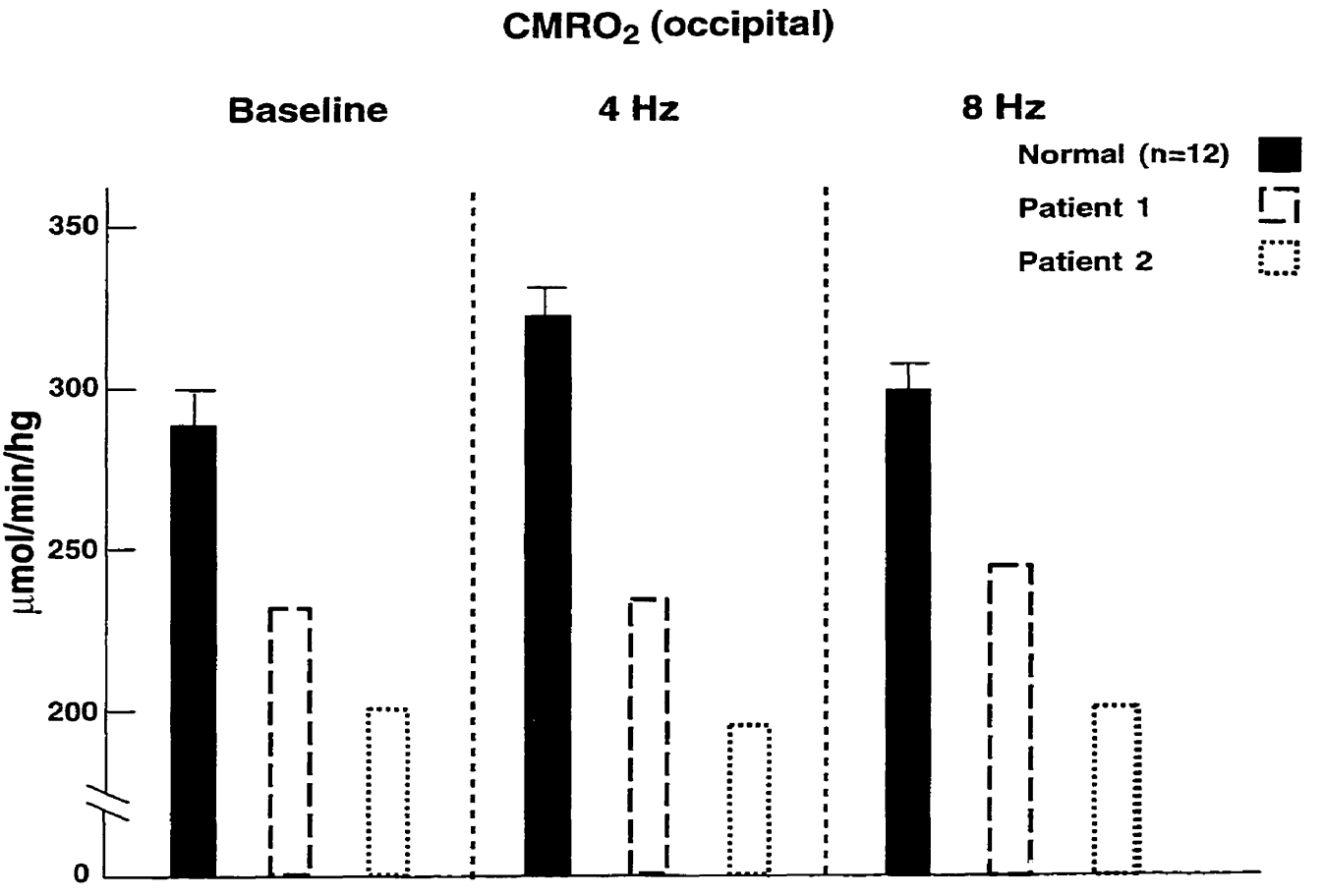
CMRO2 (occipital)
Baseline
4 Hz
8 Hz
Normal (n=12)
Patient 1
Patient 2
350
300
250
200
0
µmol/min/hg

CHAPTER 6

General Discussions

One marked characteristic of the literature dealing with cerebral circulation and its relation with metabolism is the contradictory nature of the results which have been obtained by different investigators. There is no reason for doubting that the cause of these discrepancies is to be found in complex relationship between blood flow, oxygen, and glucose metabolism.

A number of investigators have demonstrated that blood flow in the brain is tightly coupled to the metabolic requirements of tissue for glucose and oxygen (Siesjö, 1978; Yarowski and Ingvar, 1981). On the other hand, more recent studies have reported a mismatch between changes of CBF and oxygen consumption during functional activation of the human brain, despite a match between changes of regional glucose utilization and CBF (Fox and Raichle, 1986; Fox et al., 1988; Fujita et al., 1992 and 1993; Ribeiro et al., 1993). Moreover, significant increases of oxygen consumption in the striate cortex in response to a visual stimulus has been reported in this laboratory (Marrett et al., 1995; Vafaee et al., 1996; Marrett and Gjedde, 1997) as well as in other laboratories.

The goal during the course of this dissertation was to investigate the relation between blood flow and oxygen metabolism in visual cortex as one of the well studied parts of the brain and apply the results to patients who suffered from the oxidative metabolism disorder resulting from the disparity between blood flow and

oxygen metabolism, in order to shed light on pathophysiology of these disorders. For this purpose, we established a visual paradigm capable of giving rise to both CBF and $CMRO_2$ following stimulation.

We designed the yellow-blue reversing circular checkerboard as the stimulus in experiment I based on the fact that its specific colors namely yellow and blue, shape, temporal, and spatial frequencies,would be able to evoke cells rich in mitochondrial enzyme cytochrome oxidase (COX) in striate cortex (Livingstone and Hubel, 1984a). These circular cells reside in layers 2 and 3 of primary visual cortex and receive afferent fibers from intralaminar regions of lateral geniculate nucleus where most cells are double-opponent circular and contribute to color perception.

We demonstrated that our stimulus causes significant increases of oxygen consumption in visual cortex following a stimulation. The observed increase of $CMRO_2$ seems to be stimulus specific because stimulaton with an array of red LEDs flashing at the same temporal frequency (8 Hz) failed to induce significant increases of $CMRO_2$ (Fujita et al., 1992, 1993; Ribeiro et al., 1993). As the same method of $CMRO_2$ measurement was used in this study, the observed increase in $CMRO_2$ in the visual cortex could be associated with the ability of the chromatically rich stimulus to activate the cytochrome oxidase rich neurons (blobs) involved in color processing. Thus, we have shown that a specially designed stimulus gives rise to increased $CMRO_2$ in visual cortex, demonstrating that the ability of brain neurons to increase the oxygen use may vary according to the task neu-

rons perform.

Having established a stimulus capable of enhancing $CMRO_2$ following an activation, we designed experiment II to determine the relation, if any, between the frequency of the stimulus, as an index of neuronal work, and $rCMRO_2$ as a measure of oxidative metabolism. We demonstrated that $rCMRO_2$ in the visual cortex varies as a function of stimulus frequency. We also showed that unlike rCBF, which has been reported to peak at 8 Hz (Fox and Raichle, 1984 and 1985), $rCMRO_2$ reached its peak at 4 Hz and dropped off at higher frequencies. These findings represented a partial confirmation of our hypothesis of the existence of two tissue limitations.

We hypothesize that the observed behavior is the result of barrier-limited oxygen transfer to brain across cerebral capillaries which imposes a physiological limitation on the finite oxygen diffusibility in brain tissue. Although this limitation is lifted by an increase of blood flow (and possible physiological recruitment), oxygen consumption apparently does not always rise as allowed by this increase due to the existence of an additional limitation, possibly at an enzymatic step in oxidative metabolism. This limitation represents a cellular mechanism that causes the brain not to fully sustain the increase of $CMRO_2$ made possible by the blood flow increase. Based on our results, we speculate that the secondary limitation could be overcome by increasing the stimulus effects on the system as a function of time and intensity. We conclude that, a blood flow increase accompanying the

stimulus frequency of 4 Hz permits the $CMRO_2$ to increase to the observed value. When the frequency of the stimulus increases above 4 Hz, neuronal work no longer requires the $CMRO_2$ to rise.

Following the experiments I and II, we designed the experiment III to evaluate Oxidative Index (OI) equal to the $CMRO_2/CBF$ ratio. The index yielded information about the degree of flow-metabolism coupling. The discrepancy between changes of blood flow and oxygen and glucose consumption during different kinds of stimulation suggests that the mechanism underlying flow-metabolism couple is poorly understood. We proposed a model of oxygen delivery (equation 8, Chapter 4) which defines the relationship betwen blood flow and oxygen delivery. This model was based on the claim that oxygen transfer to brain across cerebral capillaries occurs in a barrier limited-fashion (Kassissia et al., 1995) and that the mitochondrial oxygen tension is too low to allow significant augmentation of oxygen diffusion gradient by lowering the mitochondrial oxygen tension. When the mitochondrial oxygen tension is negligible at the far end of the diffusion path (η=0), the predicted relationship satisfies equation 9 (Chapter 4). The model is consistent with the measured oxygen consumption when L (the average tissue conductivity of oxygen from the capillary lumen to the mitochondrion) is allowed to rise as an indication of capillary recruitment. The model is consistent with the changes of CBF and $CMRO_2$ following stimulation at 1, 4, and 8 Hz (Figs. 2 and 3, Chapter 4). As we demonstrated in Fig. 3 (Chapter 4), the oxygen consump-

tion curve drawn on the basis of CBF tuning curve (Fig. 2, Chapter 4) for η=0, predicted the measured $CMRO_2$ values at 1 and 4 Hz, while the model predicted a higher than negligible η=0 at the frequency of 8 Hz. At 4 Hz, we argue that the excess of blood flow, possibly assisted by physiological recruitment, enabled the $CMRO_2$ increase. As the frequency of the stimulus increased further, tissue factors prevented $CMRO_2$ from increasing as predicted. Although sufficient amount of blood is supplied to the tissue, the stimulus load must exceed a threshold for oxidative phosphorylation to rise. This is consistent with the hypothesis proposed in experiment II, i.e., oxygen consumption is inhibited by two limitations, first an enzymatic block which is lifted in proportion to the stimulus load, second an oxygen diffusibility block which is lifted when blood flow rises. As mentioned in Chapter 4, the poor correlation at 8 Hz may indicate the existence of other neurons supplied by a separate vascular bed with lower capillary density.

We studied two patients with mitochondrial disease to test the hypothesis that defective mtDNA causes OXPHOS disorder which in turn leads to depression of oxygen consumption. The results of CBF and $CMRO_2$ measurements following the stimulation showed that both patients consistently had lower $CMRO_2$ values. This finding is consistent with uncoupling of CBF and $CMRO_2$ and with the prediction that defective mtDNA impairs energy metabolism. We demonstrated that severity and duration of this disease has a striking effect on the measured values of the CBF and $CMRO_2$. Patient #2, who had suffered from the disease for a

longer period, consistently had lower values of $CMRO_2$ and CBF than Patient #1. The results were consistent with the hypothesis that these patients supplement their energy requirements non-oxidatively. The results replicated the finding that the absence of $CMRO_2$ following physiological stimulation may be due in part or wholly to insufficient blood flow (Vafaee et al., 1999). The results are consistent with the speculation that blood flow increases, possibly elicited by a signal from "needy" neurons, are required to allow increase of oxygen consumption.

In summary, based on the results obtained from normals subjects and patients throughout the course of this project, I conclude that oxygen consumption in visual cortex of normal subjects can be enhanced following stimulation with a proper stimulus, i.e., a stimulus capable of exciting the neurons rich in cytochrome oxidase. This finding is in line with the Roy and Sherrington principle which implies a tight coupling betwen blood flow and the supplies of glucose and oxygen to the brain. I also conclude that blood flow increase may be a pre-condition of increased oxygen delivery because the delivery is barrier-limited. Based on our data, I claim that the blood flow increase follows a signal from insufficiently oxygenated tissue. It is puzzling that the oxygen consumption sometimes fails to rise (vibrotactile stimulation), suggesting that additional factors either prevent the neurons from using the supplied oxygen, or eliminate the need to use it. Finally, I conclude that in patients with mitochondrial deficits, the capacity of brain cells for oxygen consumption and consequently for oxidative metabolism is low compared to normals.

The data suggested that insufficient blood flow supply to the brain tissue can be the reason for this abnormality.

FUTURE WORK

In order to shed more light on the issue of the re- or uncoupling of blood flow and metabolism during the changes in brain activity, I suggest more experiments be completed along the same lines as the present. It would be useful to pursue these experiments in other regions of the cerebral cortex, such as auditory cortex. To verify the present results, and strengthen future results, I intend to perform functional magnetic resonance imaging (fMRI) studies along with PET studies.

REFERENCES

Adam LE, Zaers J, Ostertag H, Trojan H, et al. (1997) Performance evaluation of the whole-body PET scanner ECAT EXACT HR+. *Proceedings of IEEE* 2:1270-1274.

Ahmed SA, Claiborne A (1989) The streptococcal flavoprotein NADH oxidase. II. Interactions of pyridine nucleotides with reduced and oxidized enzyme forms. *J Biol Chem* 264(33):19863-70.

Alberts B, Bray D, Lewis J, Raff M, et al. (1994) *Molecular Biology of the Cell* Garland Publishing Inc. New York and London pp. 653-683.

Alpert NM, Eriksson L, Chang JY, Bergström M, et al. (1984) Strategy for the measurement of regional cerebral blood flow using short-lived tracers and emission tomography. *J Cereb Blood Flow Metab* 4:28-34.

Alpert NM, Senda M, Correia JA (1990) Mapping of local cerebral pH with positron emission tomography. In: Diksic M., Reba R.C. (eds) *Radiopharmaceuticals and Brain Pathology Studied With PET and SPECT.* CRC Press, Boca Raton Ann Arbor Boston 267-278.

Andersen S, Bankier AT, Barrell BG, et al. (1981) Sequence and orgnization of the human mitochondrial genome. *Nature* 290:457-465.

Bartley SH (1937b) Some observations on the organization of the retinal response. *Am J Physiol* 120:184.

Bartley SH (1968) Temporal features of input as crucial factors in vision. In: Neff WD ed. *Contributions to Sensory Phsiology.* New York: Academic, vol. 3, pp. 81-124.

Beal MF, Hyman BT, Koroshetz W (1993) Do defects in mitochondrial energy metabolism underlie the pathology of neurodegenerative diseases? *TINS* 16:4:125-131.

Berkovic SF, Carpenter S, Evans A, et al. (1989) Myoclonus epilepsy and ragged-red fibers (MERRF). *Brain* 112:1231-1260.

Borowsky IW, Collins RC (1989) Metabolic anatomy of brain: A comparison of regional capillary density, glucose metabolism and enzyme activities. *J Comp Neurol* 288:401-413.

Brooks DJ, Lammertsma AA, Beaney RP, Leenders KL, Buckingham PD, Marshall J, Jones T (1984) Measurement of regional cerebral pH in human subjects using continous inhalation of $^{11}CO_2$ and positron emission tomography. *J Cereb Blood Flow Metab* 4:458–465.

Brooks DJ, Frackowiak RS (1989) PET and movement disorders. *J Neurol Neurosurg Psychiatry* Suppl:68-77.

Brown MD, Voljavec AS, Lott MT, et al. (1992) Mitochondrial DNA complex I and III mutations associated with Leber's hereditary optic neuropathy. *Genetics* 30:163-173.

Bustany P, Henry JF, de Rotrou J, Signoret P, et al. (1985) Correlation between clinical state and positron emission tomography measurement of local brain protein synthesis in Alzheimer's dementia, Parkinson's disease, schizophrenia and gliomas. In: Greitz T., Ingvar DH., Widen L. (eds) *The Metabolism of the Human Brain Studied With Positron Emission Tomography.* Raven Press, New York 241-249.

Burton AC (1965) *Physiology and biophysics of the circulation.* Year Book Medical Publisher Chapter 5, Chicago.

Buxton R, Frank LR, (1997) A model for the coupling between cerebral blood flow and oxygen metabolism during neuronal stimulation. *J Cereb Blood Flow Metab* 17:64-72.

Carson RE. Huang SC. Phelps ME (1981) *BLD: A Software System for Physiological Data Handling and Model Analysis.* Proceeding, Fifth Annual Symposium on Computer Applications in Med Care pp. 562-565.

Carson ER, Cobelli C, Finkelstein L (1983) *The Mathematical Modeling of Metabolic and Endocrine Systems.* Wiley, New York.

Carson RE, Huang SC, Green MV (1986) Weighted integration method for local cerebral blood flow measurements with positron emission tomography. *J Cereb Blood Flow Metab* 6:245-258.

Carson RE, Breier A, de Bartolomeis A, Saunders RC, Su TP, Schmall B, Der MG, Pickar D, Eckelman WC (1997) Quantification of amphetamine-induced changes in [11C]raclopride binding with continuous infusion. *J Cereb Blood Flow Metab* 437-447.

Ciacci F, Moraes CT, Silvestri S, et al. (1992) The 'MELAS-3243' mutation in mtDNA is found in many patients with progressive external ophthalmoplegia (PEO). *Neurology* 42(suppl 3):417.

Clarke DD, Sokoloff L (1994) Circulation and energy metabolism of the brain. In: GJ Siegel, BW Agranoff, RW Albers, PB Molinoff, eds. *Basic Neurochemistry* Raven Press, New York pp. 645-680.

Coleman RE, Hoffman JM, Hanson WM, Sostman HD, Schold SC (1990) Clinival application of PET for the evaluation of brain tumors. *J Nucl Med* 32:616-622.

Collins DL, Neelin P, Peters TM, Evans AC (1994) Automatic 3D intersubject registration of MR volumetric data in standardized Talairach space. *J Comput Assist Tomgr* 18:192-205.

Cooke BE, Evans AC, Fanthome EA, Alarie R, Sendyk AM (1984) Performance figures and images from the Therascan 3128 positron emission tomograph. *IEEE Trans Nucl Sci* NS-32:640-644.

Connett RJ, Geyeski TE (1985) Energy sources in fully aerobic rest-work transitions: a new role for glycolysis. *Am J Physiol* 248:H922.

Cormier V, Rotig A, Tardieu M, Colonna M, Saudubray JM, Munnich A (1991) Autosomal dominant deletions of the mitochondrial genome in a case of progressive encephalomyopathy. *Am J Hum Genet* 48:643-648.

Crone C (1963) The permeability of capillaries in various organs as determined by use of the "indicator diffusion method". *Acta Physiol Scand* 58:292-305.

Desimone R, Uugerleider LG (1986) Multiple visual areas in the caudal superior temporal sulcus of the macaque. *J Comp Neurol* 284: 164-189.

DiMauro S, (1992) Diseases of mitochondrial encephalomyopathies. In: RN Rosenberg, SB Prusiner, S DiMauro, RL Barchi, LM Kunkel (eds) *The Molecular and Genetic Basis of Neurological Disease.* Stoneham, MA: Butterworth-Heinamann, pp. 665-694.

DiMauro S, De Vivo DC (1994) Diseases of carbohydrate, fatty acid, and mitochondrial metabolism. In: GJ Siegel, BW Agranoff, RW Albers, PB. Molinoff, (eds) *Basic Neurochemistry.* Raven Press, New York pp. 723-748.

Eichling JO, Raichle ME, Grubb RL Jr, Ter-Pogossian MM (1974) Evidence of

the limitations of water as a freely diffusible tracer in brain of the Rhesus monkey. *Circ Res* 35:358-364.

Engel AG (1986) Carnitine deficiency syndromes and lipid storage myopathies. In: AG Engel and BQ Banker (eds) *Myology* New York: McGraw-Hill, pp. 1663-1696.

Engel J Jr, Henry DR. Risinger MW. et al. (1990) Presurgical evaluation for partial epilepsy: Relative contributions of chronic depth-electrode recordings versus FDG-PET and scalp-sphenoidal ictal EEG. *J Neurol* 40:1670-1677.

Engel SA, Rumelhart DE. Wandell BA. et al. (1994) fMRI of human visual cortex. *Nature* 359:525.

Eriksson L, Holte S. Bohm CHR. Kesselberg M, Hovander B (1988) Automated blood sampling system for positron emission tomography. *IEEE Trans Nucl Sci* NS-38:703-707.

Evans AC, Thompson CJ. Marrett S, Meyer E, Mazza M (1991) Performance evaluation of the PC-2048: A new 15-slice encoded-crystal PET scanner for neurological studies. *IEEE Trans Med Imaging* 10: 89-98.

Evans AC, Marret S, Neelin P, Collins L, Worsely K, Dai W, Milot S, Meyer E, Bub D (1992) Anatomical Mapping of Fuctional Activation in Stereotactic Coordinate Space. *Neuroimage* 1:43-53.

Fishman GS (1976) Sampling from the poisson distribution of a computer. *Computing* 17:147-156.

Fox PT, Raichle ME (1984) Stimulus rate dependence of regional blood flow in human striate cortex, demonstrated by positron emission tomography. *J Neurophysiol* 51(5):1109-1120.

Fox PT, Raichle ME, Thach WT (1985) Functional mapping of the human cerebellum with positron emission tomography. *Proc Natl Acad Sci USA* 82(21):7462-7466.

Fox PT, Raichle ME (1985) Stimulus rate determines regional blood flow in striate cortex. *Ann Neurol* 17(3):303-305.

Fox PT, Raichle ME, (1986) Focal physiological uncoupling of cerebral blood flow and oxidative metabolism during somatosensory stimulation in human subjects.

Proc Natl Acad Sci USA 83:1140-1144.

Fox PT, Raichle M, Mintun M, Dence C (1988) Nonoxidative glucose consumption during focal physiologic neuronal activity. *Science* 241:462-464.

Frackowiak RS (1985) The pathophysiology of human cerebral ischemia, a new perspective obtained with positron emission tomography. *Q J Med* 57:713-727.

Frackowiack RSL, Lenzi GL, Jones T, Heather JD (1980) Quantitative measurement of regional cerebral blood flow and oxygen metabolism in man using O-15 and positron emission tomography. Theory, procedure, and normal values. *J Comput Assist Tomogr* 4:727-736.

Frackowiak RS, Wise RJ (1983) Positron tomography in ischemic cerebrovascular disease. *Neuro Clin* 1:183-200.

Frackowiak RSJ, Herold S, Petty RKH, Morgan-Hughes JA (1988) The cerebral metabolism of glucose and oxygen measured with positron emission tomography in patients with mitochondrial diseases. *Brain* 111:1009-1024.

Frahm J, Bruhn H, Merboldt KD, Hanicke W (1992) Dynamic MR imaging of

human brain oxygenation during rest and photic stimulation. *J Magn Reson Imag* 2: 501-505.

Fu K, Hartlen R, Johns T, Genge A, Karpati G, Shoubridge EA (1996) A novel hetroplasmic $tRNA^{Leu(CUN)}$ mtDNA point mutation in a sporadic patient with mitochondrial encephalomyopathy segregates rapidly in skeletal muscle and suggests an approach to therapy. *Hum Mol Genet* 5:1835-1940.

Fujita H, Kuwabara H, Ohta S, Ribeiro L, et al. (1992) Evidence for stimulus-specific changes in oxidative metabolism. *In Proceedings, 6^{th} Annual Turku Conference on the Med Application of Cyclotrons.*

Fujita H, Meyer E, Kuwabara H, Evans AC, Gjedde A (1993) Cerebral blood flow and oxidative metabolism remain uncoupled during chronic vibrotactile stimulation in humans. *J Cereb Blood Flow Metab* 13: S798.

Fujita H, Kuwabara H, Reutens DC, Gjedde A (1999) Oxygen consumption of cerebral cortex fails to increase during continued vibrotactile stimulation. *J Cereb Blood Flow Metab* 19(3).

Fukuhara N, Tokiguchi S, Shirakawa K, et al. (1980) Myoclonus epilepsy as-

sociated with ragged-red fibres (mitochondrial abnormalities): Disease entity or a syndrome? Light- and electron-microscopic studies of two cases and review of literature. *J Neurol Sci* 47:117-133.

Giles RE, Blanc H, Cann HM, et al. (1980) Maternal inheritance of human mitochondrial DNA. *Proc Natl Acad Sci USA* 77:6715-6719.

Gjedde A, Wienhard K, Heiss WD, Kloster G, Diemer NH, Herholz K, Pawlik G (1985) Comparative regional analysis of 2-fluorodeoxyglucose and methylglucose uptake in brain of four stroke patients. With special reference to the regional estimation of the lumped constant. *J Cereb Blood Flow Metab* 5(2):163-78.

Gjedde A, Kuwabara H (1990) Kinetic analysis of glucose tracer uptake and metabolism by brain in vivo. In: Diksic M, Reba RC (eds) *Radiopharmaceuticals and Brain Pathology Studied with PET and SPECT.* CRC Press, Boca Raton Ann Arbor Boston 135-164.

Gjedde A (1990) Kinetic analysis of radioligand binding in brain in vivo. In: Diksic M, Reba RC (eds) *Radiopharmaceuticals and Brain Pathology Studied with PET and SPECT. CRC Press Boca Raton Ann Arbor Boston* pp. 337-355.

Gjedde A, Ohta S, Kuwabara H, Meyer E (1991) Is oxygen diffusion limiting for blood-brain transfer of oxygen? In: Lassen NA, Ingvar DH, Raichle MME, Friberg L, eds. *Brain Work and Mental Activity.* Alfred Benzon Symposium 31, Copenhagen: Munksgaard; 177-184.

Gjedde A (1995) Tracer kinetics. In: *Principles of Nuclear Medicine* H Wagner Jr ed. Saunders Company pp. 451-461.

Gjedde A (1997) The relation between brain function and cerebral blood flow and metabolism. *Cerebrovascular Disease.* Hunt Batjer H. ed. Lippincott-Raven Publishers pp. 23-40.

Goto Y-i, Nonaka I, Horai S (1990) A mutation in the $tRNA^{leu(UUR)}$ gene associated with MELAS subgroup of mitochondrial encephalomyopathy. *Nature* 348:651-653.

Gouras P (1991) Color vision. In: Kandal ER, Schwartz JH Jessell TM (eds) *Principles of Neural Science.* Elsevier Science publishing, New York.

Grossman LI, Shoubridge EA (1996) Mitochondrial genetics and human disease. *BioEssays* 18:983-991.

Harding AE (1991) Neurological disease and mitochondrial genes. *Trends Neurosci* 14:132-138.

Henkes HE, Van Der Tweel LH (1964) Flicker. *Doc Ophthalmol* 18:1-35.

Hering E (1964) Outlines of a theory of the light sense. LM Herrick, D Jameson (trans). Cambridge, Mass.: Harvard University Press.

Herscovitch P, Markham J, Raichle ME (1983) Brain blood flow measured with intravenous $H_2{}^{15}O$. I. Theory and error analysis. *J Nucl Med* 24:782-789.

Hoffman EJ, Phelps ME (1986) Positron emission tomography: Principles and quantification. In: Phelps ME, Mazziotta JC, Schelbert HR (eds) *Positron Emission Tomography and Autoradiography: Principles and Applications for the Brain and Heart* Raven Press. New York. 237-286.

Holt IJ, Harding AE, Morgan-Hughes JA (1988) Deletions of muscle mitochondrial DNA in patients with mitochondrial myopathies. *Nature* 331:717-719.

Holt IJ, Harding AE, Cooper JM, et al. (1989) Mitochondrial myopathies: clinical

and biochemical features of 30 patients with major deletions of muscle mitochondrial DNA. *Ann Neur* 26:699-708.

Holte S, Eriksson L, Litton J (1988) An automated blood sampling system for positron emission tomography. *IEEE Trans Nucl Sci.*

Horton JC (1984) Cytochrome oxidase patches: a new cytoarchitectonic feature of monkey visual cortex. *Phylosophical Transactions of the Royal Society of London-Series B: Biological Sciences* 304(1119): 199-253.

Howell N, Bindoff LA, McCullough DA (1991) Leber's hereditary optic neuropathy: Identification of the same mitochondrial ND1 mutation in six pedigrees. *Am J Hum Genet* 49:939-950.

Huang SC, Carson RE, Phelps ME (1982) Measurement of local blood flow and distribution volume with short-lived isotopes: A general input technique. *J Cereb Blood Flow Metab* 2:99-108.

Huang SC, Carson RE, Hoffman EJ, Carson J, et al. (1983) Quantitative measurement of local blood flow in humans by positron computed tomography and ^{15}O-water. *J Cereb Blood Flow Metab* 3:141-153.

Huang SC, Feng D, Phelps ME (1986) Model dependency and estimation reliability in measurement of cerebral oxygen utilization rate with oxygen-15 and dynamic positron emission tomography. *J Cereb Blood Flow Metab* 6:105-119.

Huang SC, Phelps ME (1986) Principles of tracer kinetic modelling in positron emission tomography and autoradiography. In: Phelps ME, Mazziotta JC, Schelbert HR (eds) *Positron Emission Tomography and Autoradiography: Principles and Applications for the Brain and Heart* Raven Press, New York, 237-286.

Hubel DH., Wiesel TN (1959) Receptive fields of single neurons in the cat's striate cortex. *J Physiol. (Lond.)* 148:574-591.

Hubel DH., Wiesel TN (1962) Receptive fields, binocular interaction and functional architecture in the cat's visual cortex. *J Physiol. (Lond.)* 160:106-154.

Hubel DH., Wiesel TN (1972) Laminar and oolumnar distribution of geniculocortical fibers in the macaque monkey. *J Comp Neurol* 146:421-450.

Hutchins GD, Hichwa RD, Koeppe RA (1986) A continuous flow input function detector for $H_2{}^{15}O$ blood flow studies in positron emission tomography. *IEEE*

Trans Nucl Sci 33:546-549.

Huoponen K, Vilkki J. Aula P, et al. (1991) A new mtDNA mutation associated with Leber hereditary optic neuroretinopathy. *Am J Hum Genet* 48:1147-1153.

Iida H, Kanno I, Miura S. Murakami M. et al. (1986) Error analysis of a quantitative cerebral blood flow measurement using $H_2{}^{15}O$ autoradiography and positron emission tomography. with respect to the dispersion of the input function. *J Cereb Blood Flow Metab* 6:536-545.

Iida H, Kanno I, Miura S. Murakami M. et al. (1987) An accurate determination of regional brain/blood partition coefficient of water using dynamic positron emission tomography: validation of Kety-Schmidt single compartment model for $H_2{}^{15}O$ based on measurement. *J Cereb Blood Flow Metab* 7:S576.

Iida H, Higano S, Tomura N. Shishido F, et al. (1988) Evaluation of regional differences of tracer appearance time in cerebral tissue using [^{15}O] water and dynamic positron emission tomography. *J Cereb Blood Flow Metab* 8:285-288.

Jones T, Chesler DA, Ter-Pogossian MM (1976) The continuous inhalation of oxygen-15 for assessing regional oxygen extraction in the brain of man. *Br J Ra-*

diol 40:339-343.

Kandel ER (1991) Phototransduction and information processsing in the retina. In: Kandel ER, Schwartz JH Jessell TM (eds) *Principles of Neural Science.* Elsevier Science publishing, New York.

Kanno I, Miura S, Yamamoto S, Iida H, et al. (1985) Design and evaluation of a positron emission tomograph: Headtome III. *J Comput Assist Tomogr* 9:931-939.

Kanno I, Iida H, Miura S, Murakami M, et al. (1987) A system for cerebral blood flow measurement using an $H_2{}^{15}O$ autoradiographic method and positron emission tomography. *J Cereb Blood Flow Metab* 7:143-153.

Karpati G, Shoubridge EA (1993) Mitochondrial encephalomyopathies due to electron transport chain defects. In: *Current Neurology,* Vol 13, Chapter 6, Mosby-Year Book, pp. 133-166.

Kassissia IG, Goresky CA, Rose CP, Schwab AJ, Simard A, Huet PM, Bach GG (1995) Tracer oxygen distribution is barrier-limited in the cerebral microcirculation. *Cir Res* 77(6):1201-1211.

Kety SS, Schmidt CF (1948) The nitrous oxide method for the quantitative determination of cerebral blood flow in man: Theory, procedure, and normal values. *J Clin Invest* 27:476-483.

Kety SS (1951) The theory and application of the exchange of inert gas at the lungs and tissue. *Pharmacol Rev* 3:1-41.

Kety SS (1960) Measurement of local blood flow by the exchange of an inert, diffusible substance. *Meth Med Res* 3:228-236.

Koeppe RA, Holden JE, Polcyn RE, Nickles RJ, Hutchins GD, Weese JL (1985) Quantitation of local cerebral blood flow and partition coefficient without arterial sampling: Theory and validation. *J Cereb Blood Flow Metab* 5:214-224.

Koeppe RA, Hutchins GD, Rothley JM, Hichwa RD (1987) Examination of assumptions for local cerebral blood flow studies in PET. *J Nucl Med* 28:1695-103.

Kuschinsky W, Paulson OB (1992) Capillary circulation in the brain. *Cerebrovasc Brain Metab Rev* 4:261-286.

Kuwabara H, Ohta S, Brust P, Meyer E, Gjedde A (1992) Density of perfused capillaries in living human brain during functional activation. *Prog Brain Res* 91: 209-215.

Kwong KK, Belliveau JW, Chesler DA, et al. (1992) Dynamic megnetic resonance imaging of humman brain activity during primary sensory stimulation. *Proc Natl Acad Sci USA* 89:5675-5679.

Lammertsma AA, Frackowiak RSJ, Hoffman JM, Huang SC, et al (1989) The $C^{15}O_2$ build-up technique to measure regional cerebral blood flow and volume of distribution of water. *J Cereb Blood Flow Metab* 9:461-470.

Lassen NA, Perl W (1979) *Tracer Kinetic Methods in Medical Physiology.* Raven Press, New York.

Leblanc R, Meyer E (1990) Functional PET scanning in the assesment of cerebral arteriovenous malformations. *J Neurosurg* 7:615-619.

Leblanc R, Meyer E, Bub D, Zatorre R, Evans AC (1992) Language localization with activation positron emission tomography scanning. *Neurosurgery* 31:369-373.

Livingstone MS, Hubel DH (1984a) Anatomy and physiology of a color system in the primate visual cortex. *J Neurosci* 4:309-356.

Livingstone MS, Hubel DH (1984b) Specificity of intrinsic connections in primate primary visual cortex. *J Neurosci* 4:2830-2835.

Luft R, Ikkos D, Palmieri G, et al. (1962) A case of severe hypermetabolism of nonthyroid origin with a defect in the maintenance of mitochondrial respiratory control: A correlated clinical, biochemical, and morphological study. *J Clin Invest* 41:1776-1804.

Marrett S, Meyer E, Kuwabara H, Evans AC, Gjedde A (1995) Differential increases of oxygen metabolism in visual cortex. *J Cereb Blood Flow Metab* 15(S1): S80.

Marrett S, Gjedde A (1997) Changes of blood flow and oxygen consumption in visual cortex of living humans. *Adv Exp Med Biol* 413:205-208.

Mason C, Kandel ER (1991) Phototransduction and information processsing in the retina. In: Kandal ER, Schwartz JH Jessell TM (eds) *Principles of Neural Science*. Elsevier Science publishing, New York.

Mazziotta JC, Phelps ME (1986) Positron emission tomography studies of the brain. In: Phelps ME, Mazziotta JC, Schelbert HR (eds) *Positron Emission Tomography Studies in the Brain: Positron Emission Tomography and Autoradiography: Principles and Applications for the Brain and Heart.* Raven Press, New York, 493-579.

McShane MA, Hammans SR, Sweeney M, et al. (1991) Pearson Syndrome and mitochondrial encephalomyopathy in a patient with a deletion of mtDNA. *Am J Hum Genet* 48:39-42.

Meyer E, Tyler JL, Thompson CJ, Redies C, et al. (1987) Estimation of cerebral oxygen utilization rate by single-bolus $^{15}O_2$ inhalation and dynamic positron emission tomography. *J Cereb Blood Flow Metab* 7:403-414.

Meyer E (1989) Simultaneous correction for tracer arrival delay and dispersion in CBF measurements by the $H_2{}^{15}O$ autoradiographic method and dynamic PET. *J Nucl Med* 30:1069-1078.

Meyer E (1990) ^{15}O studies with PET. In: Diksic M, Reba RC (eds) *Radiopharmaceuticals and Brain Pathology Studied with PET and SPECT.* CRC Press,

Boca Raton Ann Arbor Boston 165-198.

Minoshima S, Frey KA, Koeppe RA, Foster NL, Kuhl DE (1995) A diagnostic approach in Alzheimer's disease using three-dimensional stereotactic surface projections of fluorine-18-FDG PET. *J Nucl Med* 36(7):1238-1248.

Mintun MA, Raichle ME, Martin WRW, Herscovitch P (1984) Brain oxygen utilization measured with O-15 radiotracers and positron emission tomography. *J Nucl Med* 27:177-187.

Mintun MA, Raichle ME, Kilbourn MR, Wooten GF, Welch MJ (1984) A quantitative model for the in vivo assessment of drug binding sites with positron emission tomography. *Ann Neurol* 15(3):217-27.

Montagna P, Galassi R, Medori R, et al. (1988) MELAS syndrome: Characteristic migrainous and epileptic features and maternal transmission . *Neurology* 38:751-754.

Moraes CT, DiMauro S, Zeviani M, et al. (1989) Mitochondrial DNA deletions in progressive external ophthalmoplegia and Kearns-Sayer syndrome. *N Engl J Med* 320:1293-1299.

Moraes CT, Schon EA, DiMauro S (1991) Mitochondrial diseases: Towards a retional classification. In: *Current Neurology*, edited by SH Appel. St Louis: *Mosby-Year Book, Vol II*, pp. 83-119.

Movshon JA, Thompson ID, Tolhurst DJ (1978) Spatial and temporal contrast sensitivity of neurones in areas 17 and 18 of cat's visual cortex. *J Physiol London* 283:101-120.

Nelson AD, Muzic RF, Miraldi F, Muswick GJ, et al. (1990) Continuous arterial positron monitor for quantitation in PET imaging. *Am J Physio Ima* 5:84-88.

Ohira Y, Tabata I (1992) Muscle metabolism during exercise: aerobic threshold does not exist. *Am Physiol Anthropol* 11:319-323.

Ohta S, Meyer E, Gjedde A (1990) Weighted integration method with CBV correction to estimate rCBF by PET. *Eur J Nucl Med* 16: iii s178.

Ohta S, Meyer E, Thompson CJ, Gjedde A (1992) Oxygen consumption of the living human brain measured after a single inhalation of positron emitting oxygen. *J Cereb Blood Flow Metab* 12:179-192.

Ohta S, Meyer E, Fujita H, Reutens DC, Evans AC, Gjedde A (1996) Cerebral [^{15}O]water clearance in humans determined by PET: I. Theory and normal values. *J Cereb Blood Flow Metab* 16:765-780.

Ohta S, Reutens DC, Gjedde A (1999) Brief vibrotactile stimulation does not increase cortical oxygen consumption when measured by single inhalation of positron emitting oxygen. *J Cereb Blood Flow Metab* 19(3).

Ogawa S, Tank DW, Menon R, et al. (1992) Intrinsic signal changes accompanying sensory stimulation: functional brain mapping with magnetic resonance imaging. *Proc Natl Acad Sci USA* 89: 5951-5955.

Paus T, Marrett S, Worsley KJ, Evans AC (1995) Extraretinal modulation of cerebral blood flow in the human visual cortex: implications for saccadic suppression. *J Neurophysiol* 75(4):2179-2183.

Paus T, Jech R, Thompson CJ, Comeau R, Peters T, Evans AC (1997) Transcranial magnetic stimulation during positron emission tomography: a new method for studying connectivity of the human cerebral cortex. *J Neurosci* 17(9):3178-3184.

Pavlakis SG, Phillips PC, DiMauro S, et al. (1984) Mitochondrial myopathy, encephalopathy, lactic acidosis, and stroke-like episodes: A distinctive clinical syndrome. *Ann Neurol* 16:481-487.

Pette D (1985) Metabolic heterogeneity of muscle fibers. *J Exp Biol* 115:179-189.

Phelps ME, Huang SC, Hoffman EJ, Selin C, Sokoloff L, Kuhl DE (1979) Tomographic measurement of local cerebral glucose metabolic rate in humans with (F-18)2-fluoro-2-deoxy-D-glucose: validation of method. *Ann Neurol* 6(5):371-88.

Poulton J, Deadman ME, Gardiner RM (1989) Tandem direct duplications of mitochondrial DNA in mitochondrial myopathy: Analysis of nucleotide sequences and tissue distribution. *Nucleic Acids Res* 17:10233-10229.

Powers WJ, Raichle ME (1985) Positron emission tomography and its application to the study of cerebrovascular disease in man. *Stroke* 16:361-376.

Poulton J, Deadman ME, Gardiner RM (1989) Tandem direct duplications of mitochondrial DNA in mitochondrial myopathy: Analysis of nucleotide sequences

and tissue distribution. *Nucleic Acids Res* 17:10233-10229

Price C, Wise R, Friston K, Howard D, Patterson K, Frackowiak R (1992) Regional response differences within the human auditory cortex when listening to words. *Neurosci Lett* 146:179-182.

Raichle ME, Martin WRW, Herscovitch P, Mintun MA, Markham J (1983) Brain blood flow measured with intravenous $H_2{}^{15}O$. II. Implementation and validation. *J Nucl Med* 24:790-798.

Raichle ME, Grubb RL Jr, Eichling JO, Ter-Pogossian MM (1986) Measurement of brain oxygen utilization with radioactive oxygen-15: Experimental verification. *J Appl Physiol* 40:638-640.

Reivich M, Kuhl D, Wolf A, Greenberg J, et al. (1979) The [18F]fluorodeoxyglucose method for the measurement of local cerebral glucose utilization in man. *Circ Res* 44(1):127-137.

Ribeiro L, Kuwabara H, Meyer E, Fujita H, et al. (1993) Cerebral blood flow and metabolism during nonspecific bilateral visual stimulation in normal subjects. In: Uemura K, Lassen NA, Jones T, Kanno I, (eds) *Quantification of Brain Function:*

Tracer Kinetics and Image Analysis in Brain PET. Amsterdam: Elsevier, 229-234.

Roy CS, Sherrington CS (1890) On the regulation of the blood supply of the brain. *J Physiol (Lond)* 11:85-108.

Sadato N, Ibanez V, Deiber MP, Campbell G, Leonardo M, Hallett M (1996) Frequency-dependent changes of regional cerebral blood flow during finger movements. *J Cereb Blood Flow Metab* 16:23-33.

Sayers BMcA (1970) *Inferring Significance from Biological Signals.* In: Clynes M. ed. Biomedical engineering systems. McGraw-Hill, New York, 84-115.

Schickman GM (1981) Time-dependent function in vision. In: Moses RA, ed. *Adler's Physiology of the Eye.* (7^{th} ed) St. Louis MO: Mosby, chapt. 23, pp. 666-693.

Schon EA, Rizzuto R, Moraes CT, Nakase H, Zeviani M, Dimauro S (1989) A direct repeat is a hotspot for large-scale deletions of human mitochondrial DNA. *Science* 244:346-349.

Schwaiger M, Hicks R (1991) The clinical role of metabolic imaging of the heart

be positron imaging tomography. *J Nucl Med* 32:565-576.

Seitz RJ, Roland PE (1992) Vibratory stimulation increases and decreases the regional cerebral blood flow and oxidative metabolism:A positron emission tomography (PET) study. *Acta Neurol Scand* 86: 60-67.

Servidei S, Zeviani M, Manfredi G, et al. (1991) Dominantly inherited mitochondrial myopathy with multiple deletions of mitochondrial DNA: Clinical, morphological, and biochemical studies. *Neurology* 41:1053-1059.

Siesjö BK (1978) *Brain Energy Metabolism.* New York: Wiley.

Shoffner JM, Lott M, Lezza AMS et al. (1990) Myoclonic epilepsy and ragged-red fiber disease (MERRF) is associated with a mitochondrial NDA $tRNA^{lys}$ mutation. *Cell* 61:931-937.

Sokoloff L, Kety SS (1977) Regulation of cerebral circulation. *Physiol Rev* 40(Suppl. 4):38-44.

Sokoloff L (1977) Relation between physiological function and energy metabolism in the central nervous system. *J Neurochem* 29:13-26.

Sweet WH, Brownell GL (1955) Localization of intracranial lesion by scanning with positron-emitting arsenic. *J Am Med Assoc* 157:1183-1187.

Talairach J, Tournoux P (1988) *Co-Planar Stereotactic Atlas of the Human Brain: 3-Dimensional Proportional System: An Approach to Cerebral Imaging.* New York: Thieme.

Ter-Pogossian MM, Eichling JO, Davis DO, Welch MJ (1970) The measure in-vivo of regional cerebral oxygen utilization by means of oxyhemoglobin labeled with radio-active oxygen-15. *J Clin Invest* 49:381-391.

Toga AW, Collins RW (1981) Metabolic response of optical centers to visual stimuli in the albino rat: anatomical and physiological considerations. *J Comp Neurol* 199:443-464.

Tootell RBH, Silverman MS, Hamilton SL, Switkes E, De Valois RL (1988) Functional anatomy of macaque striate cortex. V. Spatial frequency. *J Neurosci* 8(5):1610-1624.

Tootell RBH, Hamilton SL, Silverman MS (1985) Topography of cytochrome ox-

idase activity in owl monkey cortex. *J Neurosci* 5:2786-2800.

Ts'o DY, Gilbert CD, Weisel TN (1986) Relationships between horizontal interactions and functional architecture in cat striate cortex revealed by cross-correlation analysis. *J Neurosci* 6:1160-1170.

Tsui E, Budinger TF (1978) Transverese section imaging of mean clearance time. *Phys Med Biol* 23:644-653.

Vafaee MS, Meyer E, Gjedde A (1993) O-15 water and O-15 labelled red blood cells require separate external dispersion corrections. *Soc Nuc Med Abstr* 34(5):51P.

Vafaee MS, Murase K, Gjedde A, Meyer E (1996) Dispersion correction for automatic sampling of O-15 labeled H_2O and red blood cells. In: Myers R, Cunningham VJ, Bailey DL, Jones T, (eds) *Quantification of Brain Function Using PET.* San Diego: Academic Press. 72-75.

Vafaee MS, Paus T, Gjedde A, Evans AC, Ptito A, Meyer E (1996) Oxidative metabolism in human visual cortex during physiological activation studied by PET. *Soc Neurosci Abstr* 22:1060.

Vafaee MS, Marrett S, Meyer E, Evans AC, Gjedde A (1998) Increased oxygen consumption in human visual cortex: Response to visual stimulation. *Acta Neurol Scand* 98:85-89.

Vafaee MS, Meyer E, Marrett S, Paus T, Evans AC, Gjedde A (1999) Frequency-dependent changes in cerebral metabolic rate of oxygen during activation of human visual cortex. *J Cereb Blood Flow Metab* 19:3:272-277.

Vafaee MS, Gjedde A (1999) Increase of oxygen consumption in visual cortex consistent with model of oxygen delivery. *submitted.*

Van Coster R, Lombes A, De Vivo DC, et al. (1991) Cytochrome c oxidase-associated Leigh syndrome: Phenotypic features and pathogenetic speculations. *J Neuro Sci* 104:97-111.

Van den Berg CJ, Bruntink R (1983) Glucose oxidation in the brain during seizures: experiments with labeled glucose and deoxyglucose. In: Hertz L, Kvamme E, McCeer EG, Schousboe A, (eds) *Glutamine, Glutamate and GABA in the central nervous system.* New York: Alan R. Liss. pp. 619-624.

Van Essen DC, Maunsuell LHR, Bixby JL (1981) The middle temporal visual

area in the maccaque: myeloarchtecture, connections, functional properties and topographic representation. *J Comp Neurol* 199: 293-326.

Wagner HN Jr (1986) Quantitative imaging of neuroreceptors in the living human brain. *Semin Nucl Med* 16(1):51-62.

Wallace DC, Zheng X, Lott MT, et al. (1988) Familial mitochondrial encephalomyopathy (MERRF): Genetic, pathophysiological, and biochemical characterization of mitochondrial DNA disease. *Cell* 55:601-610.

Wallace DC, Singh G, Lott MT, et al. (1988) Mitochondrial DNA mutation associated with Leber's heriditary optic neuropathy. *Science* 242:1427-1430.

Wallace DC (1990) Report of the committee on human mitochondrial DNA. *Cytogenet Cell Genet* 55:395-405.

Wallace DC (1992) Diseases of the mitochondrial DNA. *Annu Rev Biochem* 61:1175-1212.

Watson JDG, Meyers R, Frackowiak RSJ et al (1993) Area V5 of the human brain: Evidence from a combined study using positron emission tomography and

magnetic resonance imaging. *Cereb Cortex* 3(2): 79-94.

Weast RC, Astle MJ, Beyer WH (eds) (1985)*CRC Handbook of Chemistry and Physics*. CRC Press, 65^{th} edition, F35-F44.

Weiss DW, Souder E, Alavi A (1990) Regional cerebral metabolic and structural changes in normal aging and dementia as detected by PET and MRI. In: Diksic M, Reba RC (eds) *Radiopharmaceuticals and Brain Pathology Studied with PET and SPECT*. CRC Press. Boca Raton Ann Arbor Boston 409-426.

Widen (1991) How shall we measure regional brain work? In: Lassen NA, Ingvar DH, Raichle MME, Friberg L, (eds) *Brain Work and Mental Activity*. Alfred Benzon Symposium 31, Copenhagen: Munksgaard; 127-139.

Wong D, Wagner HN Jr, Tune LE, et al. (1986) Positron emission tomography reveals elevated D_2 dopamine receptors in drug-naive schizophrenics. *Science* 234:1558.

Wong-Riley M, Carroll E (1984) monkey visual system. *Nature* 307: 262-264.

Woods RP, Cherry SR, Mazziotta JC (1992) Rapid automated algorithm for align-

ing and reslicing PET images. *J Comput Assist Tomogr* 16: 620-633.

Woods RP, Mazziotta JC, Cherry SR (1993) MRI-PET registration with automated algorithm. *J Comput Assist Tomogr* 17: 536-546.

Worsley KJ, Evans AC, Marrett S, Neelin P (1992) A three-dimensional statistical analysis for CBF activation studies in human brain. *J Cereb Blood Flow Metab* 12: 900-918.

Worsley KJ, Marrett S, Neelin P, Vandal AC, Friston K, Evans AC (1996) A unified statistical approach for determining significant signals in images of cerebral activation. *Human Brain Mapping* 4:58-73.

Wrenn FR Jr, Good ML, Handler P (1951) Use of positron-emitting radioisotopes for localization of brain tumors. *Science* 113:525-528.

Yamamoto YL, Robertson JS (1966) *Study of Quantitative Assessment of Section Micro-regional Cerebral Blood Flow in Man by Multiple Positron Detecting System Using Krypton-79.* BNL Med Dept Circ No 28, Brookhaven National Laboratory, Islip, NY.

Yarowsky PJ, Ingvar DH (1981) Neuronal activity and energy metabolism. *Fed Proc* 40:2358-2363.

Yarowsky PJ, Kadekaro M, Sokoloff L (1983) Frequency-dependent activation of glucose utilization in the superior cervical ganglion by electrical stimulation of cervical sympathetic trunk. *Proc Natl Acad Sci USA* 80:4179-4183.

Zeki S, Shipp S (1988) The functional logic of cortical connections. *Nature* 335: 311-317.

Zeki S, Watson JDG, Lueck CJ, et al. (1991) A direct demonstration of functional specialization in human visual cortex. *J Neuro Sci* 11(3): 641-649.

Zeviani M, Moraes CT, DiMauro S (1988) Deletions of mitochondrial DNA in Kearns-Sayer Syndrome. *Neurology* 38:1339-1346.